Guilherme Rodrigues Gaspar

Licenciado em Engenharia Electrotécnica e de Computadores

Channel estimation in massive MIMO systems

Dissertação para obtenção do Grau de Mestre em
Engenharia Electrotécnica e de Computadores

Orientador: Prof. Doutor Paulo Montezuma, Professor Auxiliar, FCT-UNL

Co-orientadores: Prof. Doutor Rui Dinis, Professor Associado com Agregação, FCT-UNL

Júri:

Presidente: Prof. Doutor João Oliveira, Professor Auxiliar, FCT-UNL

Arguente: Prof. Doutor Pedro Amaral, Professor Auxiliar, FCT-UNL

Vogal: Prof. Doutor Paulo Montezuma, Professor Auxiliar, FCT-UNL

FACULDADE DE CIÊNCIAS E TECNOLOGIA
UNIVERSIDADE NOVA DE LISBOA

Setembro 2016

Channel estimation in massive MIMO systems

Aos meus avós e aos meus pais,
que nunca deixaram de me apoiar.

Acknowledgments

Firstly, I would like to address my gratitude to Professor Paulo Montezuma for the continuous support, motivation, patience and understanding over this year. I would like to thank Professor Rui Dinis that was always helpful when needed. I would also like to express my gratefulness to Faculdade de Ciências e Tecnologias da Universidade Nova de Lisboa, who instructed me so well along these years and opened so many doors. Last but not least, I want to thank all the people who have accompanied me is this journey, especially my parents, that were always by my side, and Afonso Ferreira, that could always lighten up the mood when it was most needed

Abstract

Last years were characterized by a great demand for high data throughput, good quality and spectral efficiency in wireless communication systems. Consequently, a revolution in cellular networks has been set in motion towards to 5G. Massive multiple-input multiple-output (MIMO) is one of the new concepts in 5G and the idea is to scale up the known MIMO systems in unprecedented proportions, by deploying hundreds of antennas at base stations. Although, perfect channel knowledge is crucial in these systems for user and data stream separation in order to cancel interference.

The most common way to estimate the channel is based on pilots. However, problems such as interference and pilot contamination (PC) can arise due to the multiplicity of channels in the wireless link. Therefore, it is crucial to define techniques for channel estimation that together with pilot contamination mitigation allow best system performance and at same time low complexity.

This work introduces a low-complexity channel estimation technique based on Zadoff-Chu training sequences. In addition, different approaches were studied towards pilot contamination mitigation and low complexity schemes, with resort to iterative channel estimation methods, semi-blind subspace tracking techniques and matrix inversion substitutes.

System performance simulations were performed for the several proposed techniques in order to identify the best tradeoff between complexity, spectral efficiency and system performance.

Keywords: Massive MIMO, Channel Estimation, Zadoff-Chu sequences, Pilot Contamination

Resumo

Os últimos anos foram marcados pela grande procura por um elevado aumento no tráfego de dados, na qualidade, e na eficiência espectral de transmissões em sistemas de comunicações móveis. Consequentemente, uma revolução nas redes celulares tem começado a emergir: 5G. O *massive* MIMO é um dos novos conceitos do 5G, com a ideia de ampliar os conhecidos sistemas MIMO em proporções sem precedentes, através da implementação de centenas de antenas nas estações base. No entanto, o conhecimento exato do canal é crucial neste tipo de sistemas para a divisão de utilizadores e fluxos de dados, de forma a cancelar a interferência.

A forma mais comum de estimar o canal é baseada na transmissão de pilotos. Porém, problemas como interferências e contaminação de pilotos podem surgir devido à maior quantidade de canais na transmissão sem fios. Portanto, é fulcral determinar técnicas de estimação de canal de baixa complexidade, que juntamente com descontaminação de pilotos, consigam um melhor desempenho do sistema.

Este trabalho inclui uma técnica de estimação de canal de baixa complexidade com base em sequências de treino Zadoff-Chu. Também serão estudadas diferentes abordagens à descontaminação de pilotos e redução de complexidade, baseadas em métodos iterativos de estimação de canal, técnicas *semi-blind* de rastreio de subespaços vetoriais e substitutos para inversão de matrizes.

As simulações do desempenho do sistema vão ser realizadas para as diversas técnicas propostas de forma a identificar o melhor compromisso entre complexidade, eficiência espectral e desempenho do sistema

List of Contents

List of Tables

List of Figures

1. Introduction

1.1 Motivation

In recent decades, we have seen a great evolution in the wireless communications industry. This industry has become increasingly involved in people's lives, both professionally and personally. The fact of being communicable with the rest of the world has become an all-time necessity and the result is an increasingly demand for wireless connectivity, especially in the last few years. Any Internet user demands fast wireless connections to support all needs, while at the work, at home or on-the-go. Additionally, Machine-to-Machine communications are exponentially growing, leading to an even greater demand of wireless throughput.

To meet the demand, the fifth generation (5G) of wireless communications technology is emerging. 5G is the future of cellular networking and brings new technologies such as millimeter wave (mmWave) communications and massive MIMO systems. Massive MIMO will employ a very high number of antennas to achieve huge gains in both spectral and energy efficiencies. The base stations would serve multiple users at the same time-frequency resource, through spatial multiplexing. The concept is based on the law of large numbers that states that as the number of antennas grows large, the channel responses from different antennas to each user are close to be mutually-orthogonal [1], [2].

In mobile communication systems, the receiver gets a signal with different amplitude and phases than the one that was broadcasted. Therefore, the quality of the system highly depends on the accuracy of the estimated channel. Conventional channel estimation techniques are based on known training sequences (also called pilot signals). Theses sequences are unique for every user and, preferably mutually orthogonal, so the receiver can estimate the channel responses accurately. The time interval in which a channel is assumed to be constant is denominated as coherence interval and it is where the channel estimation process must occur. Hence, the training sequence is coupled to the information sequence and sent in each considered coherence interval. This means there is a tradeoff between the length of the training sequence (proportional to the estimation's accuracy), and the data rate of payload data. Moreover, the number of mutually orthogonal training sequences is also limited by the channel coherence interval. Consequently, by largely increasing the number of antennas, and serving users, as massive MIMO proposes, the number of channels that have to be estimated and the number of orthogonal training sequence needed becomes equally large. Therefore, the training sequences must be reused in neighboring cells, leading to pilot contamination. Hence, channel estimation and pilot contamination are a major challenge in massive MIMO systems, and they are the two main subjects of this thesis.

1.2 Objectives and outline

This work introduces a low-complexity channel estimation technique based on Zadoff-Chu training sequences. In addition, different approaches were studied towards pilot contamination mitigation and lower complexities schemes, with resort to iterative channel estimation methods, semi-blind subspace tracking techniques and matrix inversion alternatives.

The thesis is organized as follows: chapter 2 presents the state of the art, which includes the massive MIMO technology, pilot contamination concept and some channel estimation methods, with their descriptions and results. Chapter 3 describes a block diagonalization precoding scheme, successful in eliminating interference among different users; a channel estimation technique using a type of training sequences with optimal periodic auto-correlation properties, called Zadoff-Chu sequences, and compares it to a well-known low-complexity channel estimation called minimum mean-square error (MMSE) channel estimation, in a multi-user downlink scenario. In chapter 4, pilot contamination mitigation is addressed by using three different channel estimation methods with different approaches. The first method relies on the iterative process of the iterative block decision feedback equalizer (IB-DFE) scheme. The iterative process eliminates residual intersymbol interference at each iteration. Thus, channel estimates could be calculated at each iteration, producing better results as the number of iterations increase. The second method is a semi-blind channel estimation technique that uses a subspace tracking algorithm to resolve the ambiguity problem, at a cost of lesser pilots than in traditional pilot-based channel estimation techniques. Using less pilots is an effective solution to mitigate pilot contamination. The last method is a Bayesian channel estimator which replaces the matrix inversion operation with a polynomial expansion and it is denominated as polynomial expansion channel (PEACH). The three techniques will be modeled in a multi-user uplink scenario. For comparison purposes, these techniques will be compared under the effect of pilot contamination, using bit error rate (BER) plots and mean square error (MSE) as performance results, for different numbers of users, transmit antennas and complexity of the schemes.

2. State of the Art

This chapter begins by describing some basic, but fundamental, features of simple wireless communications systems, in section 2.1. In section 2.2, the motivation, requirements and forthcoming technologies are also presented, followed by a description of the massive MIMO concept and its main advantages and disadvantages. Section 2.2.3 concludes this chapter by presenting the channel estimation topic in massive MIMO systems, how the undesired effect, called pilot contamination, can arise and how to approach it.

2.1 MIMO

In the decade 1970-1980 numerous studies regarding multiple channel transmission systems were published. Among them, [3]–[5] analyze some critical aspects like diversity, sequence estimation, intersymbol and interchannel interference (ISI and ICI respectively) in wired communications, and their mathematical work were valuable for future studies. In 1987, a study was presented describing the fundamental limits on systems with multiple channels in the same bandwidth and the potential for large capacity in systems with limited bandwidth [6]. In 1999, an article was published [7] concerning the problems of communicating over a flat-fading Rayleigh channel using multiple-antenna arrays. In 2001, the first commercial MIMO system was introduced by Iospan Wireless Inc.

It rather seems counter-intuitive but MIMO, also called single user MIMO (SU-MIMO) or point-to-point MIMO, relies on non-line-of-sight propagation, which means radio waves are transmitted across a path that is partially obstructed by obstacles (Figure 2.1). So, generally, it is not desirable to have a direct path between the base station and the user, because a good diversity in signal transmission is wanted. So anything that behaves like an obstacle to the signal, such as buildings, people, natural elements, etc. will improve the efficiency and total effectiveness of communication with MIMO technique. On the other hand, while multiple scatters improve the system's performance, the signal is also affected, negatively, by fading. When the signal travels over a wireless communication channel it suffers oscillations in amplitude and phase, that if not compensated compromise the ability of the receiver to recover the information properly.

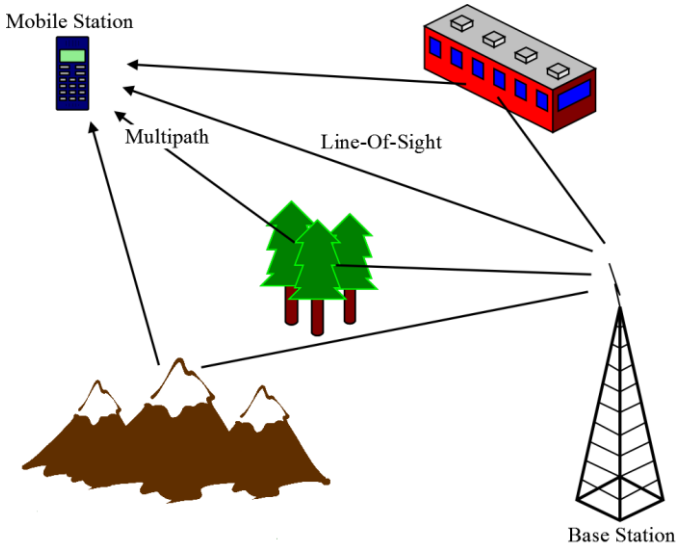

Figure 2.1 - Radio Propagation

MIMO operates with multiple receive and transmit antennas for signal transmission, as shown in Figure 2.2. Generally, the number of antennas is directly proportional to data rate (multiplexing), quality (diversity) and capacity of the transmission [8], [9]. Besides MIMO, beamforming and space-time coding schemes are another two fundamental technologies that arise in a multiple antennas wireless communication system.

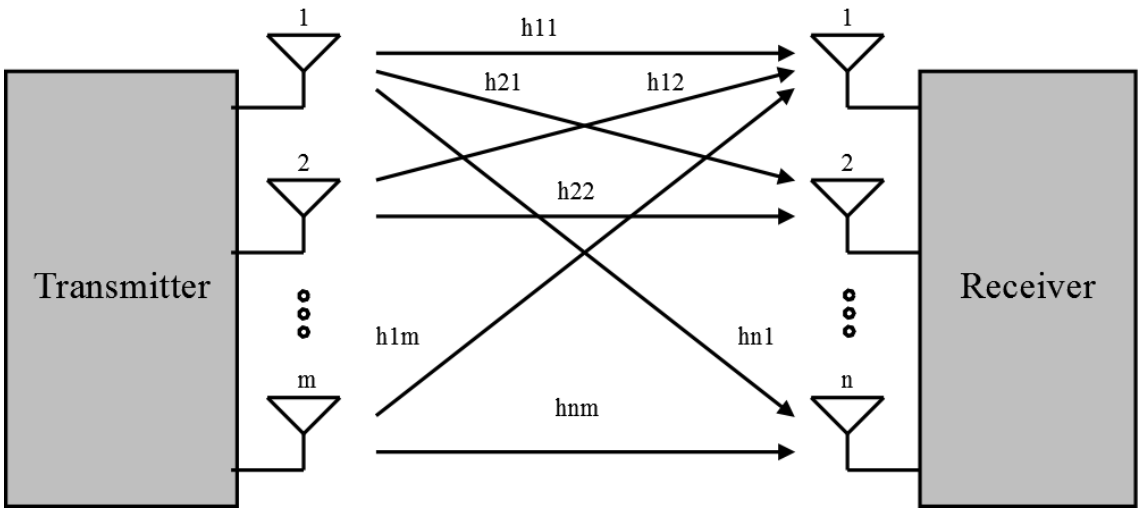

Figure 2.2 - MIMO system model with m transmit antennas and n receive antennas

2.1.1 Diversity and Multiplexing

In the real world, in a single-input single-output (SISO) wireless transmission, the signal takes multiple divergent paths due to reflections and/or refractions on obstacles across the path, especially in urban and indoors environments. Hence, the receiver detects multiple time-delayed, and attenuated versions of the original signal, resulting in the deterioration of efficiency and data

rate of the communication. Adding more antennas at receiver, it is possible to combine every received version of the signal and collectively improve these defects. Diversity can also be applied at the transmitter (called transmit diversity) when multiple antennas send the same signal. The same principle applies, where the probability of the signal reaching the receiver in good conditions is higher than with lesser antennas.

Instead of using multiple antennas to transmit the same signal, each antenna could be used to send different information, in parallel. This technique is called spatial multiplexing and increases the overall capacity of the system.

2.1.2 Beamforming

On transmission, MIMO can use the beamforming technique which consists on the transmitter focusing the transmitted energy towards the receiver instead of being omnidirectional, as is depicted on Figure 2.3. Receivers frequently detect interference signals blended with the desired signal that may affect the system's performance. However, the desired and interfering signals are usually originated in different locations. Beamforming exploits this spatial separation to cancel the unwanted interference from the desired signal, acting as a spatial filter [10].

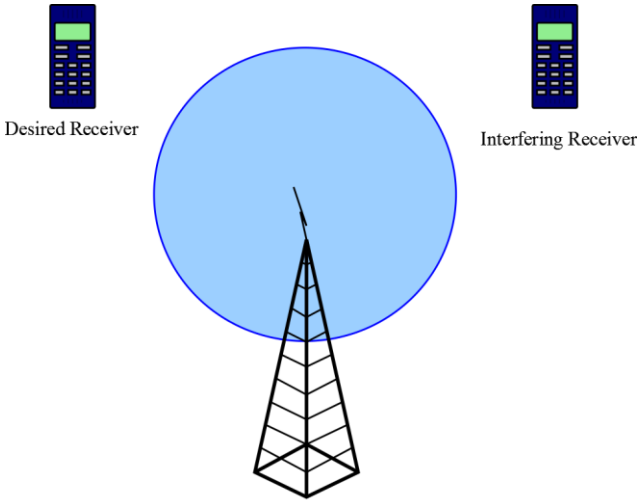

(a)

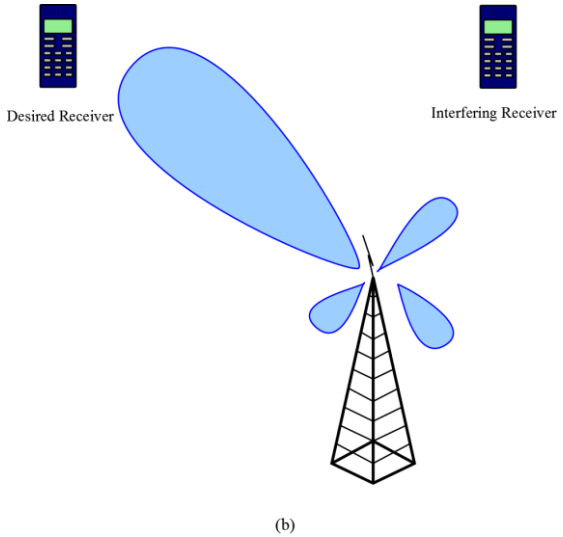

Figure 2.3 – (a) Systems with omnidirectional antennas transmission (b) System with beamforming technique

2.1.3 Channel Estimation

The wireless channel is highly complex and can be frequency- and time-selective due to fading. These phenomena include reflection, diffraction, scattering of the signal and Doppler Shift which represents the change of the frequency from the emitted to the observed wave when the distance between the receiver and the source changes. Therefore, in wireless channels, channel estimation is a vital technique mainly used in mobile wireless network systems. The receiver needs to know exactly the channel state information (CSI) to perform the equalization of the signal and to determine it can be a complex task.

Most of channel estimation techniques use training sequences on transmission. Training sequences are a set of symbols, denominated pilot symbols, known by the receiver that are coupled to the data sequence to be transmitted in order to perform the channel estimation for the next data symbols in which the channel is assumed unchanged, also called coherence time interval. Figure 2.4 depicts a typical time slot structure in systems with channel estimation based on training sequences.

Figure 2.4 - Slot structure in systems with pilot-based channel estimation

In MIMO systems due to the multiple antennas in transmitters and receivers, multiple channels must be estimated, simultaneously, as well. Therefore, a larger set of pilot symbols must be integrated in the transmission frame, reducing the payload. However, some techniques do not

require training sequences, and for that reason they are denominated as blind-estimation techniques.

2.1.4 Multi-user MIMO

MIMO technology was a big step towards the development of new communication systems. One of them is the multi-user MIMO (MU-MIMO). In a MU-MIMO scheme, the base station communicates with multiple users simultaneously (Figure 2.5).

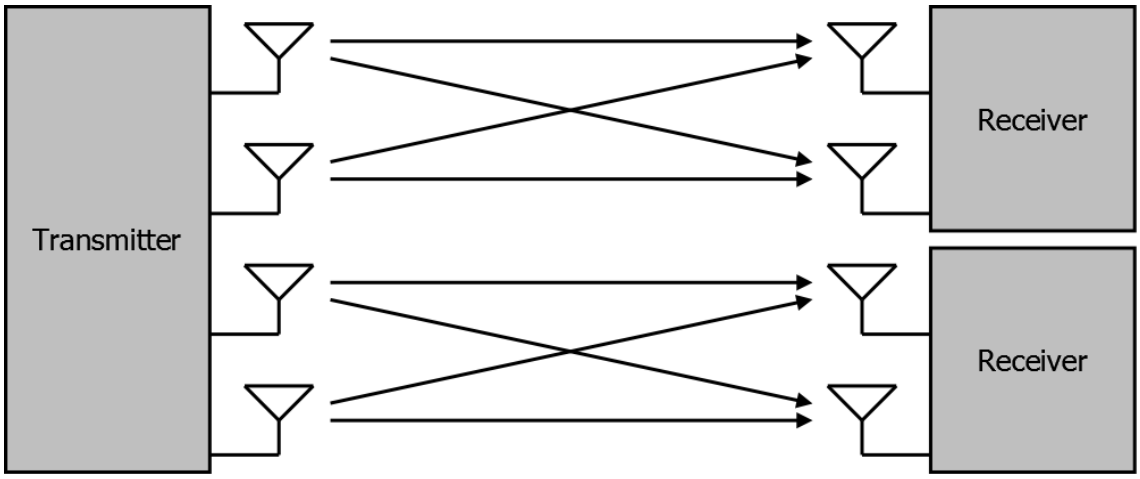

Figure 2.5 - MU-MIMO system model with 2 users

MU-MIMO schemes offer several advantages over SU-MIMO communications, which are:

- A gain in channel capacity, proportional to the minimum value between the number of BS antennas and the number of antennas at mobile stations, through multi-user multiplexing schemes [11];
- System performance is improved due to the fact that multiple users can communicate over the same spectrum;
- Spatial multiplexing gain at the BS even to single antenna receivers, allowing the arrangement of cheap and small terminals, keeping the more complicated logistics and higher performance costs in the infrastructures side;
- Communications are less affected by channel rank loss, line-of-sight propagation or antenna correlation. Although the aforementioned aspect is increased for each user's diversity, it can be avoided if multi-user diversity is extracted by the scheduler instead [12].

Nonetheless, the spatial sharing of the channel by the users results in strong co-channel interference (CCI). Handle CCI and keeping a good performance/complexity tradeoff is one of the main pursuits in MU-MIMO schemes, and generally involves the precoding of the signal, at the base station, before transmitting it. This is particularly challenging because while the base

station can manage transmissions from all of its antennas, the receivers are incapable to do so, since users are normally incapable to coordinate their channel information among them. Therefore, the base station must know the CSI perfectly in comparison with regular MIMO schemes, as precoding benefits from a precise CSI estimation. CCI can be canceled by using space-division multiple access (SDMA) schemes. One initial strategy was dirty paper coding (DPC) technique [13], that proves that the sum capacity in a multi-user downlink, or broadcast, channel is equal to the maximum aggregation of all users' data rates and full multiplexing gain can be achieved. However, DPC is impracticable in real world systems because the high computational complexity involved in coding and decoding schemes [14].

Under the assumption that the base station has an array of transmitting antennas but all users are single-antenna terminals, two low-complexity precoding schemes can be employed to eliminate CCI: Zero-Forcing (ZF) and MMSE. In this case, the receiver considers as interference all external signals and cancels them via precoding. For multiple receiving antennas, block diagonalization (BD) can be used to avoid the usage of DPC method. BD technique will be discussed in Chapter 3.

Precoding schemes such as ZF, MMSE and BD are some alternatives to DPC [15]–[18]. The basis of the abovementioned schemes relies on the surplus of degrees of freedom provided by the excess antennas at the BS, relatively to the users', to eliminate CCI.

Coordinated beamforming can be also employed to cancel CCI [19], [20]. When there are more users than transmit antennas at the base station, SDMA schemes can achieve full multiplexing gains with transmit beamforming. In larger systems, when the number of users greatly exceeds the number of transmit antennas, low-complexity schemes such as zero-forcing beamforming (ZFBF) [21], [22] or zero-forcing dirty-paper coding (ZF-DPC) [23] were proposed to achieve the optimal growth rate of the sum-capacity function [24].

2.2 Going from MIMO to Massive MIMO

With the upsurge of technology, cellphones, computers or tablets are not only the mainly devices that require wireless internet connection. Innumerous gadgets are being improved every day with wireless capabilities to adapt to the needs and habits of world's population in general. Home equipment, wearables, machinery, remote metering and many other once internet-incapable devices are resurging with more advanced technology, and mostly, require wireless transmissions of data. Plus, internet is becoming more dependable for communication, work or any other indispensable purpose. This leads to a new improved generation of cellular networks: the 5G.

2.2.1 Motivation/Requirements

To keep up with this demand, new requirements for mobile traffic need to be achieved, such as [25]:

- Traffic volume – Between the first quarter of 2015 and the first quarter of 2016, data traffic grew 60%. The high volume of traffic data is driven by the increased smartphones subscriptions and high demand for video contents. Total mobile data traffic is expected to rise at a compound annual growth rate (CAGR) of around 45%, resulting in a ten-fold increase in total traffic for all devices by 2021, reaching 52 ExaBytes per month [26] (Figure 2.6).

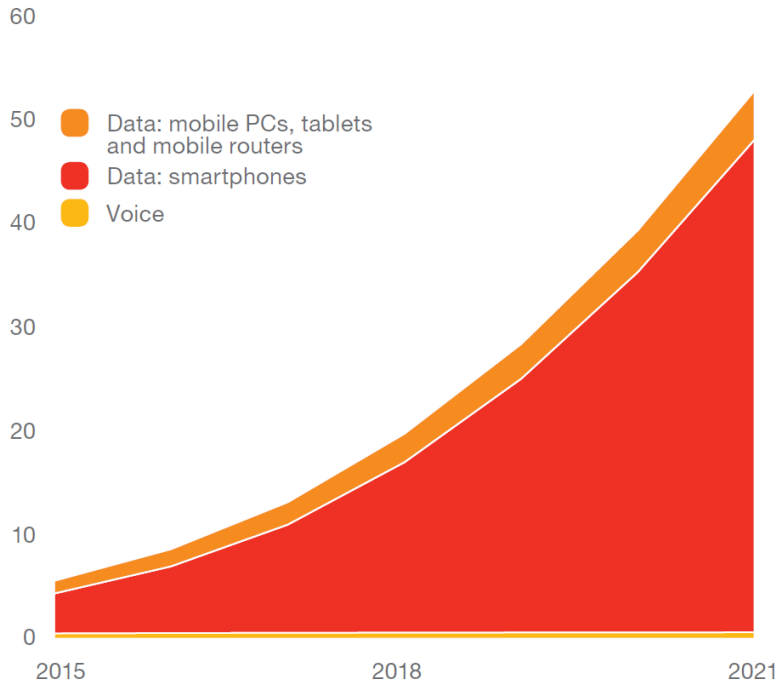

Figure 2.6 - Global Mobile Traffic (monthly ExaBytes); *source:* [26]

- Indoor or hotspot traffic – Currently, mobile traffic is mostly common indoor with 60% voice and 70% data traffic. It is anticipated in the future to approach around 90%. Picocells or femtocells are good candidates to achieve higher capacity depending on the environment, quality and type of communication service, although the deployment of femtocells is proved to be more efficient in indoor environments than picocells as it achieves the highest in-building capacity [27].

- Number of connected devices – Internet of Things (IoT) devices are expected to increase at a compounded annual growth rate (CAGR) of 23% from 2015 to 2021. In total, about 28 billion connected devices are forecasted by 2021, of which around 8.6 billion will be mobile subscriptions (Figure 2.7).

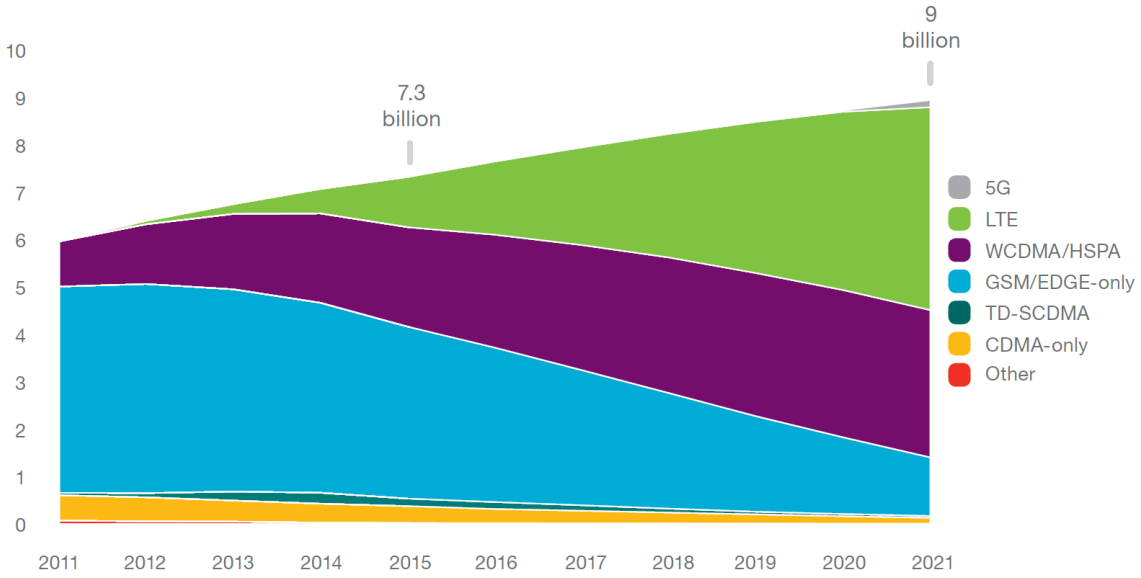

Figure 2.7 - Mobile Subscriptions by Technology (billion); *source:* [26]

- Energy consumption – An essential requirement is to deliver high network energy performance in order to follow up the required traffic volume forecasted, to reduce the total cost of ownership (TCO) and to ease the access of network connectivity in remote areas. In a classic long term evolution (LTE) network, more than 90% of energy consumption of total traffic usage is for the network to be detectable and accessible, regardless the traffic load volume, as shown in Figure 2.8.

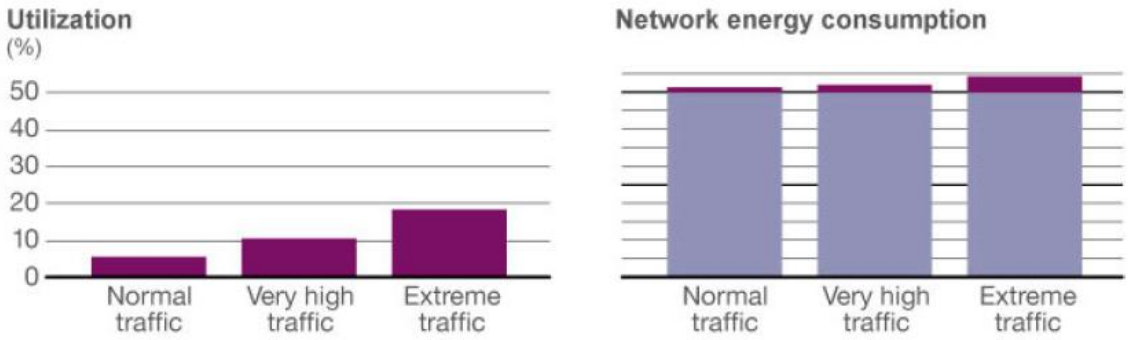

Figure 2.8 - Utilization and corresponding network energy consumption for different traffic loads; *source:* [28]

Energy performance is equally important as high traffic capacity and data rates, even when no data is being transmitted or processed. Considering this, some technologies are being conceived involving ultra-lean designs, advanced beamforming techniques, separation of user-data and system-control on radio interface, virtualized network functionality and cloud technologies [28].

2.2.2 Innovations

In order to achieve the previous requirements, wireless network technologies have to be improved and for that purpose some revolutionary features are under development such as Millimeter Wave (mmWave) communications and Massive MIMO systems. The main objective of MmWave communications is to reach an unexplored range of higher frequencies of the spectrum and Massive MIMO is to expand the antenna arrays to a whole new level.

2.2.2.1 Millimeter Waves Communications

Radio frequencies (RF) are used on almost all commercial communications in a narrow band between 300 MHz and 3 GHz. Therefore, its spectrum is increasingly scarce and getting access to it becomes a harder task as time goes by. Current efforts are only based on reusing and sharing the spectrum and do not achieve the upcoming requirements [29]. The only way to achieve large amounts of new bandwidth is to use higher frequencies, somewhere between the 3 GHz and 300GHz, where the millimeter wave (mmWave) spectrum is less crowded and much greater bandwidths are available. However, not all spectrum can be used since in some frequency ranges oxygen molecules and water vapor absorb electromagnetic energy (57 GHz – 64 GHz and 164 GHz – 200 GHz, respectively), as shown in Figure 2.9. Excluding these frequencies, mmWave communications could achieve around 100GHz of new bandwidth, 200 times more than the currently allocated spectrum, below 3 GHz [30].

In terms of free space loss, there is no difference by using different frequencies for the same antenna aperture. Furthermore, higher frequency means shorter wavelengths which lead to a higher density of antennas in mobile devices and infrastructures and it also improves non-line-of-sight communications, contrarily to current MIMO systems.

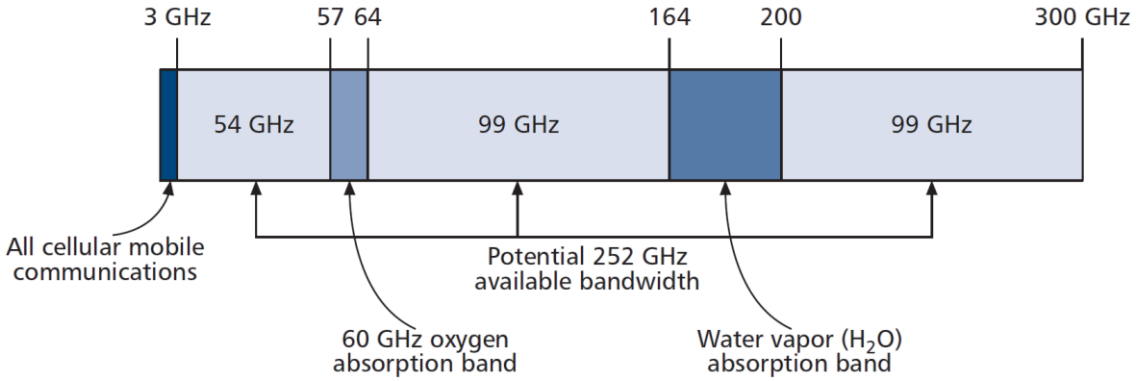

Figure 2.9 - Millimeter-wave spectrum; *source:* [30]

Figure 2.10 depicts a data rate comparison in terms of mean and 5% outage rates. Results are given in terms of gain with regards to the MIMO baseline. It is clear that millimeter wave systems could lead to unmatched data rates and revolutionary user experience as a potentially innovative technology for 5G.

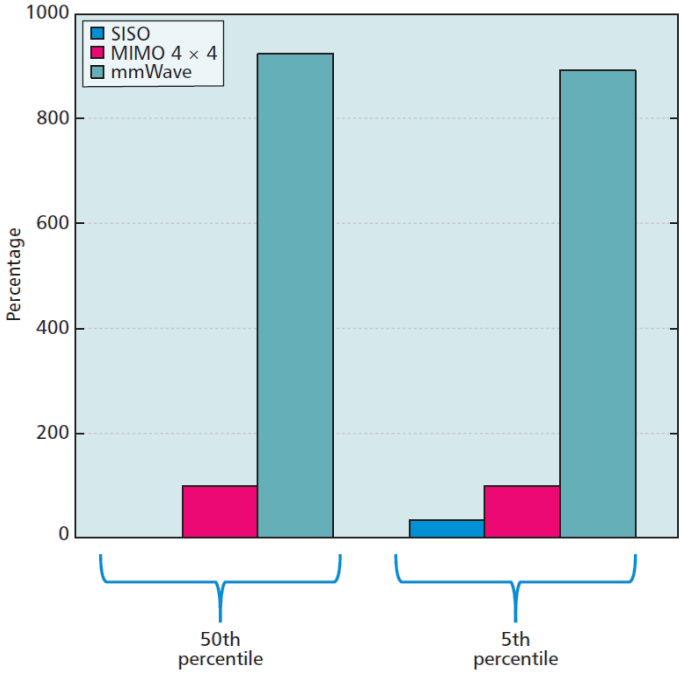

Figure 2.10 - Data rate comparison between microwave systems using 50 MHz of bandwidth (SISO and SU-MIMO) and a single user mmWave system with 500 MHz of bandwidth; *source:* [31]

On the other hand, the wave's frequency is inversely proportional to penetration capability. The analysis of [32] and [33] concludes that millimeter wave signals are highly attenuated by commonly solid materials such as concrete or brick walls, about 10 times more at 40 GHz than radio wave frequencies below 3 GHz. A solution to this problem involves the placement of mmWave femtocells inside buildings for indoor coverage.

Another two problems are the difficult propagation of mmWave transmissions through foliage and the signal scattering in raindrops. For the first case, an empirical relationship has been developed [34], that predicts the foliage loss in a range of frequencies between 200-95000 MHz in foliage depths lesser than 400 meters. As an example, at 40 GHz, a signal penetrating a large tree, around 10 meters, is about 19 dB. For the second case, raindrops have approximately the same size as the radio wavelengths, causing the scattering of the radio signal. For example, at 50 GHz, with a rain rate of 25mm/h, there is a 10db/km attenuation of the signal, as shown [34].

Low-cost, small dimension antenna designs are already being developed to be integrated with high frequencies front ends [35].

2.2.2.2 Massive MIMO

The primary idea behind massive MIMO systems is to massively scale up MU-MIMO systems, by deploying a huge number of antennas in transmitters/receivers, in the order of hundreds or more. In massive MIMO systems, the number of antennas in base stations excessively surpass the number of active users. Moreover, the base station serves all active users, simultaneously, in the same time-frequency resource.

In communications systems with few antennas, signal strength can be momentarily very low due to fading. This happens when scattered signals reach the receiver and the combined waves interfere destructively with each other and the only solution is to wait until the channel has changed enough so the data can be properly received. This delay in reception is called latency. However, as the law of large numbers predicts, if the number of scattered signals is largely increased and the number of antennas is increased as well, it will be more likely that the received signal will be closer to the expected, so fading no longer limits latency. Another result of the large number of antennas is shown in [1] where using a number of base station antennas that greatly exceeds the number of active users linear processing is nearly optimal (with single-antenna users). Additionally, by using maximum-ratio combining (MRC) or maximum-ratio transmission (MRT) in uplink or downlink, respectively, the effects of uncorrelated noise and intracell interference tend to disappear because, as the law of large numbers implies, the channel matrix for a desired user tends to be more orthogonal to an interfering user channel matrix, rendering simple spatial multiplexing procedures with optimal results. Massive MIMO also provides a large excess of degrees of freedom, which can be exploited to provide extremely cheap and power efficient RF amplifiers [36], [37].

Massive MIMO offers a high level of energy efficiency, in comparison to former wireless systems, as it can be seen in Figure 2.11. In downlink, the base station applies beamforming, which is enhanced with the increased number of antennas, resulting in a more spatially accurate transmission while reducing the radiated power. Furthermore, doubling the number of antennas at base station, the transmit power can be reduced by 3 dB, keeping the same overall performance, in optimal conditions of propagation and processing. In uplink, coherent beamforming achieves a higher array again, allowing a reduced transmit power of each user, favoring all mobile devices [38].

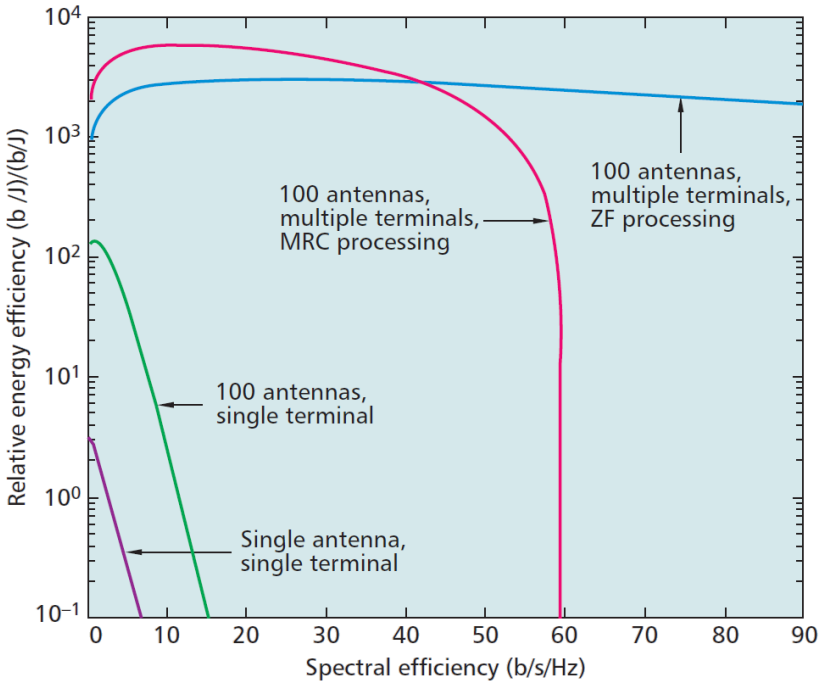

Figure 2.11 - Spectral efficiency vs. Energy efficiency in SISO, MISO and Massive MIMO systems with different processing methods; *source:* [39]

In practice, deploying very large arrays is a spatially dimensional problem. Since antennas have to be distributed half-wavelength apart, 100 antennas can occupy almost one meter of space. Though, mmWave technology eases this problem since the resort to higher frequencies allows much smaller dimension antennas designs [40]. Furthermore, architectural issues of using larger arrays were already proposed in [41]–[45].

Massive MIMO relies on favorable propagation environments. Favorable propagation occurs when the downlink channel responses to different users are uncorrelated. This can happen when channel vectors become pairwise orthogonal or there is a complex scattering environment. In [46] a series of channel measurements is performed and analyzed for various practical massive MIMO conditions in real propagation environments, concluding that the advantages of this system can also be obtained in real channels. Figure 2.12 shows the capacity achieved in a downlink system with 16 users, when the users are far apart and closely located.

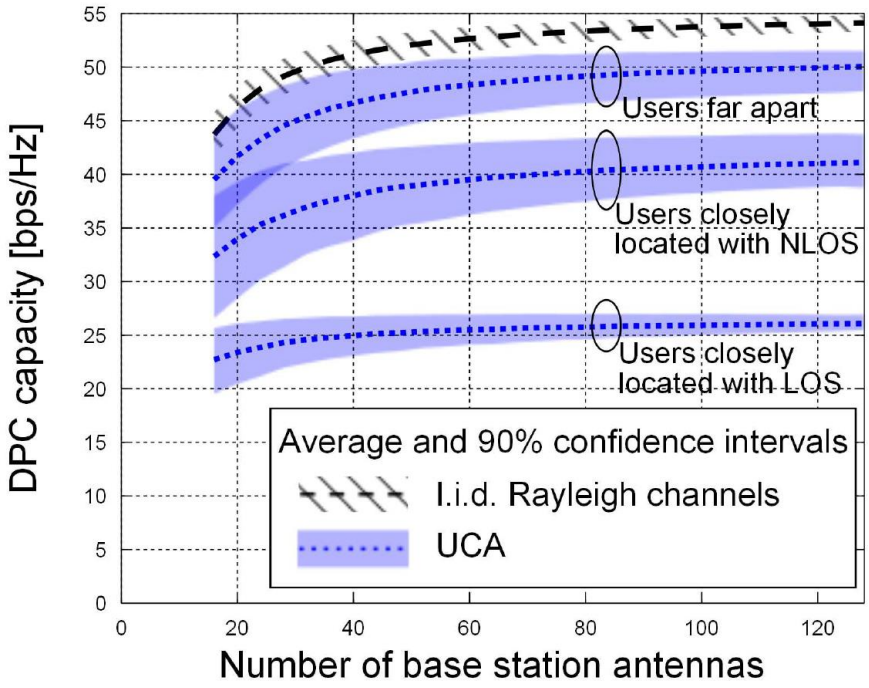

Figure 2.12 - Downlink sum-rate capacity with DPC, for 16 users in different user inter-location scenarios; *source:* [46]

2.2.3 Channel Estimation in Massive MIMO

Massive MIMO relies on spatial multiplexing, and for that reason the base station needs a precise channel knowledge. In uplink, users send training sequences and the base station estimates the channel responses of each user. For downlink, acquiring accurately the respective channel responses for every terminal can be more complicated, because the base station needs to know the forward channel beforehand. In time division duplex (TDD) architectures, it is assumed to have channel reciprocity, i.e., the reverse and forward channel are assumed to be identical in a certain coherence interval and, therefore, the estimated reverse channel responses are used for the next forward transmission. Thus, the channel reciprocity is one main advantage in TDD systems, albeit with some calibration required [47]. On the other hand, frequency division duplex (FDD) architectures require a closed-loop setup. The reverse channel is estimated by the base station with training sequences sent by the users, to alleviate computational requirements and improve battery life capacity of mobile devices. To estimate the forward channel, the base station has to, initially, send training sequences and get a (limited) feedback of the downlink's CSI by the users, since channel reciprocity is impossible in FDD systems. Therefore, the number of training sequences in TDD systems is equal to the number of users and for FDD systems is equal to the number of antennas deployed at base station. In Figure 2.13 is depicted a time slot structure with channel estimation for both FDD and TDD systems.

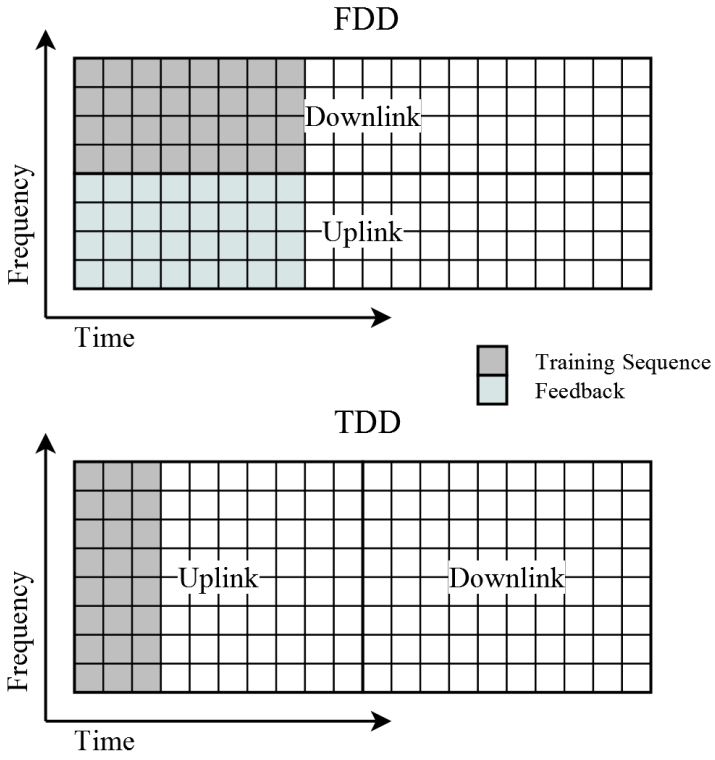

Figure 2.13 –Time slot with channel estimation for FDD and TDD systems

Despite the use of FDD in the current LTE standard, incorporating a FDD strategy is more difficult in massive MIMO systems due to orthogonality issues between antennas and large number of required channel estimations. Downlink pilots must be mutually orthogonal for optimal estimations. To accomplished that, time-frequency resources are spent proportionally to the number of antennas at the base station, which requires hundreds of times more resources in massive MIMO systems than in conventional MIMO. The number of orthogonal training sequences must be smaller than the number of pilots on the training sequences.

Another problem lies in the number of estimations to be done by the terminals in the minimum amount of time. The number of channel responses that have to be estimated by each user is proportional to the number of base station antennas. Therefore, the terminals would have to spent hundreds of times more resources to feedback the base station with the channel responses estimates, which is a critical drawback for mobile devices, and the need to feedback adds latency to transmission. Moreover, the estimated CSI can also be deteriorated by quantization errors due to the limited channel feedback and outdated due to the delay between the moment the estimation was performed and its implementation at base station. In the work of [48] the case of non-ideal CSI is analyzed at base stations and specifically the trade-off between the advantage of large number of antennas and the cost of estimating large channel vectors, in FDD systems.

Once again, scaling up large antennas arrays brings two new problems that were not previously taken into account. Alternatives to solve these problems involve the system to operate in TDD mode and rely on channel reciprocity, which is the general approach adopted in massive

MIMO systems, since the required pilot resources are independent of the number of base station antennas, or FDD schemes that require a considerably reduced CSI accuracy [49].

2.2.3.1 Pilot Contamination

Since massive MIMO is supposed to be a practical cellular network, it is distributed along multiple cells, as a multicell system. For channel estimation, every terminal has a correspondent training sequence to eliminate intra-cell interference. Additionally, channel estimation must be performed during each coherence interval, and for that reason, the number of mutually orthogonal training sequences must be smaller than the number of elements in each coherence interval. So, depending on the number of coherent time-frequency elements, the training sequences must be reused in other cells. Due to this limitation, pilot contamination may happen. A signal suffers from pilot contamination, when a receiver gets the same pilot sequence from different sources of different cells resulting in an incorrect channel estimate (Figure 2.14). Therefore, pilot contamination limits the performance of non-cooperative MU-MIMO systems [1].

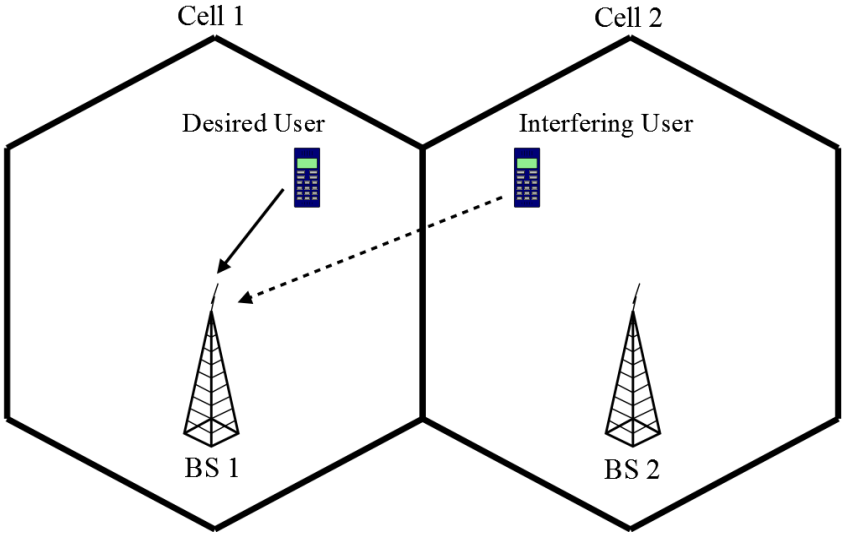

Figure 2.14 - Pilot contamination example when both users transmit mutually non-orthogonal training sequences

As the base station estimates inaccurately the desired channel responses, the precoding performed on the transmitted signal is also incorrect. The erroneous precoding decreases significantly the signal-to-interference-plus-noise ratio (SINR) of the whole transmission. Since the base station performs beamforming, in a MRT precoding scheme, the signal power is misplaced due to the estimated channel values, i.e., the desired user receives a less powered signal, and the power lost is redirected as interference to the undesired users with the same training sequence.

As the number of transmit antennas and users increases, the coherence interval may not be long enough to allow the generation of the necessary amount of training sequences to serve all

active users. In practice, to allow data transmission with good spectral efficiency as well, the number of terminals has to be significantly smaller than the number of symbols in the coherence interval. Thus, pilot contamination becomes a major problem in a massive MIMO scenario. As concluded in [50], it causes the saturation of SINR as the number of base station antennas tends to infinity. Figure 2.15 shows that as the path-loss gain (ratio between the path-loss coefficients for the channels of desired user and interfering user) increases, the saturation value of SINR also increases.

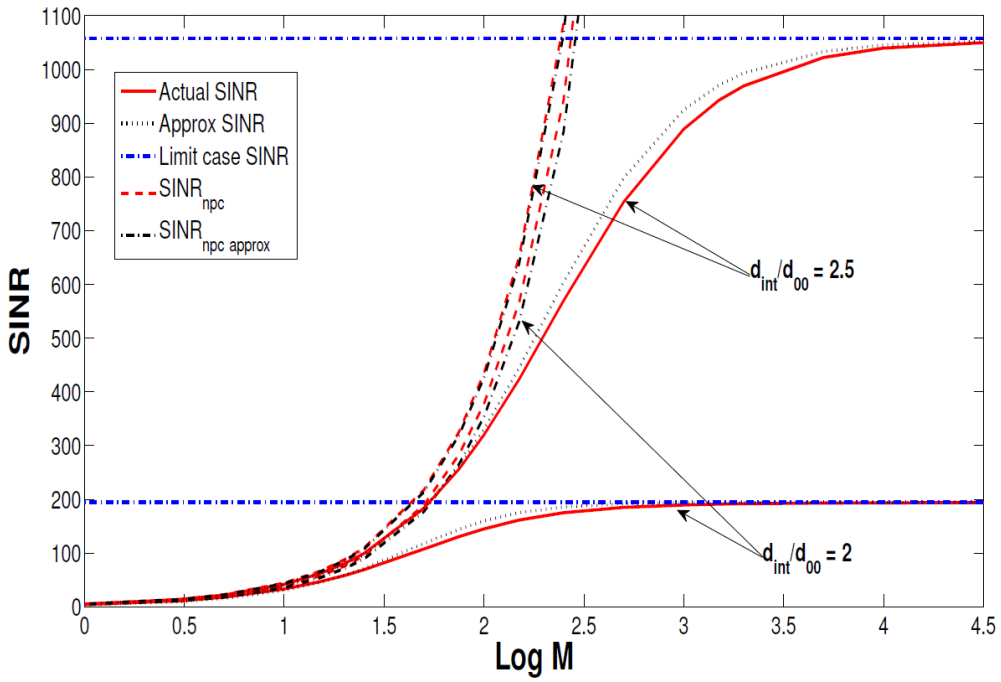

Figure 2.15 - Variation of SINR and its approximation for different path-loss gains (2 and 2,5) at 10dB interference-free SNR; *source:* [50]

Numerous methods for pilot contamination mitigation have already been proposed. In [51] a completely-blind method of pilot decontamination for uplink transmission is proposed, although, by exploiting channel reciprocity in TDD schemes, the same strategy can be applied. [52] employs a pilot contamination precoding (PCP) scheme among multiple cells, addressed to terminals with the same pilot sequence.

Eigenvalue decomposition (EVD) based approaches are also recurrent in channel estimation and mitigation of pilot contamination. Since they are semi-blind techniques, they need a much shorter training sequence, to solve ambiguity difficulties, in comparison to other pilot-based channel estimation techniques. In [53], it is shown that the channel matrix of each user can be estimated from the covariance matrix of the received signals with higher accuracy compared with linear estimation techniques. It also improves the performance by combining an iterative least-square with projection (ILSP) algorithm. An improved EVD channel estimation algorithm is proposed in [54], that eliminates pilot contamination completely. The algorithm is based on the equality between the channel fast fading coefficient matrix and the eigenvector matrix of the

covariance of received training sequence. However, EVD and EEVD techniques are founded on a critical assumption: the number of antennas at base station tends to infinity, and, therefore, performance degradation is expected, by pilot contamination, as the number of antennas is finite. Moreover, eigenvalue decomposition is a nonlinear operation, so, for large matrices, approximation errors and high computational requirements are severe problems to be taken into account. Figure 2.16 presents the MSE between the two abovementioned channel estimation techniques in function of the number of transmit antennas.

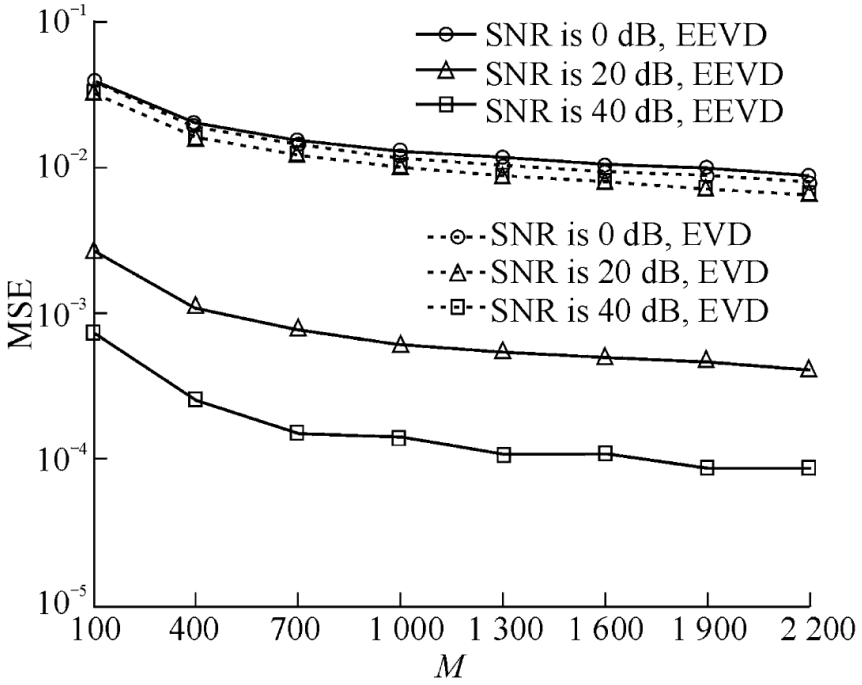

Figure 2.16 - MSE performance between EVD and EEVD channel estimation vs. the number of base station antennas, *M; source:* [54]

The coordination between base stations of different cells is also a strategy applied to reduce pilot contamination. In [55], a time-shifted training sequences method is proposed to avoid simultaneous transmissions from bordering cells, and shows that rate gains can achieve 18 times more than the aligned approach. Allocation of training sequences in multiple cells can also mitigate inter-cell interference. In [56] it is analyzed a training sequence assignment strategy where specific groups of users are assigned with identical training sequences. This latter scheme performs closely to an interference-free channel estimation scenario with reasonable numbers of antennas and users. Figure 2.17 compares the MSE between least square (LS) channel estimation, covariance-aided Bayesian (CB) estimation and coordinated pilot assignment-based (CPA) Bayesian estimation with and without inter-cell interference.

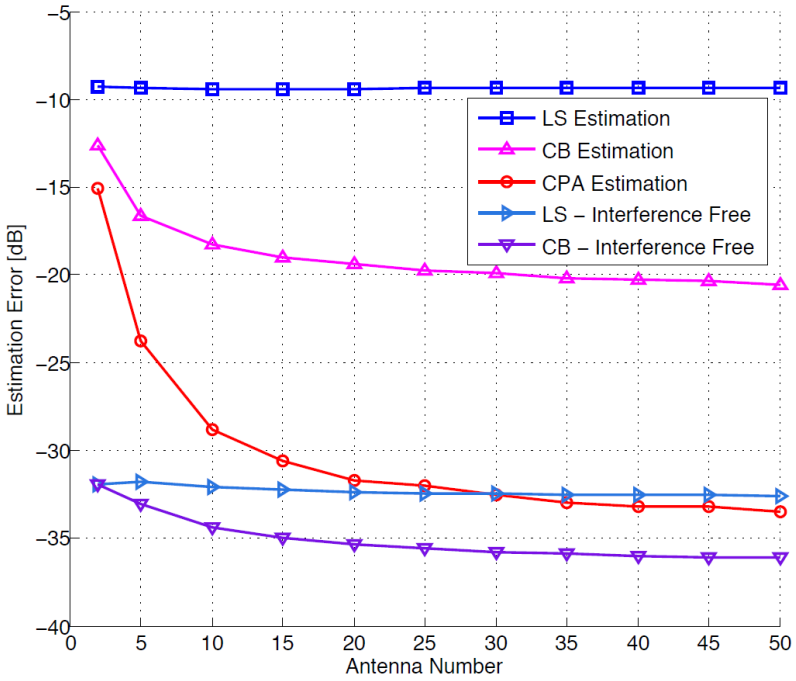

Figure 2.17 - MSE comparison between different estimation techniques and interference free cases, vs. number of base station antennas; *source:* [56]

3. Channel Estimation Techniques

Massive MIMO has shown to be a promising concept in 5G cellular networks. The increased number of antennas at the base station combined with MU-MIMO transmission techniques make massive MIMO more energy-efficient and capable to reach higher spectral efficiency. A major restrictive factor in massive MIMO is the availability of an accurate CSI, since spatial multiplexing can only be achieved if the channel responses are precisely known. For that reason, channel estimation is a main subject to be discussed in wireless communications systems, primarily when the future of the industry probably will involve a large scaling of antenna arrays.

This chapter begins by describing the adopted MU-MIMO downlink system model, followed by an explanation of the BD method, used to cancel CCI, and two low-complexity channel estimators commonly used in nowadays communication systems: LS and MMSE channel estimator. Additionally, it is introduced a channel estimation technique using Zadoff-Chu sequences as pilot signals. These sequences possess ideal periodic autocorrelation properties, which makes them ideal to be considered training sequences. To conclude the chapter, are presented the simulation results that allow a comparison purposes between the different channel estimation techniques. Simulations results will demonstrate how accurate the introduced channel estimation is, in function of the number of users and the number of pilots applied in estimation. BER and MSE are used as performance measurement and comparison purposes. Results are based on Monte Carlo experiments with 15 000 simulations and QPSK modulation. Both BER and MSE results are expressed in function of $\frac{E_b}{N_0}$, where E_b is the transmitted bit energy and where N_0 is the noise power spectral density.

3.1 System Model

The system model adopted is a downlink orthogonal frequency-division multiple access (OFDMA) transmission over a multi-user precoding MIMO system with N_u users, N_R receiving antennas at each mobile station and $N_T = N_u N_R$ transmitting antennas at the base station, resulting in a $N_T \times N_R$ MIMO configuration to each user u, with N subcarriers, through a channel $\boldsymbol{H}_u{}^{DL}$ ($\boldsymbol{H}_u{}^{DL} \epsilon \mathbb{C}^{N_R \times N_T}$), depicted in Figure 3.18.

It is also assumed that the transmitter knows exactly the CSI of all receivers and every user knows their corresponding precoding matrix. For the sake of simplicity, the time index is omitted.

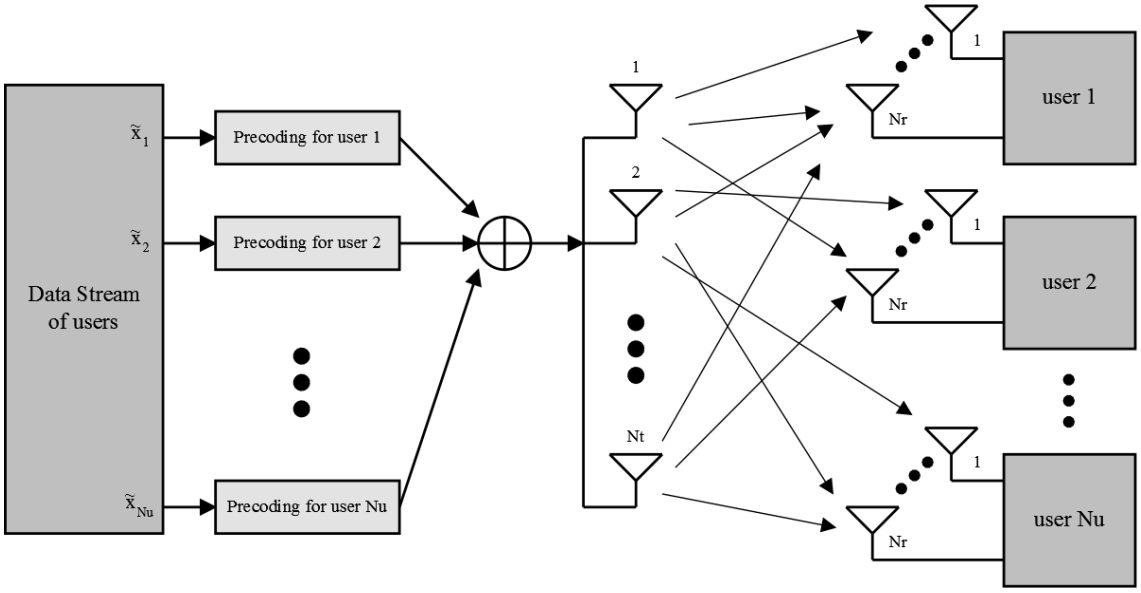

Figure 3.18 - MU-MIMO system model with precoding

The received signal for every user is given by

$$\begin{bmatrix} \boldsymbol{y}_1 \\ \boldsymbol{y}_2 \\ \vdots \\ \boldsymbol{y}_{N_u} \end{bmatrix} = \begin{bmatrix} \boldsymbol{H}_1{}^{DL} \\ \boldsymbol{H}_2{}^{DL} \\ \vdots \\ \boldsymbol{H}_{N_u}{}^{DL} \end{bmatrix} \boldsymbol{X} + \begin{bmatrix} \boldsymbol{z}_1 \\ \boldsymbol{z}_2 \\ \vdots \\ \boldsymbol{z}_{N_u} \end{bmatrix}, \tag{1}$$

or simply by

$$\boldsymbol{Y}_{BC} = \boldsymbol{H}^{DL}\boldsymbol{X} + \boldsymbol{Z}, \tag{2}$$

where $\boldsymbol{y}_u$ ($\boldsymbol{y}_u \epsilon \mathbb{C}^{N_R}$) is the received signal at the u-th user ($u = 1,2,\dots,N_u$), $\boldsymbol{X}$ ($\boldsymbol{X}\epsilon\mathbb{C}^{N_T}$) is the transmitted signal by the BS, and $\boldsymbol{z}_u$ ($\boldsymbol{z}_u\epsilon\mathbb{C}^{N_R}$) is the array relative to additive white gaussian noise (AWGN) with zero mean and variance ${\sigma_z}^2 = \frac{N_0}{2}$.

The channel matrix $\boldsymbol{H}_u{}^{DL}$ contains all SISO channel impulse responses from each BS transmitting antenna to each receiving antenna of a single user. The elements of $\boldsymbol{H}_u{}^{DL}$ are samples of independent and identically distributed (i.i.d.) complex Gaussian process, given by

$$\boldsymbol{H}_u{}^{DL} = \begin{bmatrix} h_{1,1} & \dots & h_{1,N_T} \\ \vdots & \ddots & \vdots \\ h_{N_R,1} & \dots & h_{N_R,N_T} \end{bmatrix}. \tag{3}$$

The signal received by a single user is given by

$$\boldsymbol{y}_u = \begin{bmatrix} y_1 \\ y_2 \\ \vdots \\ y_{N_R} \end{bmatrix} = \begin{bmatrix} h_{1,1} & \dots & h_{1,N_T} \\ \vdots & \ddots & \vdots \\ h_{N_R,1} & \dots & h_{N_R,N_T} \end{bmatrix} \begin{bmatrix} x_1 \\ x_2 \\ \vdots \\ x_{N_T} \end{bmatrix} + \boldsymbol{z}_u, \tag{4}$$

and, therefore, each antenna receives the signal

$$y_k = h_{k,1}x_1 + h_{k,2}x_2 + \cdots + h_{k,N_T}x_{N_T} + z_k, \qquad k = 1,2,\dots,N_u,$$

which means that each receiving antenna is subjected to CCI.

3.1.1 Channel Model

The channel considered is a frequency-nonselective or frequency flat fading channel given by [57]:

$$h_{nr,nt}(t) = \alpha(t)e^{j\theta(t)}\,, \qquad \forall nr, nt\,, \tag{5}$$

where $\alpha(t)$ denotes the envelope and $\theta(t)$ represents the phase of the equivalent channel response. This means the coherence bandwidth, B_{coh}, is larger than the signal bandwidth, B_S i.e.,

$$B_S \ll B_{coh}\,. \tag{6}$$

Hence, all frequencies of the transmitted signal experience equal gain and linear phases during the duration of a OFDM symbol. Then, the channel has a time-varying multiplicative effect on the transmitted signal.

3.1.2 Pilot Structure

There are three different types of pilots' structures that can be adopted: block type, comb type, and lattice type [58]. In the model adopted here, the pilots are arranged in a comb type format, as shown in Figure 3.19. Comb type pilot arrangement are regularly used for fast-fading channel characteristics, but not for frequency-selective channels [59], [60].

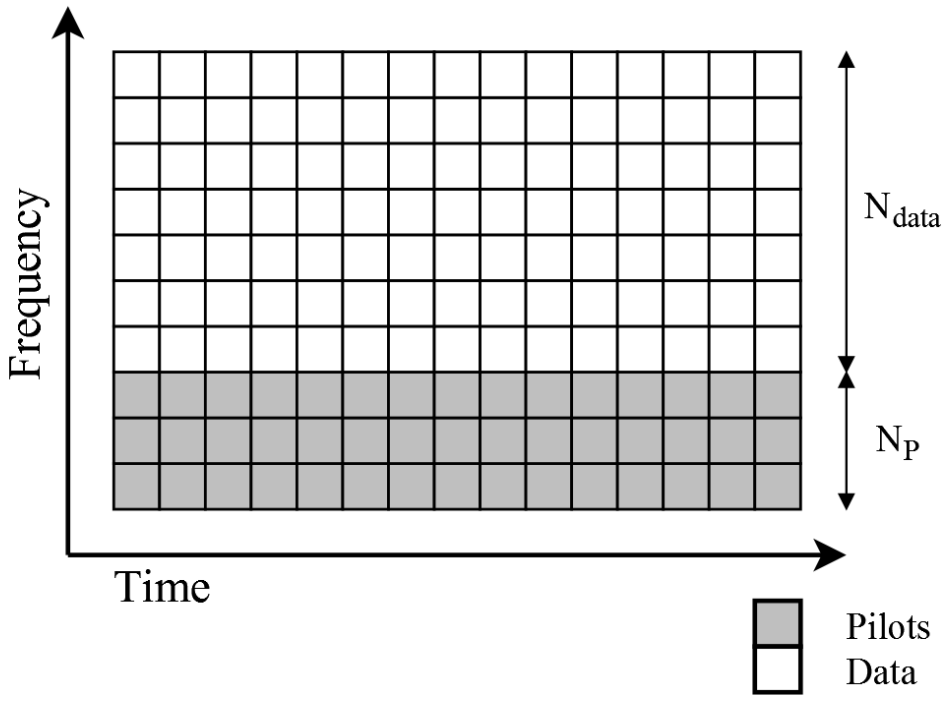

Figure 3.19 - Comb-type pilot structure

The training sequences are inserted in the first N_P subcarriers of every symbol and are used to estimate the channel responses along the frequency axis. Since the transmission is

frequency-flat over each symbol, the estimates are used in equalization for the next N_{data} subcarriers ($N_{data} = N - N_P$).

3.2 Block Diagonalization

In MU-MIMO systems with single-antenna users, precoding methods based on channel inversion are used to eliminate interference between antennas. However, in MU-MIMO systems, precoding eliminates the interference across different users but not between different antennas. So the sum capacity of the system can be increased with diversity. In these scenarios, BD is a common technique used in linear precoding schemes. This method is a generalization of channel inversion and resorts to a non-linear process called singular value decomposition (SVD). After performing BD, any signal detection method can be applied to eliminate inter-antenna interference.

In BD, each user is associated to a precoding matrix. The precoding matrix is generated in a way that the base station transmits the signal to the user through the null space of all other interfering users. Overall, the aggregated MU-MIMO channel matrix of all users is decomposed into multiple, parallel, independent SU-MIMO sub-channels corresponding to each user. However, the non-linearity process forces channel estimation to be more accurate than in a standard MIMO system.

The precoded signal for the u-th user can be written as:

$$\boldsymbol{x}_u = \boldsymbol{W}_u \tilde{\boldsymbol{x}}_u \,, \qquad u = 1, 2, \dots, N_u \,, \tag{7}$$

where $\boldsymbol{x}_u$ ($\boldsymbol{x}_u \epsilon \mathbb{C}^{N_T}$) is the coded array of transmitting symbols, $\boldsymbol{W}_u$ ($\boldsymbol{W}_u \epsilon \mathbb{C}^{N_T \times N_R}$) the precoding matrix and $\tilde{\boldsymbol{x}}_u$ ($\tilde{\boldsymbol{x}}_u \epsilon \mathbb{C}^{N_R}$) is the vector with N_R parallel data symbols concerning the user u. The signal that each user u receives can be expressed as:

$$\boldsymbol{y}_u = \boldsymbol{H}_u{}^{DL} \sum_{k=1}^{N_u} \boldsymbol{W}_k \tilde{\boldsymbol{x}}_k + \boldsymbol{z}_u \,, \qquad u = 1, 2, \dots, N_u \,. \tag{8}$$

The same equation can be rearranged as

$$\boldsymbol{y}_u = \boldsymbol{H}_u{}^{DL} \boldsymbol{W}_u \tilde{\boldsymbol{x}}_u + \sum_{k=1, k \neq u}^{N_u} \boldsymbol{H}_u{}^{DL} \boldsymbol{W}_k \tilde{\boldsymbol{x}}_k + \boldsymbol{z}_u \,, \qquad u = 1, 2, \dots, N_u \,, \tag{9}$$

where $\boldsymbol{H}_u{}^{DL} \boldsymbol{W}_k$ is an effective channel matrix for the u-th user receiver and the k-th user transmit signal ($u, k = 1,2, \dots, N_u$). In matrix format, the received signals are represented as:

$$\begin{bmatrix} \boldsymbol{y}_1 \\ \boldsymbol{y}_2 \\ \vdots \\ \boldsymbol{y}_{N_u} \end{bmatrix} = \begin{bmatrix} \boldsymbol{H}_1{}^{DL} \boldsymbol{W}_1 & \boldsymbol{H}_1{}^{DL} \boldsymbol{W}_2 & \dots & \boldsymbol{H}_1{}^{DL} \boldsymbol{W}_{N_u} \\ \boldsymbol{H}_2{}^{DL} \boldsymbol{W}_1 & \boldsymbol{H}_2{}^{DL} \boldsymbol{W}_2 & \dots & \boldsymbol{H}_2{}^{DL} \boldsymbol{W}_{N_u} \\ \vdots & \vdots & \ddots & \\ \boldsymbol{H}_{N_u}{}^{DL} \boldsymbol{W}_1 & \boldsymbol{H}_{N_u}{}^{DL} \boldsymbol{W}_2 & & \boldsymbol{H}_{N_u}{}^{DL} \boldsymbol{W}_{N_u} \end{bmatrix} \begin{bmatrix} \tilde{\boldsymbol{x}}_1 \\ \tilde{\boldsymbol{x}}_2 \\ \vdots \\ \tilde{\boldsymbol{x}}_{N_u} \end{bmatrix} + \begin{bmatrix} \boldsymbol{z}_1 \\ \boldsymbol{z}_2 \\ \vdots \\ \boldsymbol{z}_{N_u} \end{bmatrix}, \tag{10}$$

when $\boldsymbol{H}_u{}^{DL}\boldsymbol{W}_k \neq 0_{N_R\times N_R}, \forall\, u \neq k$ there is CCI, where $0_{N_R\times N_R}$ is a zero matrix. From (10) it can be seen that CCI-free transmission is guaranteed as long as the effective channel matrix is block-diagonalized, to ensure that

$$\boldsymbol{H}_u{}^{DL}\boldsymbol{W}_k = 0_{N_R\times N_R}, \forall\, u \neq k\,. \tag{11}$$

Let denote $\widetilde{\boldsymbol{H}}_u{}^{DL}$ ($\widetilde{\boldsymbol{H}}_u{}^{DL}\mathbb{C}^{N_R(N_u-1)\times N_T}$) as the congregate interfering channel matrix that contains the channel responses of all users except the u-th user

$$\widetilde{\boldsymbol{H}}_u{}^{DL} = \left[\left(H_1{}^{DL}\right)^H \ \ldots\ \left(H_{u-1}{}^{DL}\right)^H \left(H_{u+1}{}^{DL}\right)^H \ \ldots\ \left(H_k{}^{DL}\right)^H\right]^H, \tag{12}$$

where $(\bullet)^H$ denotes the complex-conjugate transpose operation, or Hermitian transpose. Thus, since $N_T = N_R N_u$, (11) is equivalent to

$$\widetilde{\boldsymbol{H}}_u{}^{DL}\boldsymbol{W}_u = 0_{(N_T-N_R)\times N_R}\,, \qquad u = 1, 2, \ldots, N_u\,. \tag{13}$$

Therefore, results a CCI-free transmission:

$$\boldsymbol{y}_u = \boldsymbol{H}_u{}^{DL}\boldsymbol{W}_u\widetilde{\boldsymbol{x}}_u + \boldsymbol{z}_u. \tag{14}$$

which corresponds in matrix format to

$$\begin{bmatrix}\boldsymbol{y}_1\\ \boldsymbol{y}_2\\ \vdots\\ \boldsymbol{y}_{N_u}\end{bmatrix} = \begin{bmatrix}\boldsymbol{H}_1{}^{DL}\boldsymbol{W}_1 & 0 & \ldots & 0\\ 0 & \boldsymbol{H}_2{}^{DL}\boldsymbol{W}_2 & \ldots & 0\\ \vdots & \vdots & \ddots & \\ 0 & 0 & & \boldsymbol{H}_{N_u}{}^{DL}\boldsymbol{W}_{N_u}\end{bmatrix}\begin{bmatrix}\widetilde{\boldsymbol{x}}_1\\ \widetilde{\boldsymbol{x}}_2\\ \vdots\\ \widetilde{\boldsymbol{x}}_{N_u}\end{bmatrix} + \begin{bmatrix}\boldsymbol{z}_1\\ \boldsymbol{z}_2\\ \vdots\\ \boldsymbol{z}_{N_u}\end{bmatrix}. \tag{15}$$

The interference can be cancelled using the diagonalization process called SVD [61], [62]. To obtain the precoding matrix $\boldsymbol{W}_u$ which satisfies the condition of (13). It is possible to separate $\widetilde{\boldsymbol{H}}_u{}^{DL}$ into a product of three matrices.

$$\widetilde{\boldsymbol{H}}_u{}^{DL} = \widetilde{\boldsymbol{U}}_u\widetilde{\boldsymbol{\Lambda}}_u\widetilde{\boldsymbol{V}}_u{}^H, \tag{16}$$

where $\widetilde{\boldsymbol{U}}_u$ ($\widetilde{\boldsymbol{U}}_u \in\mathbb{C}^{N_R(N_u-1)\times N_R(N_u-1)}$) and $\widetilde{\boldsymbol{V}}_u$ ($\widetilde{\boldsymbol{V}}_u \in\mathbb{C}^{N_T\times N_T}$) are orthogonal matrices and $\widetilde{\boldsymbol{\Lambda}}_u$ ($\widetilde{\boldsymbol{\Lambda}}_u\in\mathbb{C}^{N_R(N_u-1)\times N_T}$) is a diagonal matrix containing the square roots of eigenvalues from $\widetilde{\boldsymbol{U}}_u$ or $\widetilde{\boldsymbol{V}}_u$. Since $\widetilde{\boldsymbol{\Lambda}}_u$ will not be a square matrix, there will be empty columns. In that case, $\widetilde{\boldsymbol{V}}_u$ can be represented as

$$\widetilde{\boldsymbol{V}}_u{}^H = \left[\widetilde{\boldsymbol{V}}_u{}^{NZ}\,\widetilde{\boldsymbol{V}}_u{}^{Z}\right]^H, \tag{17}$$

where $\widetilde{\boldsymbol{V}}_u{}^{Z}$ are the last orthonormal eigenvectors, or singular vectors, corresponding to the zero singular values of $\widetilde{\boldsymbol{\Lambda}}_u$ and $\widetilde{\boldsymbol{V}}_u{}^{NZ}$ to the non-zero singular values. Thus, $\widetilde{\boldsymbol{V}}_u{}^{Z}$ is an orthogonal basis for the null space of $\widetilde{\boldsymbol{H}}_u{}^{DL}$, since we may write

$$\begin{aligned}\widetilde{\boldsymbol{H}}_u^{\,DL}\widetilde{\boldsymbol{V}}_u^{\,Z} &= \widetilde{\boldsymbol{U}}_u\left[\widetilde{\boldsymbol{\Lambda}}_u^{\,NZ} \quad 0\right]\begin{bmatrix}\left(\widetilde{\boldsymbol{V}}_u^{\,NZ}\right)^H\\ \left(\widetilde{\boldsymbol{V}}_u^{\,Z}\right)^H\end{bmatrix}\widetilde{\boldsymbol{V}}_u^{\,Z}\\ &= \widetilde{\boldsymbol{U}}_u\widetilde{\boldsymbol{\Lambda}}_u^{\,NZ}\left(\widetilde{\boldsymbol{V}}_u^{\,NZ}\right)^H\widetilde{\boldsymbol{V}}_u^{\,Z}\\ &= \widetilde{\boldsymbol{U}}_u\widetilde{\boldsymbol{\Lambda}}_u^{\,NZ}0\\ &= 0\,,\end{aligned} \tag{18}$$

which means that when the signal is transmitted in the direction of $\widetilde{\boldsymbol{V}}_u^{\,Z}$, every interfering user will not receive any signal. Therefore, $\widetilde{\boldsymbol{V}}_u^{\,Z}$ will be the precoding matrix for user u, given by

$$\boldsymbol{W}_u = \widetilde{\boldsymbol{V}}_u^{\,Z}\,. \tag{19}$$

Figure 3.20 shows the effectiveness of BD method in eliminating CCI. When compared to a CCI-absent transmission scheme in the same conditions.

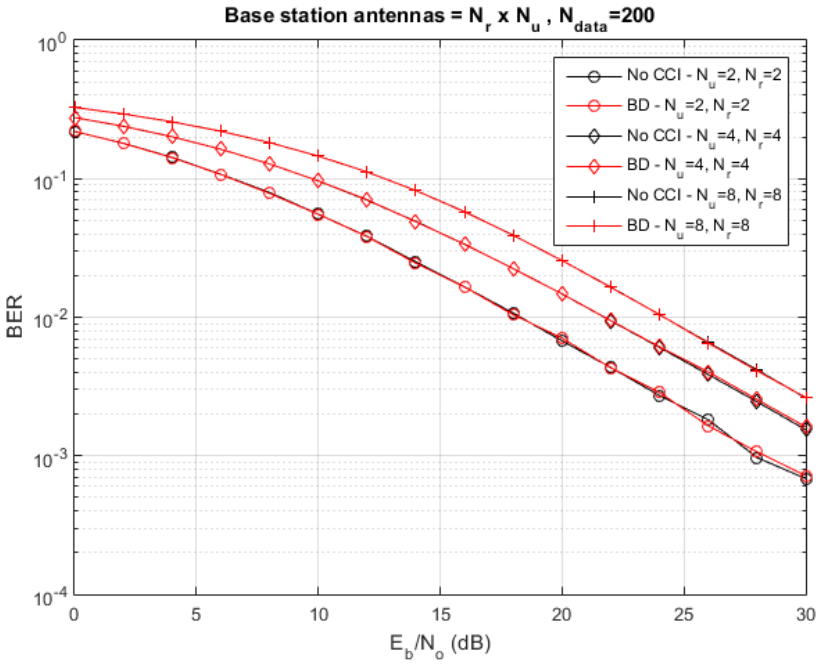

Figure 3.20 - BER plot for different numbers of users and receive antennas

With perfect CSI knowledge at the mobile stations, the BD method can satisfactorily eliminate CCI in a multiple-antenna users' scenario. Due to the lower complexity when compared with the DPC, the BD will be the adopted precoding scheme in the following simulations of this chapter. N_{data} value will be kept equal to 200 as well.

3.3 One Dimension Channel Estimators

LS channel estimator and MMSE channel estimator are two basic, pilot-based channel estimation techniques. These estimators are categorized as one dimension (1D) estimators, this means that the channel estimation is done by resorting to training sequences, of length N_P, in one dimension, either in frequency or time domain. Due to their simplicity they are widely used for pilot-based channel estimation [54], [58-60].

3.3.1 Least-Squares Channel Estimation

The LS channel estimator minimizes the squared error quantity between the received signal and the estimated one and may be described as

$$\widehat{\boldsymbol{h}}^{LS} = \arg\min_{\widetilde{\boldsymbol{h}}^{LS}} \left\| \boldsymbol{y} - \widetilde{\boldsymbol{h}}^{LS}\boldsymbol{S} \right\|^2 , \tag{20}$$

where $\boldsymbol{S}$ ($\boldsymbol{S} \epsilon \mathbb{C}^{N_T \times N_P}$) is the matrix containing the transmitted training sequences $\boldsymbol{s}_{nt}$ ($nt = 1,2,\dots,N_T$) of all transmit antennas such as:

$$\boldsymbol{S} = \begin{bmatrix} \boldsymbol{s}_1 \\ \boldsymbol{s}_2 \\ \vdots \\ \boldsymbol{s}_{N_T} \end{bmatrix}. \tag{21}$$

The channel estimates of the channel impulse responses between all transmit antennas and the n-th receiving antenna are given by

$$\widehat{\boldsymbol{h}}_n^{LS} = \boldsymbol{y}_n \boldsymbol{S}^H [\boldsymbol{S}\boldsymbol{S}^H]^{-1} , \tag{22}$$

or, generically, for non-white Gaussian noise by

$$\widehat{\boldsymbol{h}}_n^{LS} = \boldsymbol{y}_n \boldsymbol{R}_{zz}^{-1} \boldsymbol{S}^H [\boldsymbol{S}\boldsymbol{R}_{zz}^{-1}\boldsymbol{S}^H]^{-1} , \tag{23}$$

where $(\bullet)^{-1}$ denotes the inverse operation and $\boldsymbol{R}_{zz}$ is the auto-correlation matrix of the noise given by:

$$\boldsymbol{R}_{zz} = {\sigma_z}^2 \boldsymbol{I}_{N_R \times N_R} , \tag{24}$$

where $\boldsymbol{I}_{N_R \times N_R}$ is the identity matrix.

The MSE of the LS channel estimate is equal to:

$$MSE_{LS} = \frac{{\sigma_z}^2}{{\sigma_x}^2}. \tag{25}$$

From (25), it becomes obvious that the MSE is inversely proportional to the SNR ($SNR = {\sigma_x}^2/{\sigma_z}^2$), which means that the LS estimator is susceptible to noise enhancement, particularly

when the channel is in deep fading. However, since this technique does not consider channel statistical parameters, it is extensively used for channel estimation.

3.3.2 Minimum Mean-Square Error Channel Estimation

MMSE channel estimation is a more accurate version of the LS channel estimation. Let us consider the block diagram shown in Figure 3.21, where $\boldsymbol{M}$ is the weight matrix and $\widehat{\boldsymbol{h}}^{MMSE}$ corresponds to the MMSE estimate.

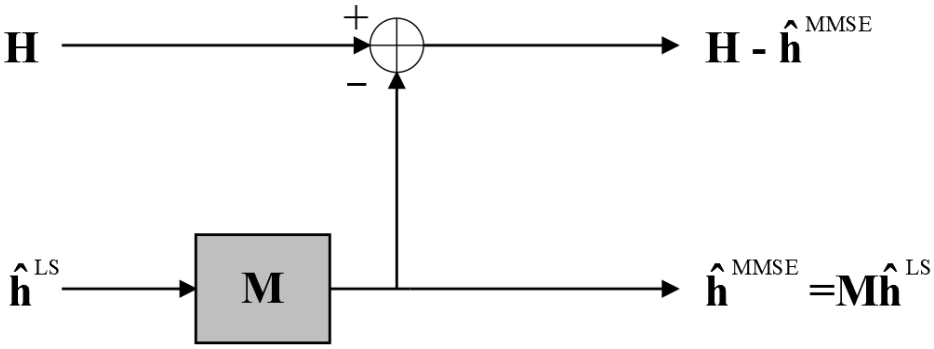

Figure 3.21 - Block Diagram of MMSE Channel Estimation

The MMSE channel estimator minimizes the MSE between the true channel, $\boldsymbol{H}$, and the MMSE estimated channel, $\widehat{\boldsymbol{h}}^{MMSE}$, by finding a good linear estimate in terms of $\boldsymbol{M}$ and the value of LS estimate, $\widehat{\boldsymbol{h}}^{LS}$:

$$\widehat{\boldsymbol{h}}^{MMSE} = \arg \min_{\widetilde{\boldsymbol{h}}^{MMSE}} \left\| \boldsymbol{H} - \widetilde{\boldsymbol{h}}^{MMSE} \right\|^2 , \tag{26}$$

with

$$\widehat{\boldsymbol{h}}^{MMSE} = \widehat{\boldsymbol{h}}^{LS} \boldsymbol{M} . \tag{27}$$

According to the principle of orthogonality, the estimation error vector $\varepsilon = \boldsymbol{H} - \widehat{\boldsymbol{h}}^{MMSE}$ is orthogonal to $\widehat{\boldsymbol{h}}^{LS}$, resulting in

$$\boldsymbol{R}_{\boldsymbol{H}\widehat{\boldsymbol{h}}^{LS}} - \boldsymbol{M}\boldsymbol{R}_{\widehat{\boldsymbol{h}}^{LS}\widehat{\boldsymbol{h}}^{LS}} = 0 , \tag{28}$$

where $\boldsymbol{R}_{\boldsymbol{H}\widehat{\boldsymbol{h}}^{LS}}$ represents the cross-correlation matrix between $\boldsymbol{H}$ and $\widehat{\boldsymbol{h}}^{LS}$, and $\boldsymbol{R}_{\widehat{\boldsymbol{h}}^{LS}\widehat{\boldsymbol{h}}^{LS}}$ the auto-correlation matrix of $\widehat{\boldsymbol{h}}^{LS}$ given by

$$\boldsymbol{R}_{\widehat{\boldsymbol{h}}^{LS}\widehat{\boldsymbol{h}}^{LS}} = \boldsymbol{R}_{\boldsymbol{HH}} + \frac{{\sigma_z}^2}{{\sigma_x}^2}\boldsymbol{I} . \tag{29}$$

Solving (28) in function of $\boldsymbol{M}$ results:

$$\boldsymbol{M} = \boldsymbol{R}_{\boldsymbol{H}\widehat{\boldsymbol{h}}^{LS}} \boldsymbol{R}_{\widehat{\boldsymbol{h}}^{LS}\widehat{\boldsymbol{h}}^{LS}}{}^{-1} . \tag{30}$$

By combining equations (30) and (29), equation (27) can be rewritten as:

$$\widehat{\boldsymbol{h}}^{MMSE} = \widehat{\boldsymbol{h}}^{LS}\boldsymbol{R}_{\boldsymbol{H}\widehat{\boldsymbol{h}}^{LS}}\left(\boldsymbol{R}_{\boldsymbol{HH}} + \frac{{\sigma_z}^2}{{\sigma_x}^2}\boldsymbol{I}\right)^{-1}. \tag{31}$$

Assuming that every channel response energy is normalized, such as:

$$E\left\{\left|h_{nr,nt}\right|^2\right\} = {\sigma_h}^2, \qquad \forall nr, nt, \tag{32}$$

the estimate solution of the Equation (31) for the n-th receiving antenna can be simplified to:

$$\widehat{\boldsymbol{h}}_n^{MMSE} = \boldsymbol{x}_n\boldsymbol{S}^H\left(\boldsymbol{S}\boldsymbol{S}^H + \frac{{\sigma_z}^2}{{\sigma_h}^2}\boldsymbol{I}\right)^{-1}. \tag{33}$$

Generally, for non-white Gaussian noise we have

$$\widehat{\boldsymbol{h}}_n^{MMSE} = \boldsymbol{x}_n\boldsymbol{R}_{zz}^{-1}\boldsymbol{S}^H\left(\boldsymbol{S}\boldsymbol{R}_{zz}^{-1}\boldsymbol{S}^H + \frac{{\sigma_z}^2}{{\sigma_h}^2}\boldsymbol{I}\right)^{-1}. \tag{34}$$

Since MMSE estimation relies on minimizing the MSE, it has a better performance than LS channel estimation. The downside lies on the fact that it depends on the channel statistics. Hence, this method has a higher complexity than the LS estimator. To reduce the complexity of MMSE channel estimator, a technique called modified MMSE is suggested in [63].

In this work, the MSE of the estimated channel is defined as

$$MSE = \frac{\left\|\boldsymbol{H}_u{}^{DL} - \widehat{\boldsymbol{H}}_{\boldsymbol{u}}^{MMSE}\right\|_F}{N_T N_R} \tag{35}$$

where $\|\bullet\|_F$ denotes the Frobenius norm of a matrix.

Figure 3.22 and Figure 3.23 show the BER and MSE results, to compare the accuracy of the MMSE estimator for a different numbers of pilots in a scheme with 2 users and 2 receive antennas per each one.

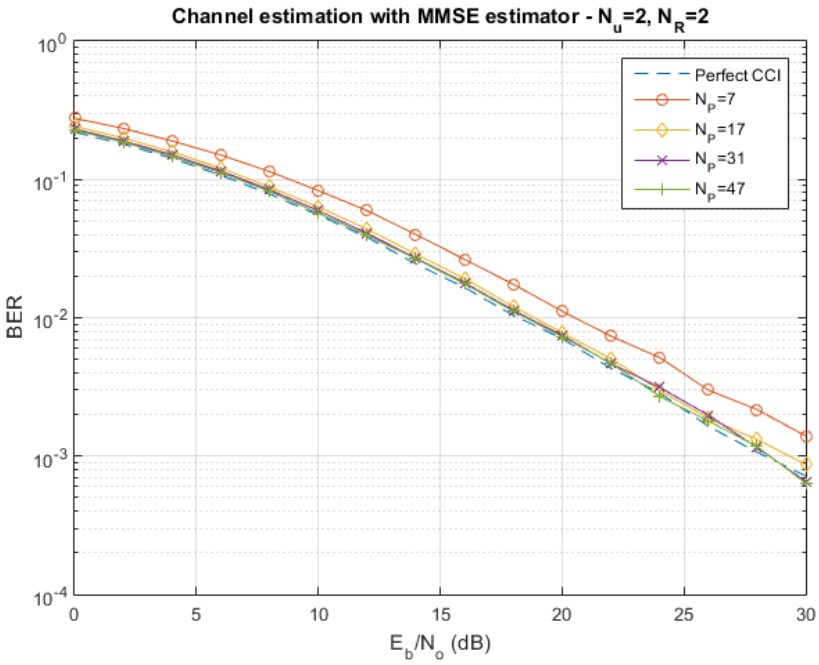

Figure 3.22 - BER plot of transmission to 2 users with MMSE estimator, for different numbers of pilots

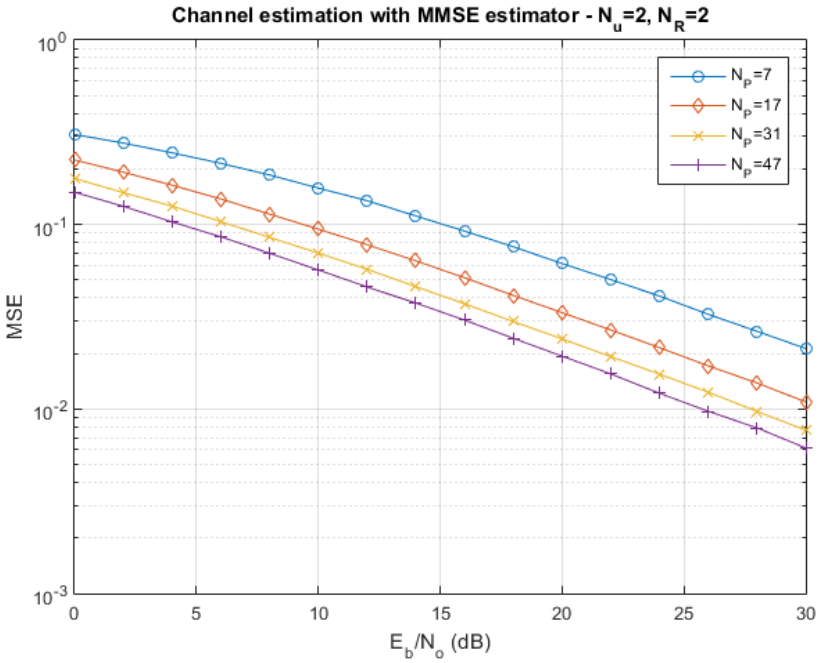

Figure 3.23 - MSE of transmission to 2 users with MMSE estimator, for different numbers of pilots

It is clear that for $N_P = 7$, estimation performance is degraded, but for the other values of N_P the estimation is accurate. Obviously, as the number of pilots increase, the channel estimation is more precise. The following plots, Figure 3.24 and Figure 3.25, consider an 8 users scheme for the same comparison purposes as before.

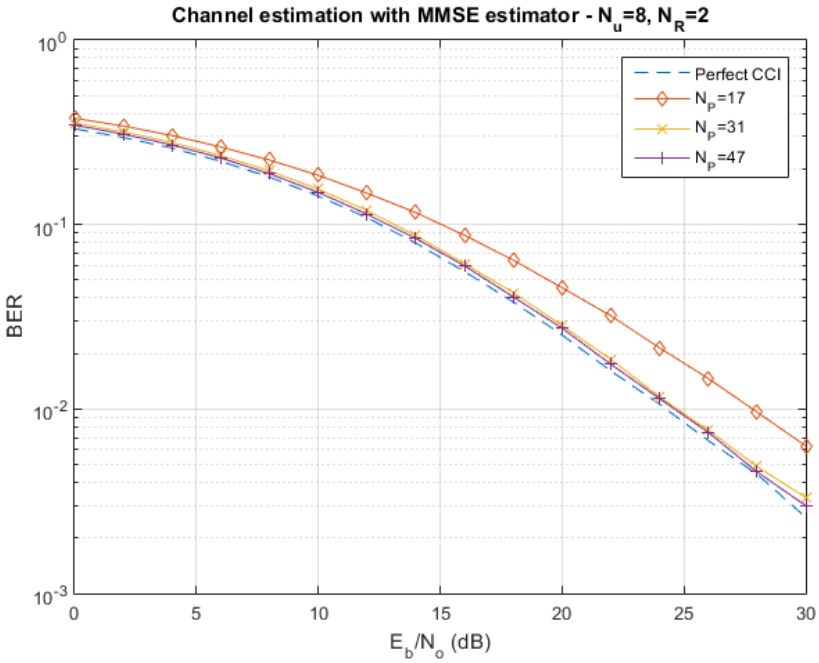

Figure 3.24 - BER plot of transmission to 8 users with MMSE estimator, for different numbers of pilots

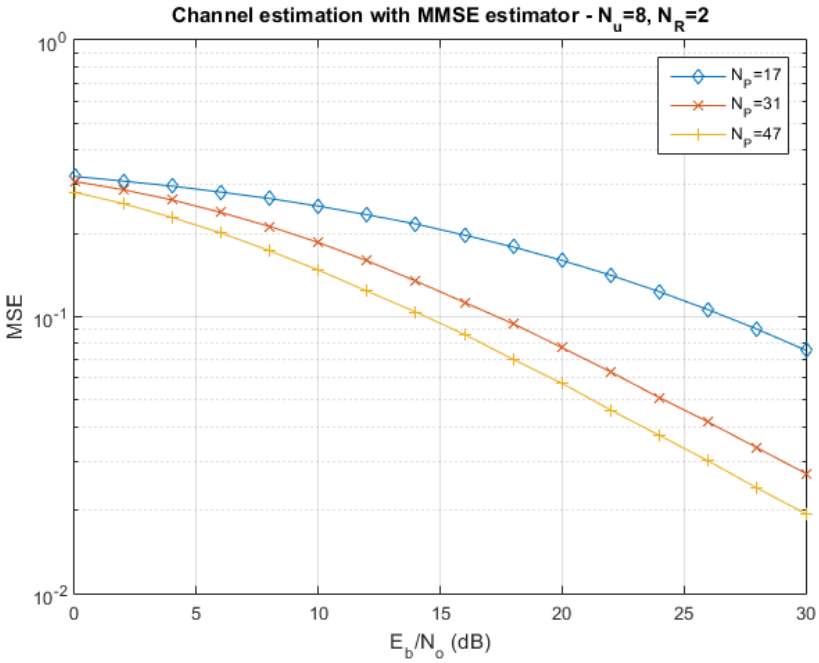

Figure 3.25 - MSE of transmission to 8 users with MMSE estimator, for different numbers of pilots

When the number of pilots is close to the number of base station antennas ($N_T = 4, N_P = 7$ for the first case, and $N_T = 16, N_P = 17$ for the second one), it is visible a degradation in the performance of the estimators. Apart from that, for the rest of the set of training sequence lengths the BER plot shows an approximated performance to the exact CSI.

To put massive MIMO into context, Figure 3.26 and Figure 3.27 show the performance of the MMSE estimator when the base station deploys a large array of antennas ($N_T = 64$), serving 8 users simultaneously, each one with 8 receive antennas. It can be seen that, as the number of antennas increases, the estimator becomes less accurate. Moreover, the channel estimation process becomes more complex, since a larger matrix has to be inverted.

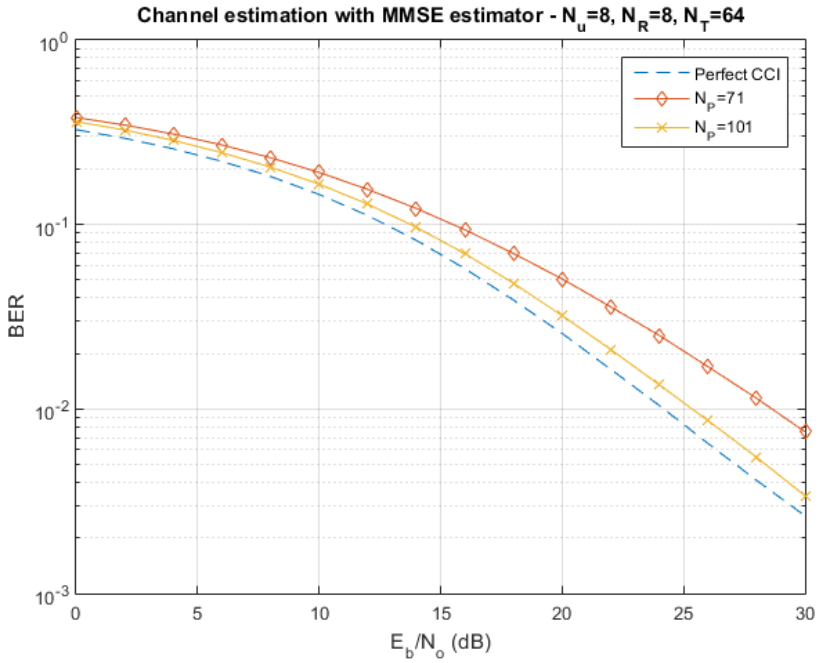

Figure 3.26 - BER plot of massive MIMO scheme with 64 base station antennas using MMSE estimator, for $N_P = 71$ and $N_P = 101$

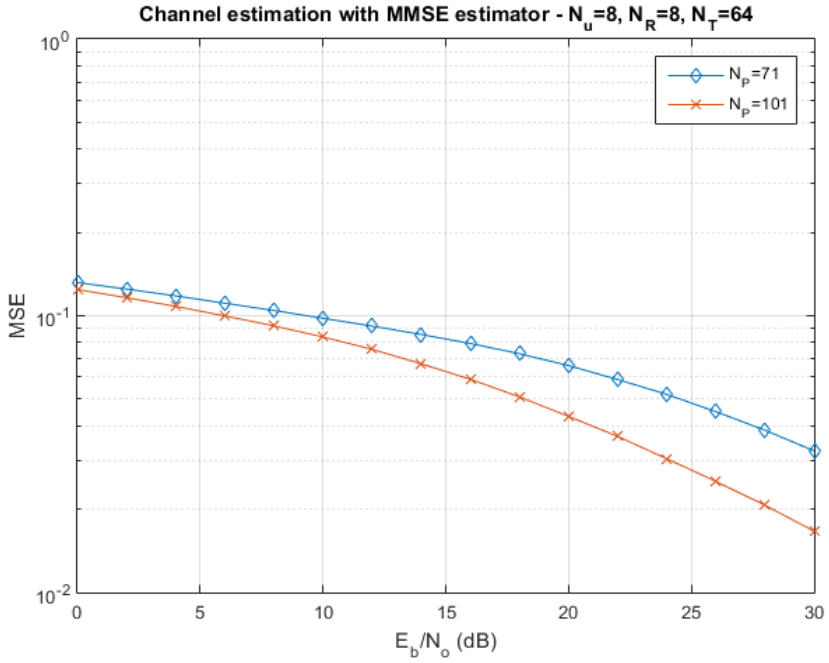

Figure 3.27 - MSE plot of massive MIMO scheme with 64 base station antennas using MMSE estimator, for $N_P = 71$ and $N_P = 101$

In order to improve efficiency and lower complexity of channel estimation, the next section introduces the Zadoff-Chu sequences.

3.4 Channel Estimation with Zadoff-Chu training sequences

Zadoff-Chu (ZC) sequences are complex-valued mathematical sequences in which cyclically shifted versions of the same sequence are orthogonal to each other, that is, they have zero correlation. A non-shifted sequence is known as "root sequence" and is defined as:

$$x_U(n) = e^{-j\frac{\pi U n(n+1)}{N_{ZC}}}, 0 \leq n \leq N_{ZC}, \tag{36}$$

where U is the root index that determines a specific sequence, n is the time index and N_{ZC} is the length of the sequence. If N_{ZC} is a prime number, each root index ($U = 1,2,\dots,N_{ZC}-1$) generates different Zadoff-Chu sequences.

Zadoff-Chu sequences belong to the class of perfect polyphase sequences [66], also called Constant Amplitude Zero Autocorrelation (CAZAC) sequences. A CAZAC sequence is a periodic signal with modulus one and discrete cyclic autocorrelation equal to zero, i.e., each circularly shifted version of the same sequence is mutually orthogonal. Hence, the discrete Fourier transform (DFT) of any Zadoff-Chu sequence has constant amplitude. Furthermore, the cross-correlation between two prime-length Zadoff-Chu sequences of different root indices coprimes to N_{ZC} is constant and equal to $\sqrt{N_{ZC}}$.

Zadoff-Chu sequences are used in several channels of LTE standard, more specifically in primary synchronization signal (PSS), reference signal (RF) both uplink and downlink, physical uplink control channel (PUCCH), physical uplink traffic channel (PUSCH) and physical random access channel (PRACH).

Since all cyclically shifted versions of a Zadoff-Chu sequence are orthogonal to each other, they can be used as training sequences for channel estimation in transmissions with multiple antennas, simultaneously.

Let us assume $\boldsymbol{S}$ as the matrix containing the transmitted training sequences, in (21). Each training sequence $\boldsymbol{s}_{nt}$ $(nt = 1,2,\dots,N_T)$ is a circularly shifted version of a Zadoff-Chu sequence with the same root index, of length N_{ZC}, so,

$$\langle \boldsymbol{s}_a, \boldsymbol{s}_b \rangle = 0, \qquad a \neq b, \tag{37}$$

where $\langle \bullet, \bullet \rangle$ refers to the Hermitian inner product operation.

Subsequently, the constraint $N_{ZC} > N_T$ is imposed so every sequence is pairwise orthogonal and, therefore, each channel response is distinguished. This is a major drawback in massive MIMO systems, where N_T is intended to be large.

In reception, the nr-th receive antenna $(nr = 1,2,\dots,N_R)$ obtains the following signal:

$$\begin{gathered}\boldsymbol{y}_{nr} = \boldsymbol{s}_1 h_{nr,1} + \boldsymbol{s}_2 h_{nr,2} + \cdots + \boldsymbol{s}_{nr} h_{nr,nt} + \cdots + \boldsymbol{s}_{N_T} h_{nr,N_T}, \\ (nt = 1,2,\dots,nr,\dots,N_T).\end{gathered} \tag{38}$$

So, $h_{nr,nt}$ $(nt = nr)$ is the desired channel while $h_{nr,nt}$ $(nt \neq nr)$ are the interfering channels. Therefore, using the Hermitian inner product operation in $\boldsymbol{y}_{nr}$ with the appropriate training sequence $\boldsymbol{s}_{nr}$ the unwanted interference parcels will be canceled, resulting

$$\langle \boldsymbol{y}_{nr}, \boldsymbol{s}_{nr} \rangle = |\boldsymbol{s}_{nr}|^2 \bar{h}_{nr,nr} \,, \tag{39}$$

where $|\bullet|$ refers to the norm function and $\bar{\bullet}$ denotes the complex conjugate.

Since the square of a vector's norm is equal to the length of the vector, the expression can be simplified as:

$$\langle \boldsymbol{y}_{nr}, \boldsymbol{s}_{nr} \rangle = N_{ZC} \bar{h}_{nr,nr} \,. \tag{40}$$

Thus, to estimate the value of the corresponding channel response, $\hat{h}_{nr,nr}$, it is just needed to divide by N_{ZC} and proceed with complex conjugate operation.

$$\hat{h}_{nr,nr} = \frac{\overline{\langle \boldsymbol{y}_{nr}, \boldsymbol{s}_{nr} \rangle}}{N_{ZC}}. \tag{41}$$

This estimator does not perform matrix inversions and, therefore, it has much lower complexity than a MMSE estimator, specially in a massive MIMO scenario, where the channel matrix is very large.

As before, Figure 3.28 and Figure 3.29 show the accuracy of the channel estimation technique described in this section, for a system with 2 users and 2 receive antennas per each. It is perceptible the reduced accuracy when $N_P = 7$. However, although MMSE estimator has higher complexity due to channel inversions, it performs worse than channel estimation based on Zadoff-Chu training sequences. The following simulations compare the latter technique with the MMSE channel estimation.

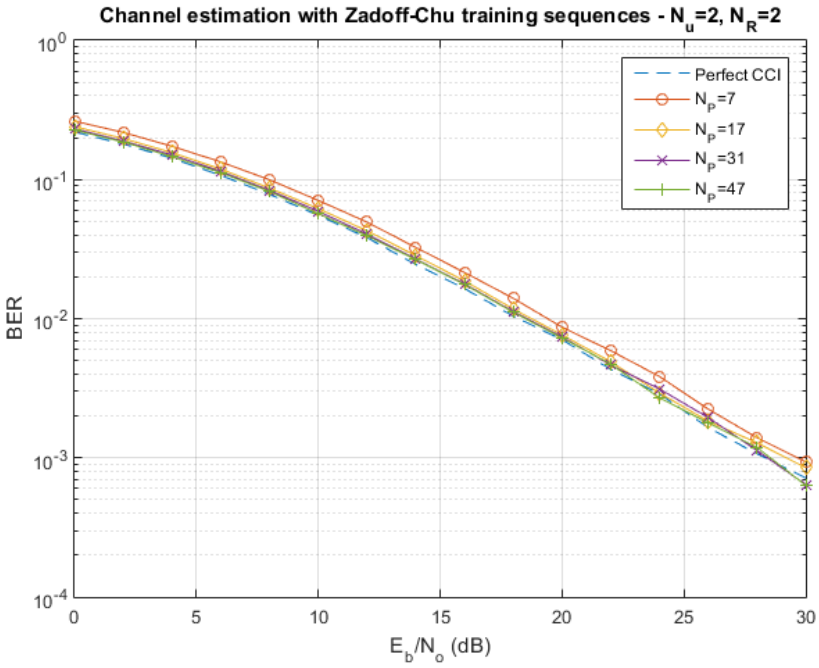

Figure 3.28 - BER plot of transmission to 2 users with channel estimation using Zadoff-Chu training sequences, for different numbers of pilots

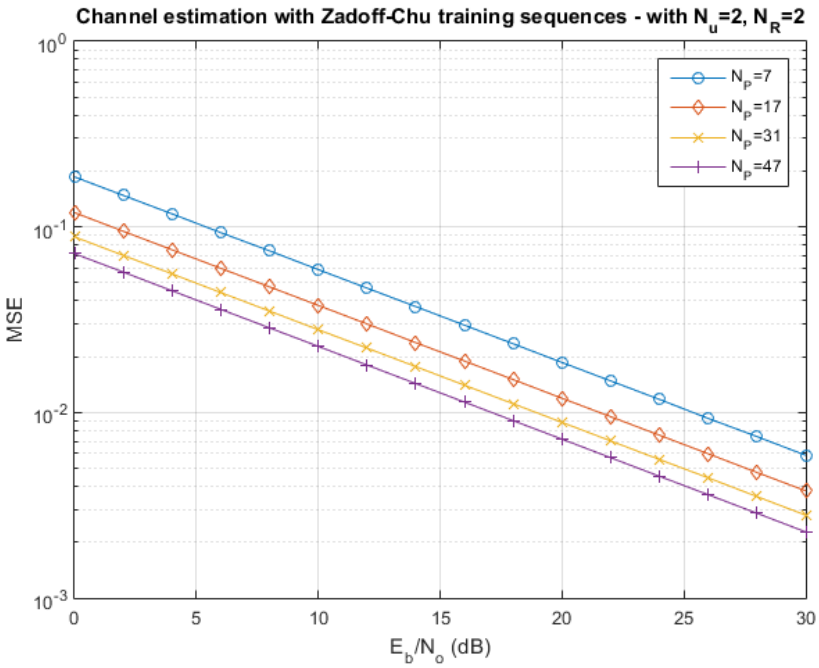

Figure 3.29 - MSE of transmission to 2 users with channel estimation using Zadoff-Chu training sequences, for different numbers of pilots

For $N_P = 7$, there is a great improvement in ZC-based channel estimation, specially for an increasing number of antennas. As shown in Figure 3.32, for 8 active users with 2 receiving antennas each, there is a BER improvement around 3dB when using the smallest training sequence length ($N_P = 17$). Moreover, Zadoff-Chu channel estimation technique's MSE do not depend on

the number of base station antennas, but in the length of the training sequences. Plus, the number of receive antennas equipped at each user enhances the MSE results, as depicted in Figure 3.34.

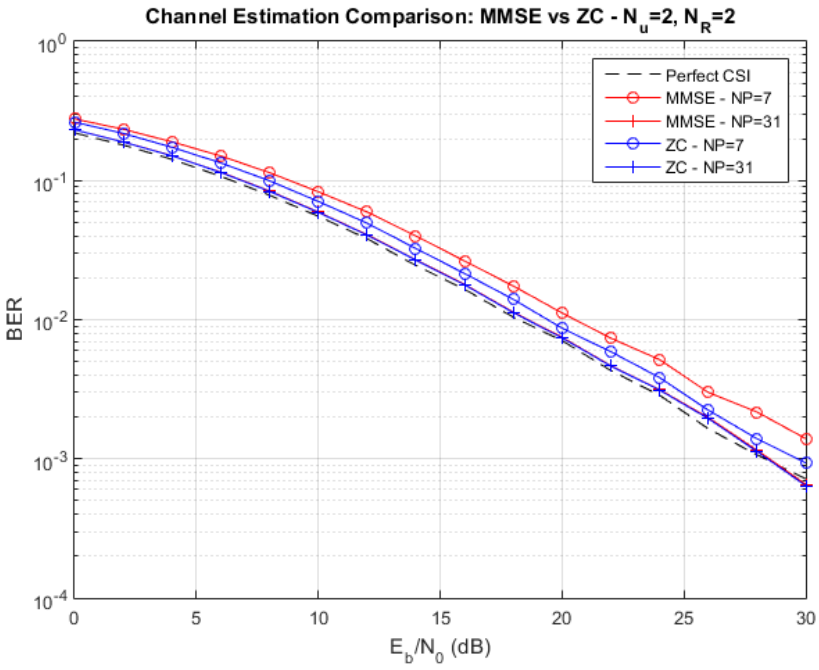

Figure 3.30 - BER comparison between MMSE estimator and ZC method, for $N_P = 7$ and $N_P = 31$

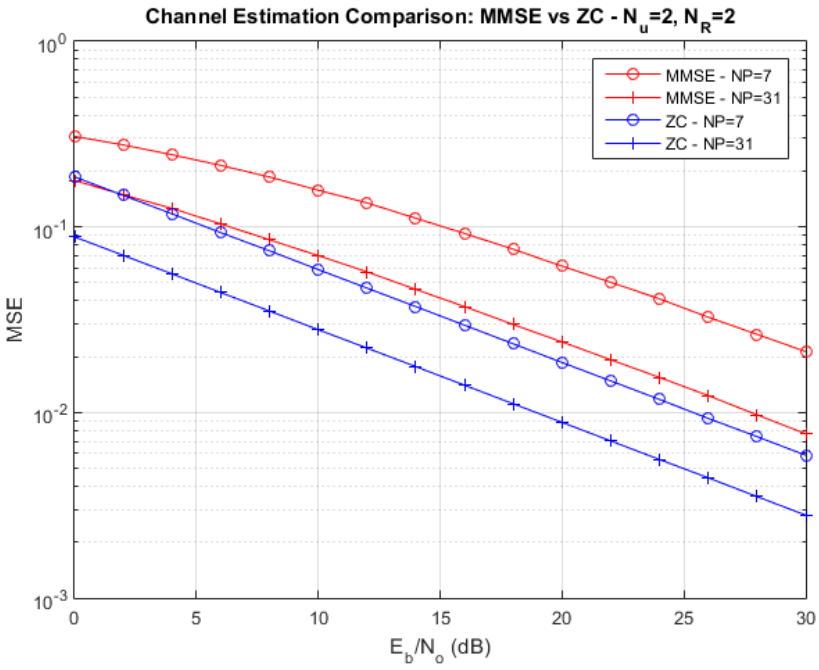

Figure 3.31 - MSE comparison between MMSE estimator and ZC method, for $N_P = 7$ and $N_P = 31$

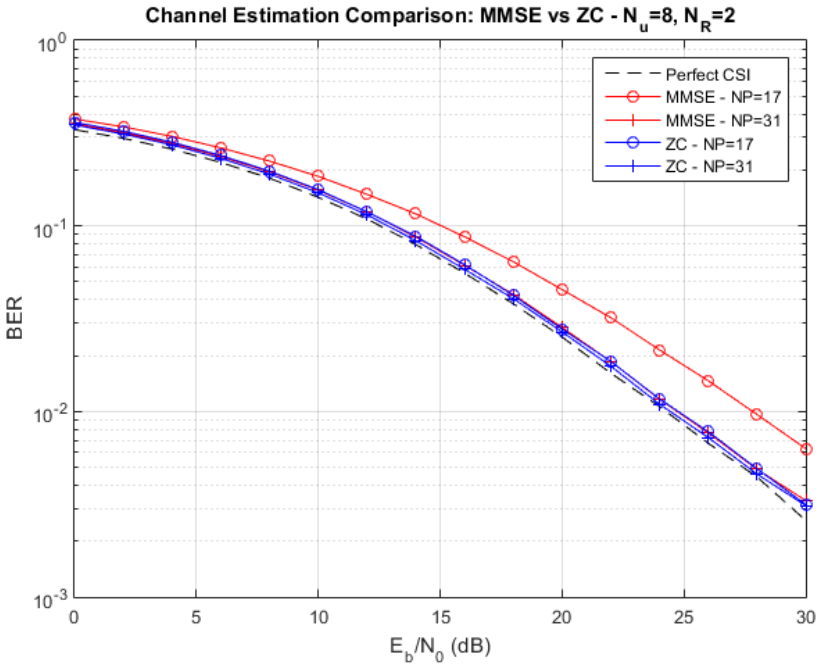

Figure 3.32 - BER comparison between MMSE estimator and ZC method, for $N_P = 17$ and $N_P = 31$

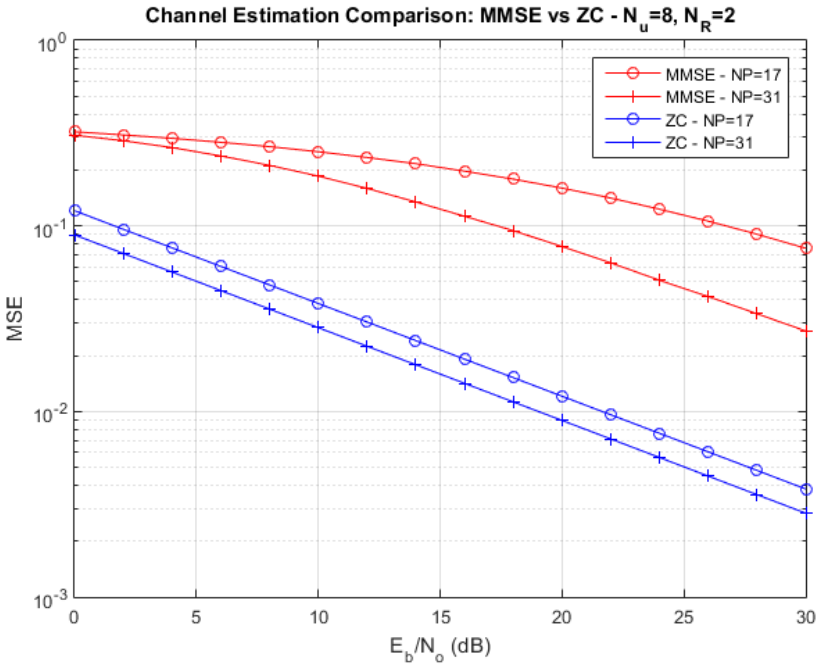

Figure 3.33 - MSE comparison between MMSE estimator and ZC method, for $N_P = 17$ and $N_P = 31$

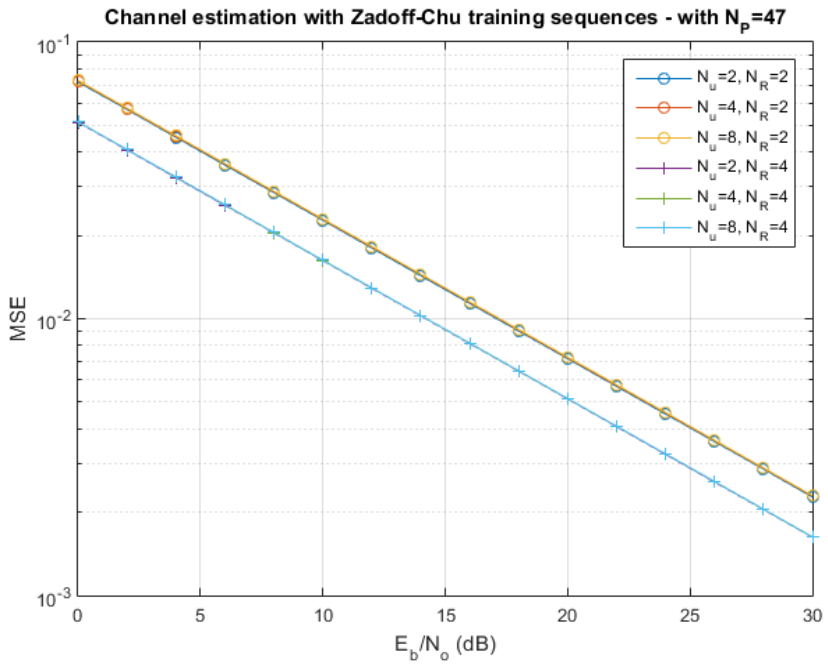

Figure 3.34 - MSE of transmission with channel estimation using Zadoff-Chu training sequences, for ranging values of N_u and N_R

Zadoff-Chu sequences admit perfect autocorrelation and good cross-correlations properties. These properties make them suitable training sequences in channel estimation. When compared with MMSE estimator, the ZC-based channel estimation technique achieves lower complexity and better performances at the minimum limit number of pilots. Massive MIMO schemes tends to prejudice this technique because the number of pilots are lower bounded by the number of base station antennas. However, for large channel matrices, complexity intensification is not as critical as in channel inversion-based estimators, such as LS and MMSE. Hereupon, in the introduced ZC-based channel estimation there must have a compromise between the number of active transmit antennas and data payload.

4. Pilot Contamination

Channel estimation has an important role in massive MIMO transmission, in order to reduce CCI. However, the reuse of training sequences in neighboring cells imposes a limitation on the achievable rate in a massive MIMO system. This limitation arises from the phenomenon called pilot contamination. The number of distinct training sequences should be higher than the number of users that are being served in the system. Moreover, the number of mutually orthogonal training sequences that can be generated is upper bounded by the length of those sequences. Thus, there is a tradeoff between the length of the training sequences and the data transmission payload. The tradeoff worsens as the channel coherence interval becomes smaller. In order to mitigate pilot contamination and reduce the bandwidth usage by training sequences, semi-blind and blind channel estimation techniques have been developed. In comparison to traditional pilot-based channel estimation techniques, they require fewer, or even none, pilots to estimate the CSI, relieving the effect of pilot contamination and increasing spectral efficiency. Blind and semi-blind channel estimation techniques rely on channel's statistics to determine the channel estimate.

In this chapter, three different channel estimation methods will be described and compared. The first one consists in an adaptation of the IB-DFE. By taking advantage of the iterative process, CSI can also be, iteratively, estimated. The second method is a complexity-reduced adaptive semi-blind channel estimator that uses a subspace tracking algorithm to resolve the ambiguity problem. The algorithm is named fast single compensation approximated power iteration (FSCAPI). FSCAPI is simplified to achieve higher estimation speeds, albeit good tracking performance. The last technique is a low-complexity channel estimator called PEACH. PEACH estimator approximates the MMSE estimator, replacing the matrix inversion with a polynomial expansion.

The same system model of chapter 3 is adopted, however, with an uplink scenario with single-antenna users and the base station having $N_R \geq N_u$ antennas. The same notation is applied.

Simulation results will distinguish the best technique to be used in an uplink MU-MIMO system with pilot contamination, over BER and MSE measurements.

4.1 System Model

The system model considered is an uplink MU-MIMO scenario, shown in Figure 4.35. The base station is equipped with N_R antennas and serves simultaneously N_u ($N_u \leq N_R$) single-antenna users. At time n, the received signal vector $\boldsymbol{y}(n)$ ($\boldsymbol{y}(n) \epsilon \mathbb{C}^{N_R}$) at the base station is given byww

$$\boldsymbol{y}(n) = \boldsymbol{H}\boldsymbol{x}(n) + \boldsymbol{z}(n)\,, \qquad n = 1, 2, \ldots, N\,, \tag{42}$$

where $\boldsymbol{H}$ ($\boldsymbol{H}\epsilon\mathbb{C}^{N_R \times N_u}$) is the channel matrix composed by i.i.d. samples of complex Gaussian process of zero mean and unit variance, $\boldsymbol{x}(n)$ ($\boldsymbol{x}(n)\epsilon\mathbb{C}^{N_u}$) is the transmitted vector of aggregated symbols by the N_u users and $\boldsymbol{z}(n)$ ($\boldsymbol{z}(n)\epsilon\mathbb{C}^{N_R}$) is a vector of AWGN with zero mean and variance ${\sigma_z}^2 = \frac{N_0}{2}$,assumed to be known at the base station.

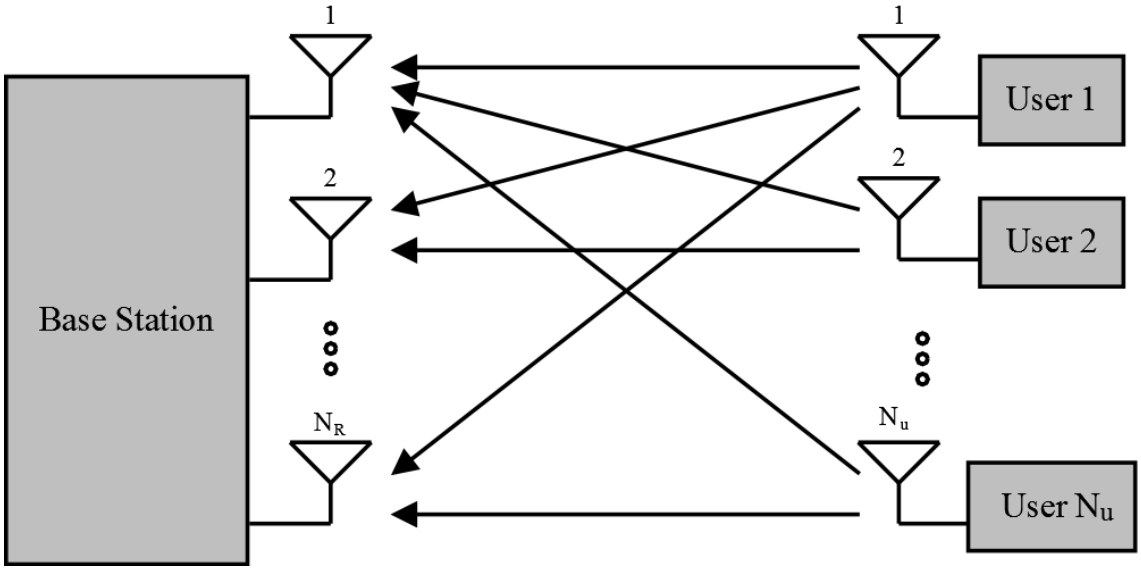

Figure 4.35 - Uplink MU-MIMO system model with single-antenna users

The channel model is identical to the one of chapter 3, which means that the channel is constant during each coherence time interval of length N. The pilot structure model is also identical, where the pilots are transmitted in comb type process over N_P symbols. The received training sequences, $\boldsymbol{Y}^P$ ($\boldsymbol{Y}^P\epsilon\mathbb{C}^{N_R \times N_P}$), are given by

$$\boldsymbol{Y}^P = \boldsymbol{H}\boldsymbol{S} + \boldsymbol{Z}^P\,, \tag{43}$$

where the pilot matrix, $\boldsymbol{S}$ ($\boldsymbol{S}\epsilon\mathbb{C}^{N_u \times N_P}$), corresponds to the collectively transmitted training sequence by N_u users and $\boldsymbol{Z}^P$ ($\boldsymbol{Z}^P\epsilon\mathbb{C}^{N_R \times N_P}$) is the AWGN noise matrix, which lines have the same characteristic as $\boldsymbol{z}$ in (42).

At time n ($n = 1,2, \ldots, N_P$), the pilot signal received by the nr-th ($nr = 1,2, \ldots, N_R$) base station antenna is given by

$$y_{nr}^P(n) = h_{nr,1}s_1(n) + h_{nr,2}s_2(n) + \cdots + h_{nr,N_u}s_{N_u}(n) + z_{nr}^P(n)\,. \tag{44}$$

4.1.1 Pilot Contamination Model

Pilot contamination effect caused by the reuse of training sequences from other users in neighboring cells is modeled as in Figure 4.36.

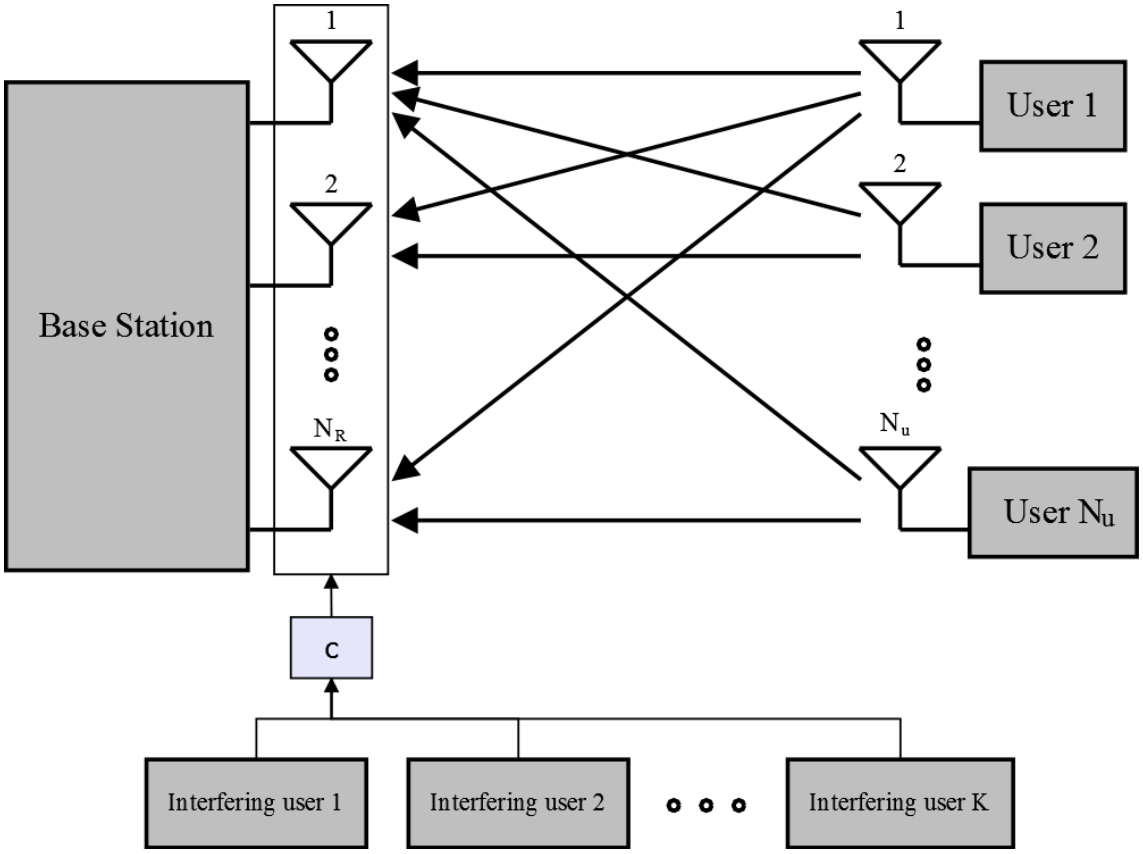

Figure 4.36 - Uplink MU-MIMO system model with pilot contamination

The received pilots affected by pilot contamination are given by

$$\boldsymbol{Y}^{PC} = \boldsymbol{Y}^{P} + c(\boldsymbol{H}^{PC}\boldsymbol{S} + \boldsymbol{Z}^{PC}) \tag{45}$$

where c $(0 < c < 1)$ is the attenuation constant that adjusts the power of the interference training sequences sent by K interfering users. For $c = 0$ pilot contamination is inexistent, and for $c = 1$ the interfering channel has the same power has the desired channel. $\boldsymbol{H}^{PC}$ $(\boldsymbol{H}^{PC} \epsilon \mathbb{C}^{N_R \times K})$ denotes the interfering channel, $\boldsymbol{S}^{PC}$ $(\boldsymbol{S}^{PC} \epsilon \mathbb{C}^{K \times N_P})$ is the interfering pilot matrix with K interfering training sequences (equal to the number of interfering as users) and $\boldsymbol{Z}^{PC}$ $(\boldsymbol{Z}^{PC} \epsilon \mathbb{C}^{N_R \times N_P})$ is the correspondent interfering AWGN noise matrix which lines have the same characteristics as $\boldsymbol{z}$ in (42).

The nr-th base station antenna receives the following signal

$$y_{nr}^{PC} = y_{nr}^{P} + c\left(h_{nr,1}^{PC} s_1 + h_{nr,2}^{PC} s_2 + \cdots + h_{nr,K}^{PC} s_K + z_{nr}^{PC}\right) \tag{46}$$

where the time index n is omitted for notation simplicity. The received signal is now affected with inter-cell interference from K interfering users.

From (44), the previous equation can be rewritten as

$$\begin{aligned} y_{nr}^{PC} = {} & s_1\left(ch_{nr,1}^{PC} + h_{nr,1}\right) + \cdots + s_K\left(ch_{nr,K}^{PC} + h_{nr,K}\right) + \cdots + s_{N_u} h_{nr,N_u} \\ & + z_{nr}^{P} + z_{nr}^{PC}\,, \end{aligned} \tag{47}$$

meaning the estimator is incorrectly aimed to estimate the sum of the desired channel and the correspondent interfering channel for K user channels.

4.2 IB-DFE with iterative channel estimations

In order to avoid excess battery usage and to lower the cost of mobile devices, LTE adopted for the uplink the single-carrier frequency domain equalization (SC-FDE). Although very similar to OFDM, the SC-FDE allocates the high computational necessities to the receiver: The Inverse Fast Fourier Transform (IFFT) is done by the receiver, instead of the transmitter, as in OFDM. Besides that, SC-FDE has also a lower Peak-to-Average Power Ratio (PAPR). Analogously to OFDM, the multiuser version of SC-FDE, implemented nowadays in wireless communications, is the signal-carrier frequency division multiple access (SC-FDMA) [67], [68].

Usually, for SC-FDE schemes the receiver is a linear equalizer. However, non-linear (also called decision-directed) equalizers have better performances than the linear ones [69]. Nonlinear equalizers take into account previous symbol decisions made by the receiver to cancel the ISI, and for that reason they are also called as Decision-Feedback Equalizer (DFE). The structure of DFE is shown is Figure 4.37. Since ISI is caused by multipath when separated paths are received at different times, the interference can be cancelled by knowing the previous symbols and removing their corresponding ISI contribution of future received symbols, through a feedback filter structure. The drawback of this approach lies on error propagation, when there are wrong decisions of the prior symbols, especially at low SNR. Furthermore, the improved performance, in comparison to linear equalizers, is traded by increased complexity [69]. Nonetheless, time-domain DFE have a good performance/complexity tradeoff. This tradeoff worsens in severely time-dispersive channels, making time-domain DFEs too complex.

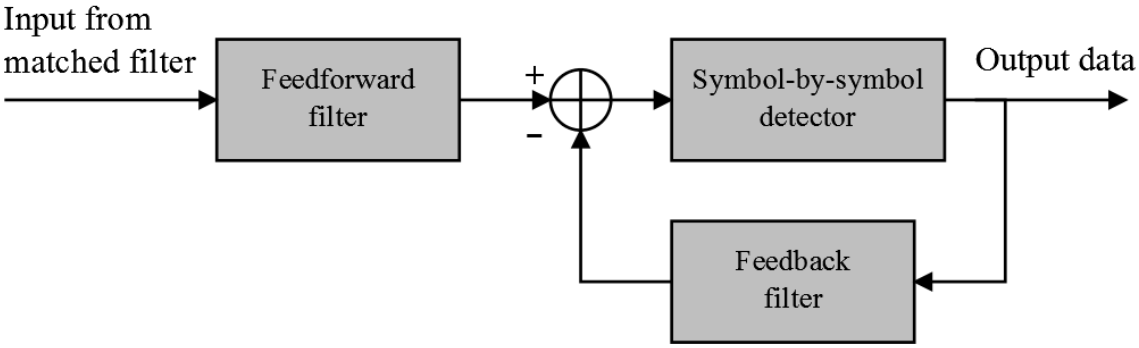

Figure 4.37 - DFE structure

To reduce DFE's complexity, a hybrid time-frequency approach was proposed in [70] where the feedforward filter works in the frequency domain and the feedback filter remains in time-domain. Although with better performance than a linear DFE, the error propagation is still

possible. The IB-DFE can be employed as an alternative to improve the performance of SC-FDE. In IB-DFE, both feedback and feedforward filters are implemented in the frequency domain. The IB-DFE receiver structure is depicted in Figure 4.38.

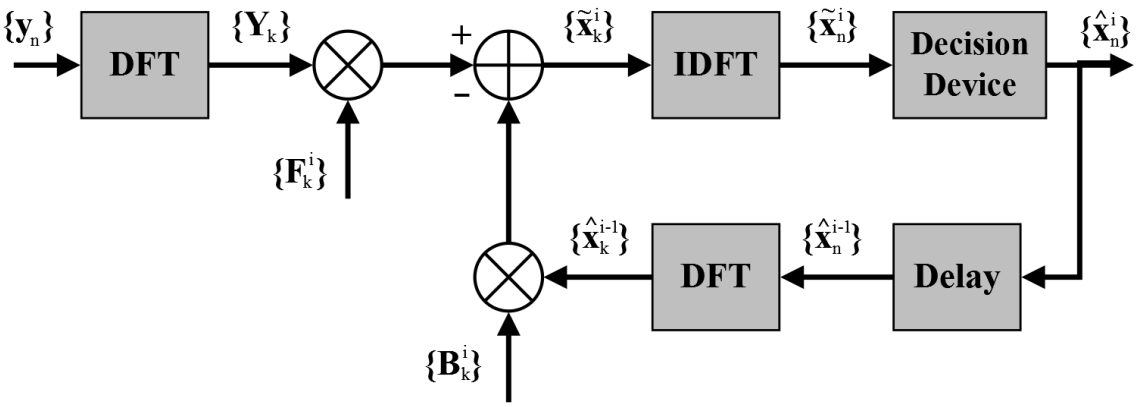

Figure 4.38 - IB-DFE receiver structure

The output samples of the equalizer, for the i-th iteration, are given by

$$\tilde{X}_k^i = F_k^i Y_k - B_k^i \hat{X}_k^{i-1}\,, \tag{48}$$

where B_k^i and F_k^i are the feedback and feedforward filter coefficients, respectively, and $\hat{X}_k^{i-1}$ denotes the Discrete Fourier Transform (DFT) of the decision block, $\hat{x}_n^{i-1}$, of the previous iteration, related to the transmitted time-domain block, where and k represents the frequency index.

The feedforward and feedback coefficients, F_k^i and B_k^i respectively, are given by

$$F_k^i = \frac{\kappa^i {H_k}^\star}{{}^1\!/_{SNR} + \left(1-\rho^{(i-1)^2}\right)|H_k|^2}, \tag{49}$$

$$B_k^i = \rho^{(i-1)}\left(F_k^i H_k - \gamma^i\right), \tag{50}$$

where $(\bullet)^\star$ denotes the complex conjugate operation.

The factor κ^i of the feedforward equalizer coefficient, F_k^i, is chosen to assure that γ^i is normalized, i.e.,

$$\gamma^i = \frac{1}{N}\sum_{k=0}^{N-1} F_k^i H_k = 1\,, \tag{51}$$

and ρ^i is the correlation factor, that measures the blockwise reliability of the decisions used in the feedback loop, given by

$$\rho^i = \frac{E\left[x_n{}^\star \hat{x}_n{}^i\right]}{E[|x_n|^2]} = \frac{E\left[X_k{}^\star \hat{X}_k{}^i\right]}{E[|X_k|^2]}. \tag{52}$$

The feedforward and feedback coefficients of (49) and (50) are optimum to maximize the Signal-to-Interference plus Noise Ratio (SINR). Plus, since IB-DFE takes into account the

reliability of estimates employed in the feedback loop, error propagation problems are also reduced.

For the first iteration, there is no previous information about X_k, so IB-DFE is equivalent to the linear FDE, as $B_k^0 = \hat{X}_k^0 = 0 \Rightarrow \rho = 0$ and

$$F_k^i = \frac{\kappa^i {H_k}^\star}{1/_{SNR} + |H_k|^2}, \tag{53}$$

which corresponds to the optimum FDE coefficient under the MMSE criterion.

As the number of iterations increase, the correlation factor ρ approximates to 1, which means residual ISI will be almost entirely canceled.

Insofar as ρ is the blockwise reliability of the estimates $\hat{X}_k^{i-1}$, (48) can be rewritten as

$$\tilde{X}_k^i = F_k^i Y_k - B_k^i \bar{X}_k^{i-1}, \tag{54}$$

where $\bar{S}_k^{i-1}$ is the overall block average of X_k^{i-1} at the FDE output and given by

$$\bar{S}_k^{i-1} = \rho^{(i-1)} \hat{X}_k^{i-1}. \tag{55}$$

It should be noted that, to improve performance, symbol averages could be used, instead of using blockwise averages. Decision with "blockwise averages" are called hard decisions (HD-IBDFE) and soft decisions (SD-IBDFE) using the "symbol averages". HD-IBDFE and SD-IBDFE are studied in detail in [71].

The performance of IB-DFE for three different system setups is depicted in Figure 4.39. It is assumed a perfect CSI knowledge.

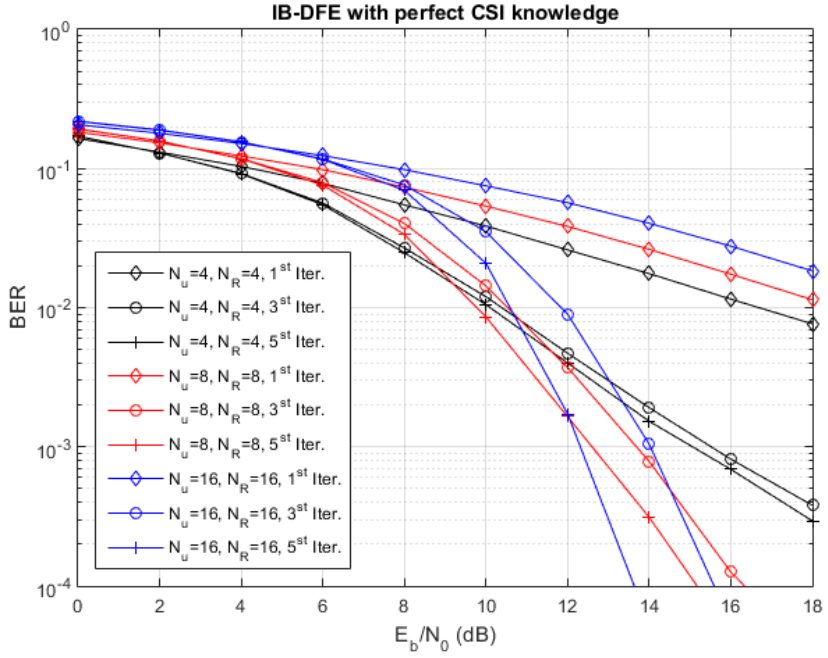

Figure 4.39 - IB-DFE performance with perfect CSI knowledge

The first iteration provides worst results for an increase number of antennas. However, additional iterations improve the system's performance for higher values of SNR. These are encouraging results for the implementation of an iterative channel estimation technique.

4.2.1 Iterative channel estimations

IB-DFE schemes cancel ISI, iteratively. To take advantage of the iteration process, CSI may be iteratively estimated as well, using the previously discussed channel estimation techniques. For the first iteration, equivalent to SC-FDE, the CSI is estimated with the Zadoff-Chu sequences and no iterative channel estimation occurs. For $i > 1$, the frequency-domain estimated symbols of the previous iteration, $\hat{X}_k^{i-1}$, can be used, instead of the pilots, to estimate the CSI more accurately. Using MMSE channel estimation technique, the channel estimate for the ith iteration is given by

$$H_k^i = \left[\left(\hat{X}_k^{i-1}\right)^H \hat{X}_k^{i-1} + \frac{{\sigma_z}^2}{{\sigma_h}^2} \boldsymbol{I} \right]^{-1} \left(\hat{X}_k^{i-1}\right)^H Y_k \,, \tag{56}$$

In the following figures the performance of the iterative channel estimation scheme for two different system setups in function of the number of pilots used is shown.

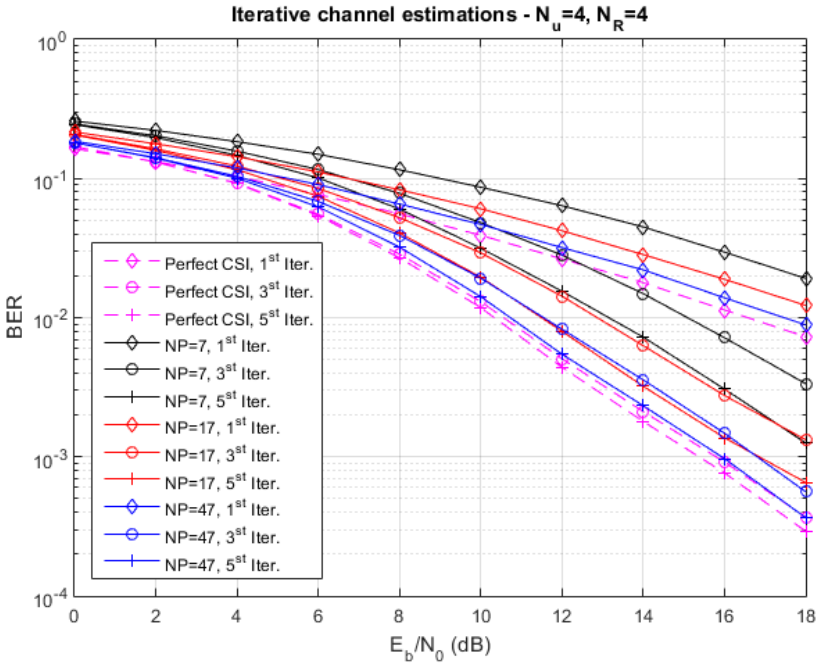

Figure 4.40 - BER performance of iterative channel estimation, for $N_u = N_R = 4$, in function of number of iterations and pilots used

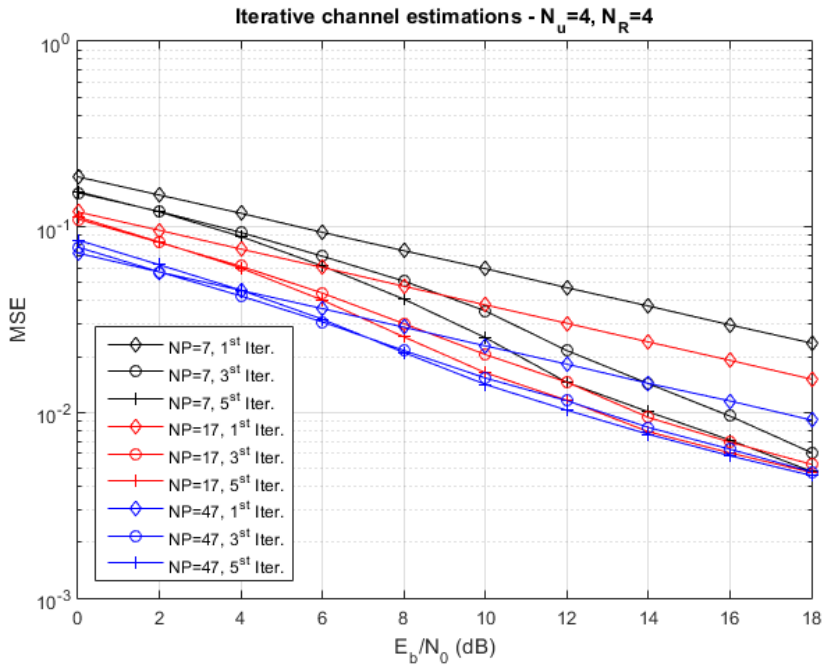

Figure 4.41 - MSE performance of iterative channel estimation, for $N_u = N_R = 4$, in function of number of iterations and pilots used

As expected, the higher number of pilots along with the increment of iterations leads to a better BER performance. However, in Figure 4.41 it is visible on the iterative estimates (3rd and 5th iteration), a convergence of the MSE slope as the SNR increases.

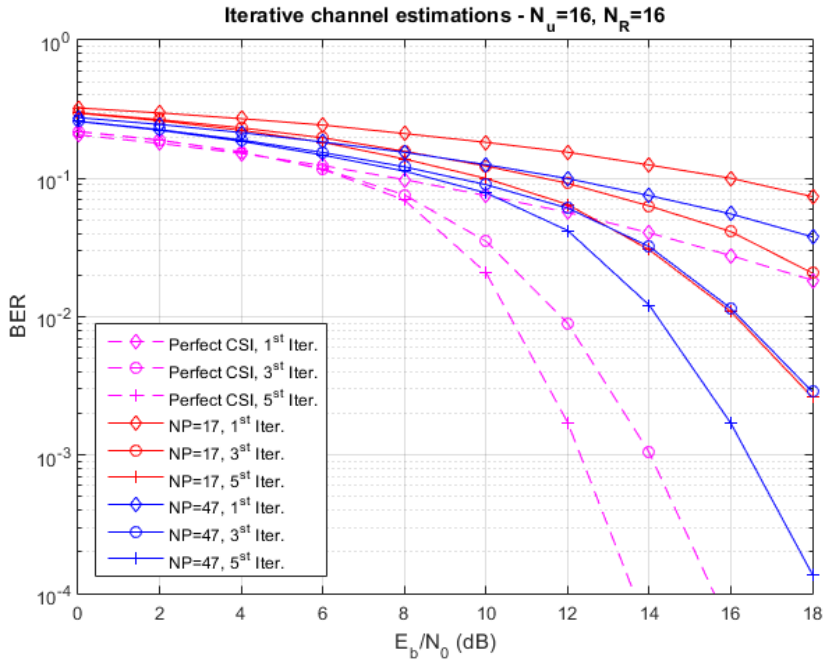

Figure 4.42 - BER performance of iterative channel estimation, for $N_u = N_R = 16$, in function of number of iterations and pilots used

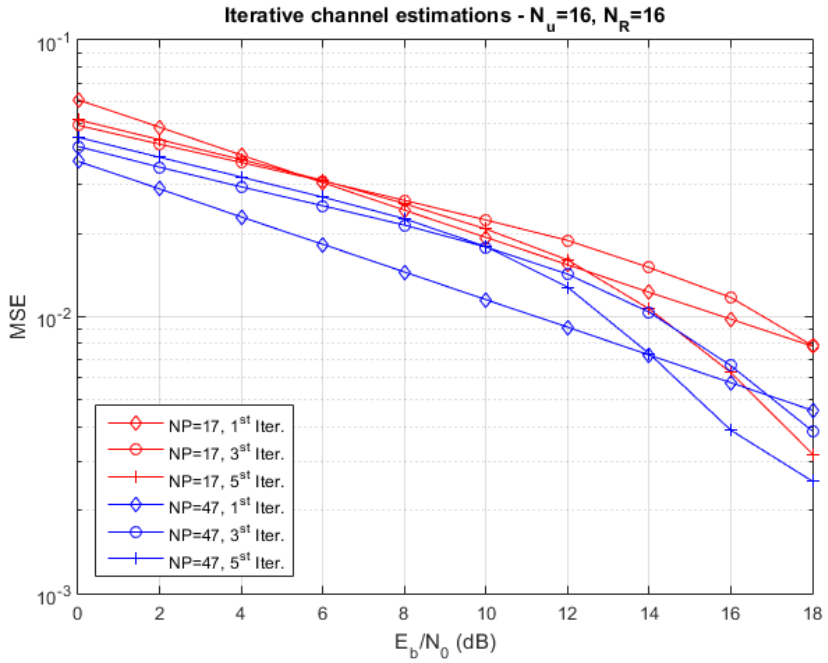

Figure 4.43 - MSE performance of iterative channel estimation, for $N_u = N_R = 16$, in function of number of iterations and pilots used

For a higher number of users and same number of pilots, BER results show a larger disparity of the estimated channel system when compared with the system assuming perfect CSI knowledge – from 1dB to 4dB in the best scenario presented. It is also noticeable the MSE slope convergence starting at a higher level of SNR.

Thus, we may conclude that the channel estimation technique aforementioned shows that the iteration process of IB-DFE can decrease the MSE, actively, after a certain SNR level.

4.3 FSCAPI-based channel estimation

Pilot contamination arises by the repeated use of same training sequences by several users. Thus, becomes crucial for massive MIMO systems to develop estimators capable of accurately estimate CSI with fewer pilots than traditional pilot-based channel estimation techniques. Hence, semi-blind channel estimators are effective in mitigating the effect of pilot contamination, as shown in [53] and [54]. These latter estimators are based in EVD algorithms and few pilots are used to resolve the problem of the ambiguity matrix. Another method to resolve the ambiguity problem is to exploit the asymptotic orthogonality of the users' channel, supported by the law of large numbers. However, this last method is commonly implemented with SVD. Although it achieves better estimation results than EVD-based estimators [72], both SVD and EVD-based channel estimation techniques are exhaustive processes with computational complexity $O({N_R}^3)$, proportional to the dimension of the received signal. Therefore, in massive

MIMO scenarios, where the number of the base station antennas is large, these schemes are not reliable.

To avoid high-complexity and very time consuming algorithms, in [73] and [74] some subspace tracking algorithms were proposed. The FSCAPI-based estimator is an adaptation of the fast approximated power iteration (FAPI) in [74]. The FSCAPI subspace tracking algorithm simplifies the iterative process of the correlation matrix, in order to resolve the ambiguity issue. This way, it achieves lower computational complexity, albeit better tracking results. The complexity of FSCAPI tracking algorithm has complexity $O(N_R N_u)$ [75].

4.3.1 Ambiguity matrix problem and solution

The covariance matrix of the received signal can be given by

$$\begin{aligned} \boldsymbol{R}_y &= E\{\boldsymbol{y}\boldsymbol{y}^H\} \\ &= E\{\boldsymbol{H}\boldsymbol{x}\boldsymbol{x}^H\boldsymbol{H}^H + \boldsymbol{z}\boldsymbol{z}^H\} \\ &= \boldsymbol{H}\boldsymbol{H}^H + \boldsymbol{I}_{N_R}. \end{aligned} \tag{57}$$

To acknowledge the signal subspace, the covariance matrix $\boldsymbol{R}_y$ can be decomposed using SVD such as

$$\boldsymbol{R}_y = [\boldsymbol{U}_s \;\; \boldsymbol{U}_n]\boldsymbol{\Lambda}[\boldsymbol{U}_s \;\; \boldsymbol{Y}_n]\,, \tag{58}$$

where $\boldsymbol{U}_n$ ($\boldsymbol{U}_n \epsilon \mathbb{C}^{N_R \times N_u}$) is the noise subspace and $\boldsymbol{U}_s$ ($\boldsymbol{U}_s \epsilon \mathbb{C}^{N_R \times (N_R - N_u)}$) is the signal subspace.

In [72] it was proven that $\boldsymbol{U}_s$ determines the channel matrix $\boldsymbol{H}$, depending on a scalar multiplicative ambiguity matrix $\boldsymbol{A}$ ($\boldsymbol{A} \epsilon \mathbb{C}^{N_u \times N_u}$). Therefore, the channel estimates can be given by

$$\widehat{\boldsymbol{H}} = \boldsymbol{U}_s \boldsymbol{A}\,. \tag{59}$$

To calculate the ambiguity matrix, a short training sequence is used. The received training sequence is given in (43). According to [72], the ambiguity matrix can be calculated as

$$\boldsymbol{A} = (\boldsymbol{U}_s)^H \widehat{\boldsymbol{H}}^P\,, \tag{60}$$

where $\widehat{\boldsymbol{H}}^P$ is the pilot-based channel estimate resulting of the LS channel estimation in (22).

Therefore, the channel estimate $\widehat{\boldsymbol{H}}$ is given by

$$\widehat{\boldsymbol{H}} = \boldsymbol{U}_s (\boldsymbol{U}_s)^H \widehat{\boldsymbol{H}}^P\,. \tag{61}$$

4.3.2 FSCAPI subspace tracking algorithm

The following FSCAPI subspace tracking algorithm, proposed in [75], was adopted due to its fast convergence and good tracking performance and it is presented in Table 1.

Table 1 - FSCAPI subspace tracking algorithm; *source:*[75]

Initialization:

$$\boldsymbol{W}(0) = \begin{bmatrix} \boldsymbol{I}_{N_u} \\ 0_{(N_R - N_u) \times N_u} \end{bmatrix}, \quad \boldsymbol{Z}(0) = \boldsymbol{I}_{N_u}$$

For $n = 1, 2, \dots, (N_{data})$

Input vector: $\boldsymbol{y}(n)$

$$\boldsymbol{r}(n) = \boldsymbol{W}(n-1)^H \boldsymbol{y}(n)$$

$$\boldsymbol{d}(n) = \boldsymbol{Z}(n-1)\boldsymbol{r}(n)$$

$$\boldsymbol{g}(n) = \frac{\boldsymbol{d}(n)}{\beta + \boldsymbol{r}(n)^H \boldsymbol{d}(n)}$$

$$e^2(n) = \|\boldsymbol{y}(n)\|^2 - \|\boldsymbol{r}(n)\|^2$$

$$s(n) = 1 + e^2(n)\|\boldsymbol{g}(n)\|^2$$

$$\tau(n) = \frac{e^2(n)}{s(n) + \sqrt{s(n)}}$$

$$\phi(n) = 1 - \tau(n)\|\boldsymbol{g}(n)\|^2$$

$$\boldsymbol{r}'(n) = \phi(n)\boldsymbol{r}(n) + \tau(n)\boldsymbol{g}(n)$$

$$\boldsymbol{d}'(n) = \boldsymbol{Z}(n-1)^H \boldsymbol{r}'(n)$$

$$\boldsymbol{Z}(n) = \beta^{-1}(\boldsymbol{Z}(n-1) - \boldsymbol{g}(n)\boldsymbol{d}'(n)^H)$$

$$\boldsymbol{e}'(n) = \phi(n)\boldsymbol{y}(n) - \boldsymbol{W}(n-1)\boldsymbol{r}'(n)$$

$$\boldsymbol{W}(n) = \boldsymbol{W}(n-1) + \boldsymbol{e}'(n)\boldsymbol{g}(n)$$

End for

In the algorithm of Table 1, $\boldsymbol{W}(n)$ ($\boldsymbol{W}(n) \epsilon \mathbb{C}^{N_R \times N_u}$) is the tracked signal subspace for the n-th sample, β ($0 < \beta < 1$) is the forgetting factor and N_{data} ($N_{data} = N - N_P$) denotes the length of the received signal without the pilots. The forgetting factor controls the influence of old data. Then, the tracked signal subspace $\boldsymbol{W}(N_{data})$ is the estimation of $\boldsymbol{U}_s$, so

$$\boldsymbol{U}_s = \boldsymbol{W}(N_{data})\,. \tag{62}$$

Therefore, the estimation of the channel matrix is given by

$$\widehat{\boldsymbol{H}}^{FSCAPI} = \boldsymbol{W}(N_{data})\big(\boldsymbol{W}(N_{data})\big)^H \widehat{\boldsymbol{H}}^P \tag{63}$$

For all simulations based on this method, the selected forgetting factor is $\beta = 0{,}996$.

In Figure 4.44 and Figure 4.45 is shown the discussed channel estimation technique performance with the same setups as the previous section.

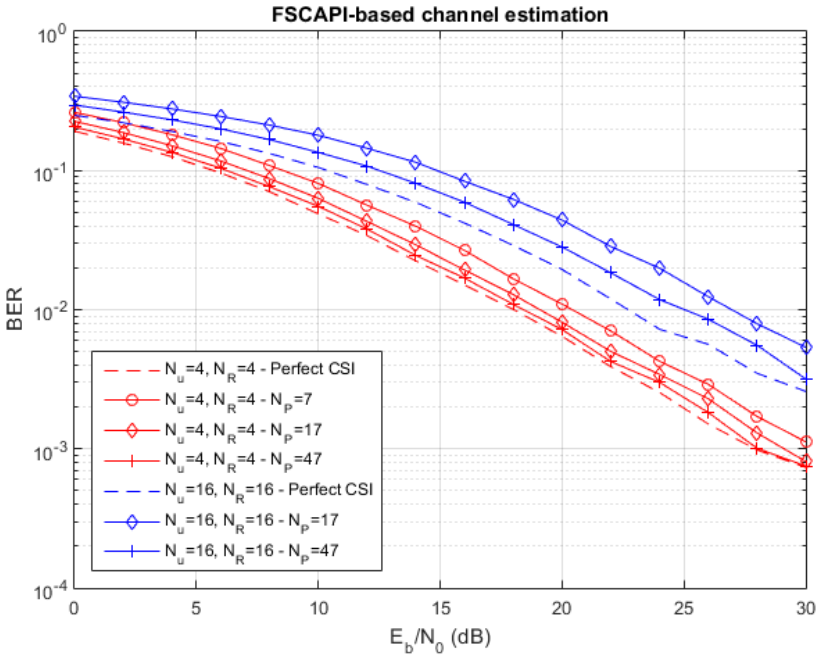

Figure 4.44 - BER performance of FSCAPI-based channel estimation, for $N_u = N_R = 4$ and $N_u = N_R = 16$ based on the number of pilots used

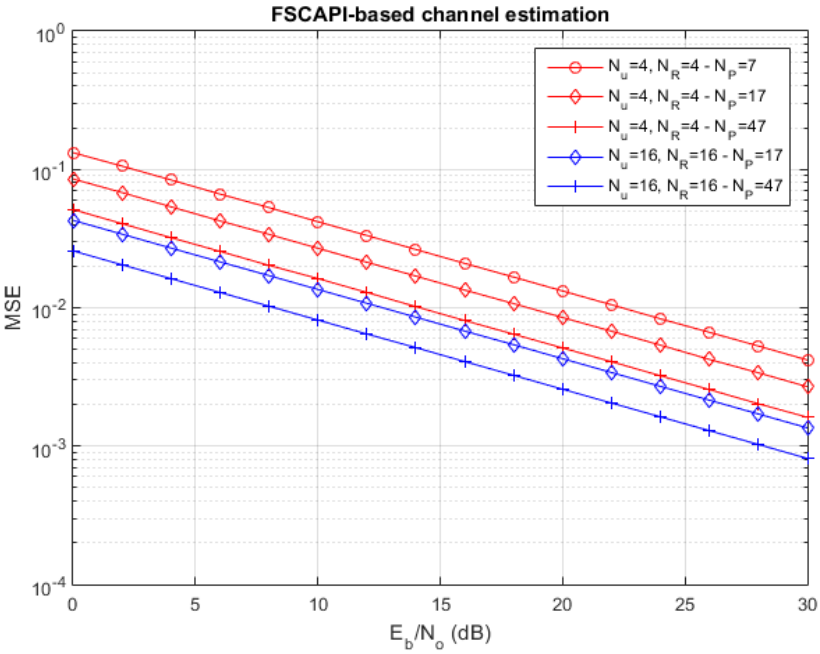

Figure 4.45 - MSE performance of FSCAPI-based channel estimation, for $N_u = N_R = 4$ and $N_u = N_R = 16$ based on the number of pilots used

The FSCAPI-based channel estimation shows better MSE performance for higher number of base station antennas, as it can be seen in Figure 4.45. There is, approximately, a 6dB enhancement on quadrupling the base stations antennas. This can be justified by an improvement on the orthogonality of the channel matrix as number of base stations antennas increases.

4.4 PEACH estimators

The MMSE estimator was already described in chapter 3. This estimator solves a linear system of equations with the use of an inverse operation. Mathematically, this operation has cubic computational complexity. Although the complexity can be reduced under ideal propagation conditions, pilot contamination in massive MIMO systems creates a spatially correlated interference, that reduces the estimation performance and spectral efficiency [2], [51], [56].

In multi-user detection schemes, MMSE detector performs matrix inversions as well, increasing the complexity of the system. The computational complexity of MMSE estimator scales with $O\left({N_R}^3 {N_T}^3\right)$. In massive MIMO systems, where a large scale of antenna arrays is deployed, MMSE estimators are not feasible. For that reason, low-complexity approaches were developed based on polynomial expansion [75–77]. In this studies, the inverse operation is approximated by an L-order matrix polynomial. However, L does not need to be proportional to the system size to achieve satisfying results [78], and so, it is selected to return a good tradeoff between complexity and detection performance.

Based on the polynomial expansion method to reduce complexity, in [79] low-complexity channel estimators, named unweighted PEACH and weighted PEACH (W-PEACH) estimators are proposed. In order to replace the MMSE channel estimation technique, PEACH approximates the MMSE estimator by changing the matrix inversion into a polynomial expansion. Similar to MMSE estimator, PEACH estimators aim to minimize MSE between the estimated channel and the true channel.

4.4.1 Theoretical development

The main idea of replacing the inverse operation with a polynomial expansion is explained in [79], which says that the inverse of the eigenvalues, λ_b, of a Hermitian matrix $\boldsymbol{G}$ ($\boldsymbol{G} \epsilon \mathbb{C}^{B \times B}$) can be approximated by an L-order Taylor polynomial, such as:

$$\boldsymbol{G}^{-1} = \alpha\left(\boldsymbol{I} - (\boldsymbol{I} - \alpha\boldsymbol{G})\right)^{-1} \approx \alpha \sum_{l=0}^{L} (\boldsymbol{I} - \alpha\boldsymbol{G})^{l}\,, \tag{64}$$

where the approximation holds with equality is valid when $L \to \infty$ and α is a scaling factor that must satisfy

$$0 < \alpha < \frac{2}{max_b \lambda_b(\boldsymbol{G})}. \tag{65}$$

For this reason, L does not need to scale with the matrix dimensions to reach the desired accuracy. Thus, L is selected depending on the desired tradeoff between approximation error and complexity. In regard to simulations, the selected polynomial order is $L = 8$. The polynomial

order is based on the MSE comparison presented in [79], which, for this order level, PEACH estimator proves to be approximately equivalent to the MMSE estimator.

4.4.2 Unweighted PEACH estimator

Combining the approximation of (64) with the MMSE channel estimation solution in (33) the unweighted PEACH estimate is given by

$$\widehat{\boldsymbol{H}}^{PEACH} = \boldsymbol{Y}^{P}\boldsymbol{S}^{H}\sum_{l=0}^{L}\alpha\left(\boldsymbol{I}-\alpha\left(\boldsymbol{S}\boldsymbol{S}^{H}+\frac{{\sigma_z}^2}{{\sigma_h}^2}\boldsymbol{I}\right)\right)^{l}, \tag{66}$$

where α, for complexity reasons, is chosen to be

$$\alpha = \frac{2}{tr(\boldsymbol{S}\boldsymbol{S}^{H}+\frac{{\sigma_z}^2}{{\sigma_h}^2}\boldsymbol{I})}. \tag{67}$$

where $tr(\bullet)$ is denoted as the trace operation of a matrix, defined to be the sum of the elements on the main diagonal.

Since (66) no longer has channel inversions, its computational complexity is $O\left(L{N_T}^2{N_R}^2\right)$. It is noteworthy to mention that for massive MIMO schemes, where $L \ll N_T N_R$ PEACH estimator is a great improvement on a complexity point of view, comparing to MMSE estimator.

4.4.3 Weighted PEACH estimator

In order to improve the unweighted PEACH channel estimation technique, different weights can be assign to α to optimize the overall estimation for a specific order L. W-PEACH is obtained by expanding $\left(\boldsymbol{I}-\alpha\left(\boldsymbol{S}\boldsymbol{S}^{H}+\frac{{\sigma_z}^2}{{\sigma_h}^2}\boldsymbol{I}\right)\right)^{l}$ as a binomial series, and replacing constants with weights [79].

The channel estimation result of W-PEACH is

$$\widehat{\boldsymbol{H}}^{WPEACH} = \boldsymbol{Y}^{P}\boldsymbol{S}^{H}\sum_{l=0}^{L}w_l\alpha^{l+1}\left(\boldsymbol{S}\boldsymbol{S}^{H}+\frac{{\sigma_z}^2}{{\sigma_h}^2}\boldsymbol{I}\right)^{l}, \tag{68}$$

where $\boldsymbol{w} = [w_0, \dots, w_L]^T$ are the scalar weights, denoting $[.]^T$ as the transpose operation.

The vector of weights coefficients, w, is calculated to minimize the MSE and is given by

$$\boldsymbol{w} = \boldsymbol{A}^{-1}\boldsymbol{b} \tag{69}$$

where the i-th and j-th element of $\boldsymbol{A}$ ($\boldsymbol{A}\epsilon\mathbb{C}^{(L+1)\times(L+1)}$) and the i-th element of $\boldsymbol{b}$ ($\boldsymbol{b}\epsilon\mathbb{C}^{L+1}$) are given by

$$[\boldsymbol{A}]_{ij} = \alpha^{i+j} tr\left(\boldsymbol{S}^H \left(\boldsymbol{S}\boldsymbol{S}^H + \frac{{\sigma_z}^2}{{\sigma_h}^2}\boldsymbol{I}\right)^{\boldsymbol{i+j-1}} \boldsymbol{S}^H\right), \tag{70}$$

$$[\boldsymbol{b}]_i = \alpha^i tr\left(\boldsymbol{S}^H \left(\boldsymbol{S}\boldsymbol{S}^H + \frac{{\sigma_z}^2}{{\sigma_h}^2}\boldsymbol{I}\right)^{\boldsymbol{i-1}} \boldsymbol{S}^H\right). \tag{71}$$

To further decrease the computational complexity of the weights calculation, [79] proposes an algorithm based on a continuous update of the weights over a sliding time window.

The following figures show the BER and MSE performance of the WPEACH estimator described in this section.

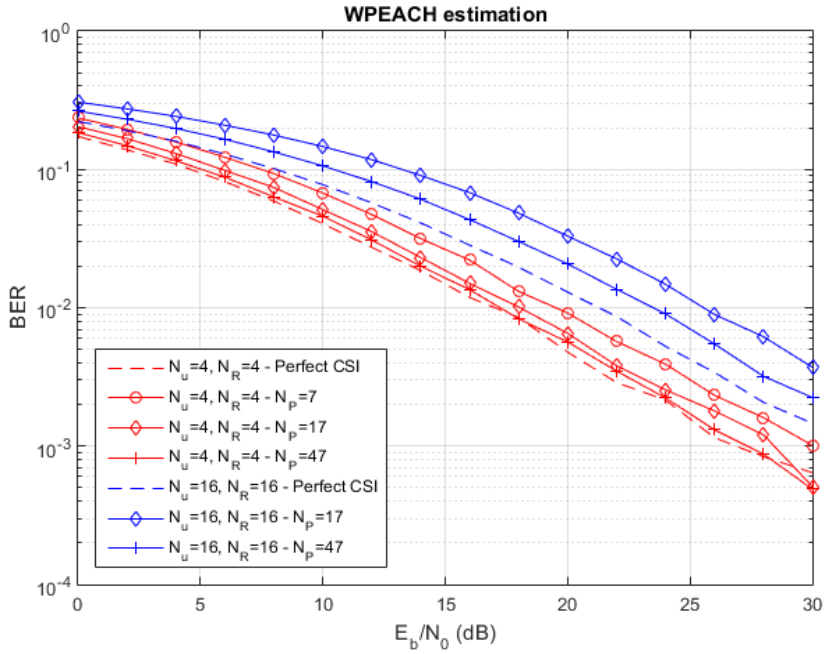

Figure 4.46 - BER performance of WPEACH estimator ($L = 8$), for $N_u = N_R = 4$ and $N_u = N_R = 16$ based on the number of pilots used

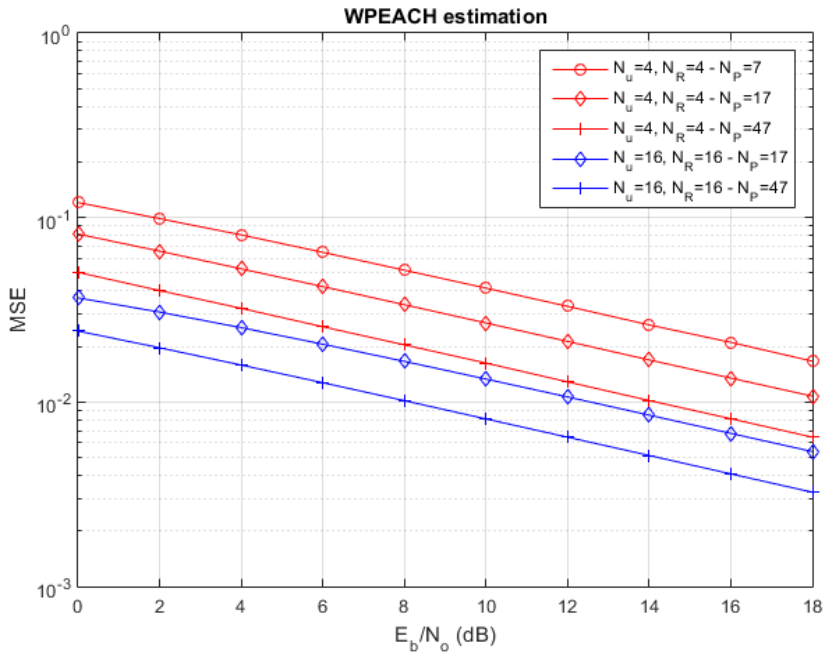

Figure 4.47 - MSE performance of WPEACH estimator ($L = 8$), for $N_u = N_R = 4$ and $N_u = N_R = 16$ based on the number of pilots used

From the results it can be seen that WPEACH estimator achieves very similar results as the FSCAPI-based channel estimator in the previous section. The two techniques only differ at low SNR levels, where is shown a small discrepancy in the MSE value, benefiting the WPEACH estimator. Figure 4.48 and Figure 4.49 display the three estimator's MSE performances for a clear comparison between them. The exhibited simulation of the iterative channel estimation technique corresponds to the 5th iteration.

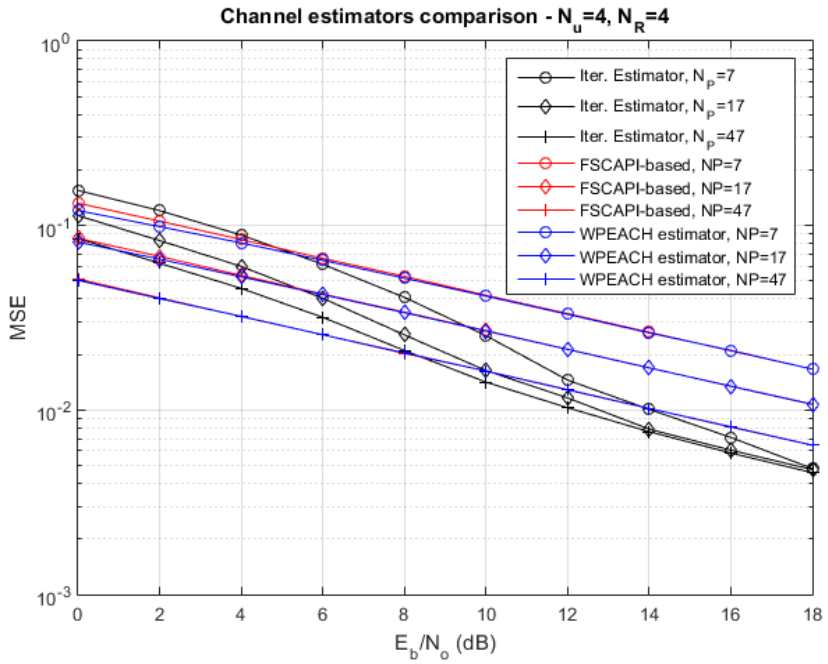

Figure 4.48 - MSE comparison between channel estimation techniques, for $N_u = N_R = 4$

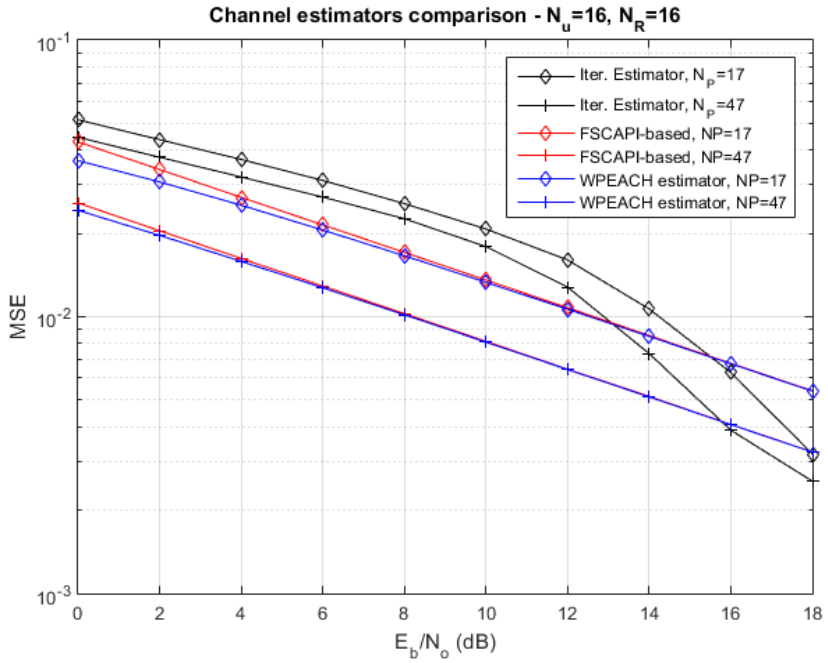

Figure 4.49 - MSE comparison between channel estimation techniques, for $N_u = N_R = 16$

It is clear that, as the number of antennas increases, the iterative channel estimation technique is not as effective as the other two estimators at low SNRs. But, after a certain SNR value, also proportional to the number of antennas, the MSE's slope of the iterative estimator rapidly converges and excels the others.

To put massive MIMO system into context, the following simulations present the case where the base station deploys a larger number of antennas than active users ($N_R = 100$ and $N_u = 10$), highly benefiting from receive diversity and channel matrix orthogonality.

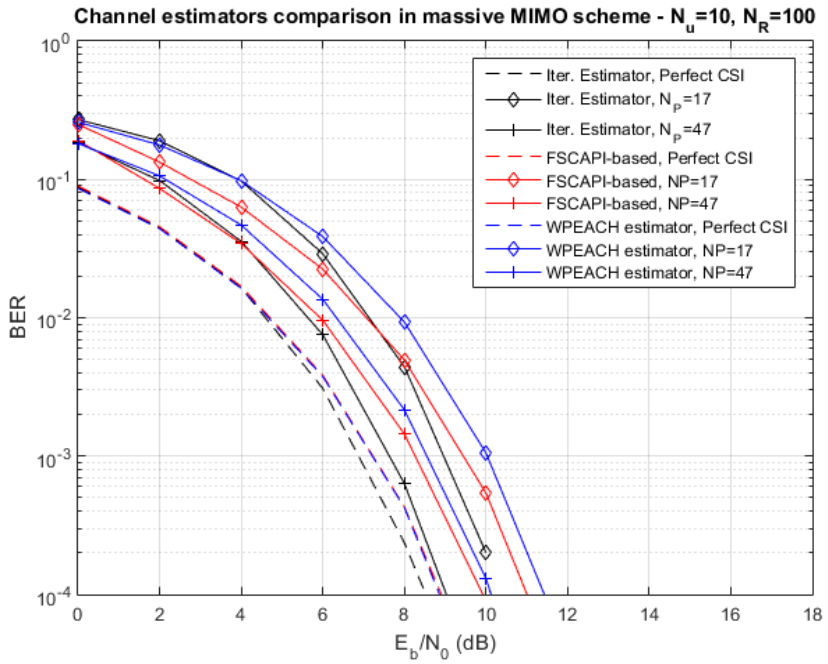

Figure 4.50 - BER comparison between channel estimation techniques, for $N_u = 10$ and $N_R = 100$

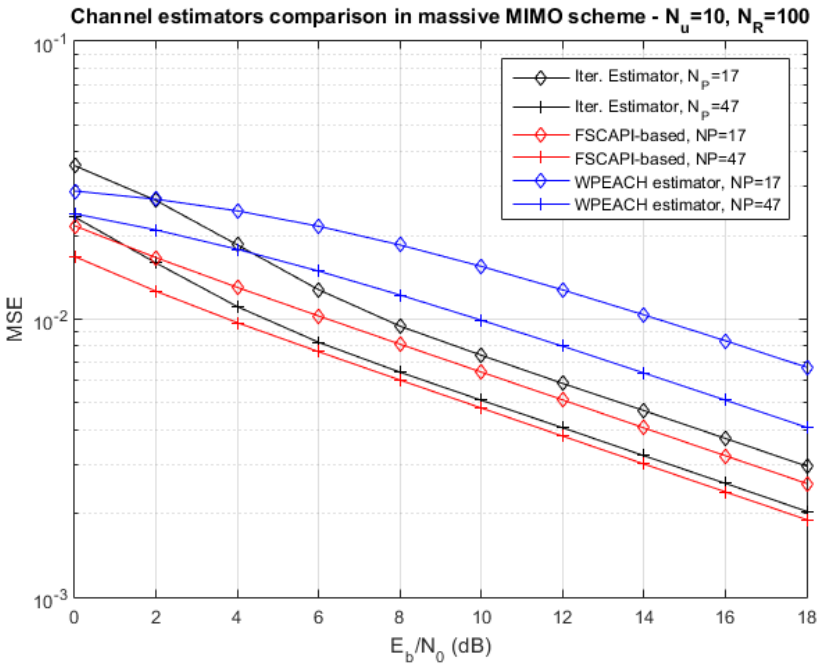

Figure 4.51 - MSE comparison between channel estimation techniques, for $N_u = 10$ and $N_R = 100$

Due to the reasons mentioned above, FSCAPI-based estimator outperforms achieving the lowest MSE between the three. The need of fewer pilots makes this estimator the most interesting technique to adopt in uplink massive MIMO schemes, so far. However, the robustness to inter-cell interference is the main challenge to surpass, and will be analyzed in the next section.

4.5 Comparison results in a massive MIMO scheme

In this section, it will be demonstrated the differences between the three channel estimation techniques, discussed along this chapter, in a massive MIMO scheme with pilot contamination, modeled in section 4.1.1. The system is composed by $N_R = 100$ base station antennas, $N_u = 10$ active users and $K = 5$ interfering users. The interfering users correspond equivalently to the number of training sequences that are going to be contaminated by an interfering channel weakened by the factor of c. The chosen attenuation factors are $c_1 = -6\text{dB}$ and $c_2 = -10\text{dB}$.

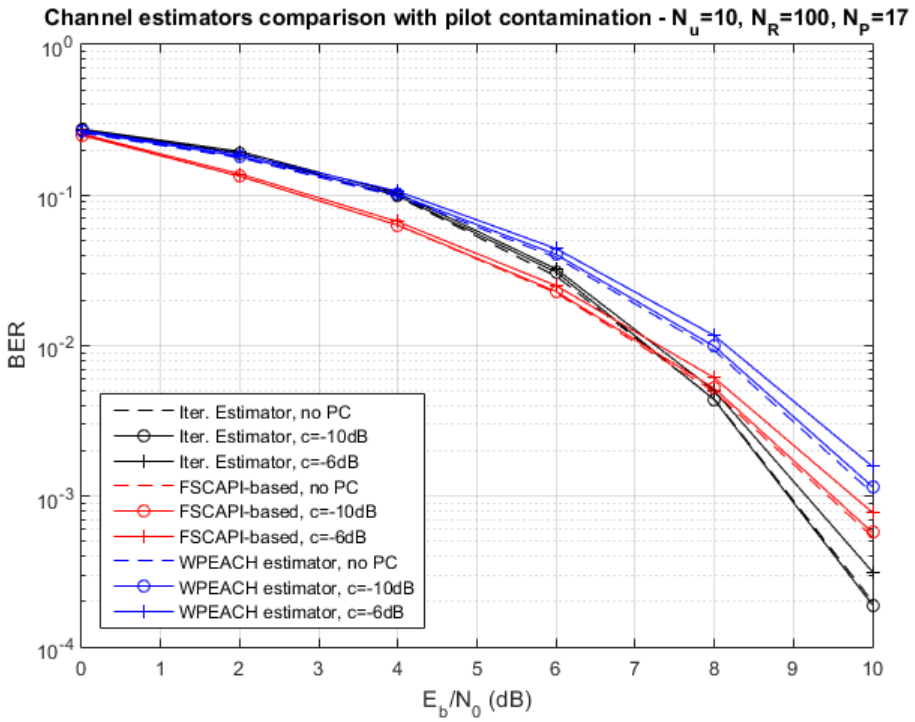

Figure 4.52 - BER comparison between channel estimation techniques in massive MIMO scheme with pilot contamination ($c = -6$dB and $c = -10$dB) and $N_u = 10$, $N_R = 100$, $N_P = 17$

In the BER results of Figure 4.52 the effect of the inter-cell interference is visible. Although it is clear that pilot contamination undesirably affects the performance of the system, MSE simulations will clarify which of the estimators is the best choice do adopt in pilot contamination scenarios. Figure 4.53 and Figure 4.54 show the MSE values for the presented massive MIMO scheme for $N_P = 17$ and $N_P = 47$, respectively.

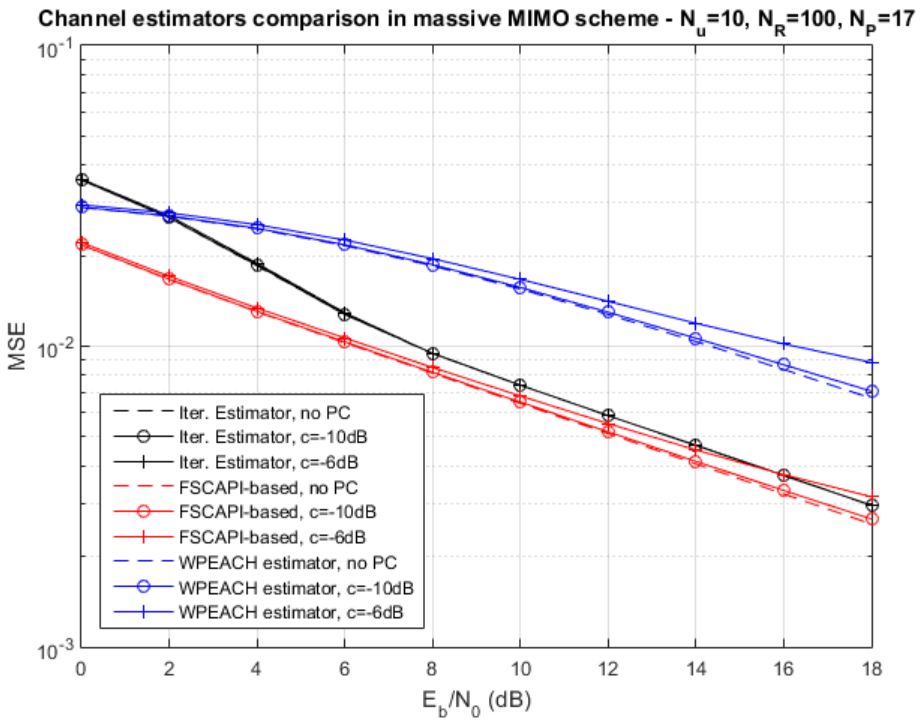

Figure 4.53 - MSE comparison between channel estimation techniques in massive MIMO scheme with pilot contamination ($c = -6\text{dB}$ and $c = -10\text{dB}$) and $N_u = 10$, $N_R = 100$, $N_P = 17$

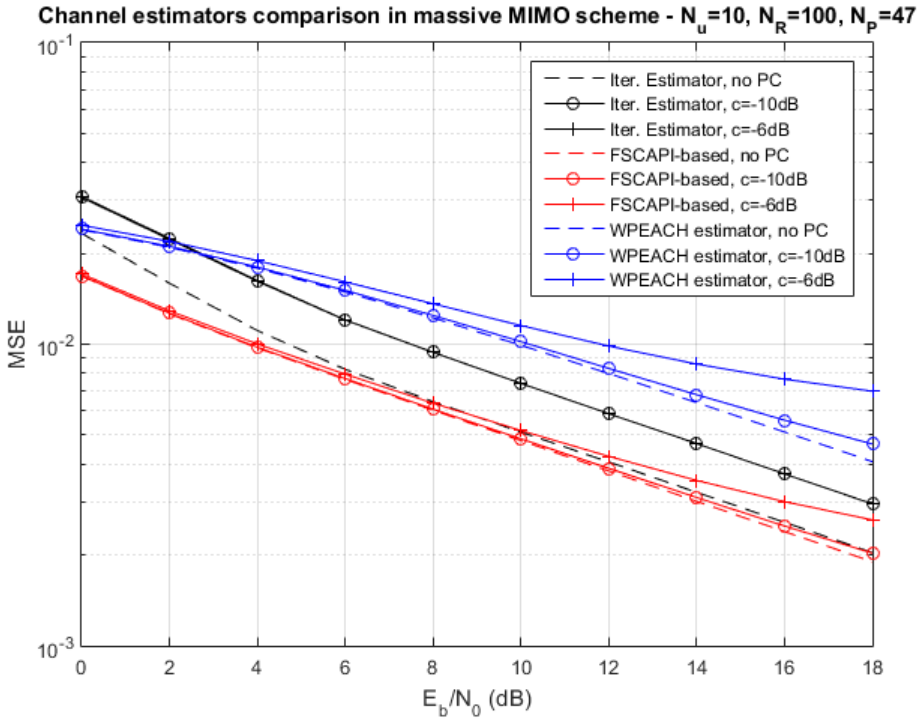

Figure 4.54 - MSE comparison between channel estimation techniques in massive MIMO scheme with pilot contamination ($c = -6\text{dB}$ and $c = -10\text{dB}$) and $N_u = 10$, $N_R = 100$, $N_P = 47$

As expected, the MSE saturates to a non-zero value under pilot contamination. Hereupon, the most effective channel estimation technique is concluded to be the FSCAPI-based estimator, for many aspects:

- For an increasing SNR, FSCAPI-based estimator is the latest to show the effect of pilot contamination, at 6dB, while the WPEACH estimator starts at 2dB and the iterative one is practically always affected.
- It presents the lowest saturation level of all estimators, followed by the iterative channel estimator.
- The linear computational complexity makes FSCAPI-based estimator an optimal technique in massive MIMO scenarios.
- It greatly benefits from large base station antennas arrays, since the subspace tracking algorithm relies on the orthogonality of channel matrix. Since FSCAPI-based estimator has very low computational complexity, large channel matrices do not affect as much the efficiency of the process.
- By being a semi-blind technique it relieves the pilot contamination effect [1] and increases data payload.

For all the aforementioned reasons, the FSCAPI-based channel estimation technique proposed in section 4.3 is a perfect candidate for the future of massive MIMO uplink transmissions.

5. Conclusions

5G is recognized to be the groundbreaking future of cellular networking. From 5G, massive MIMO is an innovative concept to revolutionize wireless communication systems, and it is intended to be implemented in the near future. This new concept, is capable of hundredfold growths in spectral efficiency and overall system's performance by deploying a large-scale antenna arrays at the base stations. In this work, some problems are analyzed that arise with massive MIMO, more specifically, the increased complexity of channel estimation of large channel matrices and inter-cell interference caused by the reuse of training sequences in adjacent cells. As far as complexity concerns, matrix inversions and factorizations are the main problem of channel estimations techniques. A channel estimation technique with Zadoff-Chu sequences was introduced in order to replace channel estimation based on matrix inversions, such as the MMSE estimator. Moreover, pilot contamination was studied and three channel estimation techniques were proposed to achieve the best compromise between complexity, spectral efficiency and system performance.

5.1 Synthesis and final remarks

In chapter 2 the state-of-the-art was presented, with a description of the fundamentals of 5G, i.e., the motivation, requirements and main ideas behind it. To end it, the importance of channel estimation in wireless systems, the problems of channel estimation in massive MIMO systems and current efforts to solve them were also clarified.

Chapter 3 focus was on the BD precoding scheme that showed to be very effective in cancelling CCI, especially in multiple antenna mobile stations. It was also compared the well-known MMSE estimator with the introduced channel estimation technique based on Zadoff-Chu training sequences. The latter exhibits better performance results for few pilots and since it does not resort to channel inversion of matrices, it has much lower complexity than MMSE estimator. The problem in adapting this technique in a system with large number of antennas, is that the number of pilots per sequence has to be greater than the desired number of different sequences (proportional to the active transmit antennas), in order to generate pairwise orthogonal pilot signals. Hence, a tradeoff between number of active transmit antennas and data payload as to be studied, hereafter.

In chapter 4, it was described the pilot contamination model, and three channel estimation techniques were proposed to mitigate the inter-cell interference, denominated as pilot contamination. Simulations results were presented for different antenna setups, including the massive MIMO concept, with a great diversity order. The pilot contamination scenario was

simulated for different attenuation constants, and from the results it was possible to concluded that the FSCAPI-based estimator was, definitely, the most efficient and accurate estimator for a massive MIMO scenario, with or without inter-cell interference scenario modeled among the others. Nonetheless, the other two estimators are more influenced by pilot contamination than the FSCAPI-based one.

5.2 Future Works

The results presented in this work can be used for future efforts in order to haste the 5G revolution. The main subject of the thesis is crucial for the development of massive MIMO and imposes a critical limitation on the anticipated system's performance.

When no pilots are required, pilot contamination ceases to exist. Hence the most optimistic approach would be the development towards low-complexity, blind channel estimation techniques. However, based on the work results, subspace tracking algorithms have many advantages taken from the concept of massive MIMO, and should be extensively studied.

6. References

[1] T. L. Marzetta, “Noncooperative cellular wireless with unlimited numbers of base station antennas,” *IEEE Trans. Wirel. Commun.*, vol. 9, no. 11, pp. 3590–3600, Nov. 2010.

[2] F. Rusek, D. Persson, Buon Kiong Lau, E. G. Larsson, T. L. Marzetta, and F. Tufvesson, “Scaling Up MIMO: Opportunities and Challenges with Very Large Arrays,” *IEEE Signal Process. Mag.*, vol. 30, no. 1, pp. 40–60, Jan. 2013.

[3] L. H. Brandenburg and A. D. Wyner, “Capacity of the Gaussian Channel With Memory: The Multivariate Case,” *Bell Syst. Tech. J.*, vol. 53, no. 5, pp. 745–778, 1974.

[4] A. R. Kaye and D. A. George, “Transmission of Multiplexed PAM Signals Over Multiple Channel and Diversity Systems,” *IEEE Trans. Commun. Technol.*, vol. 18, no. 5, pp. 520–526, 1970.

[5] W. Van Etten, “Maximum Likelihood Receiver for Multiple Channel Transmission Systems,” *IEEE Trans. Commun.*, vol. 24, no. 2, pp. 276–283, 1976.

[6] J. H. Winters, “On the capacity of radio communication systems with diversity in a Rayleigh fading environment,” *Sel. Areas Commun. IEEE J.*, vol. SAC-5, no. 5, pp. 871–878, 1987.

[7] T. L. Marzetta and B. M. Hochwald, “Capacity of a mobile multiple-antenna communication link in Rayleigh flat fading,” *IEEE Trans. Inf. Theory*, vol. 45, no. 1, pp. 139–157, 1999.

[8] E. Telatar, “Capacity of multi-antenna Gaussian channels,” *Eur. Trans. Telecommun.*, vol. 10, no. 6, pp. 585–595, 1999.

[9] A. M. Sayeed and V. Raghavan, “Maximizing MIMO capacity in sparse multipath with reconfigurable antenna arrays,” *IEEE J. Sel. Top. Signal Process.*, vol. 1, no. 1, pp. 156–166, 2007.

[10] B. D. Van Veen and K. M. Buckley, “Beamforming: A Versatile Approach to Spatial Filtering,” *IEEE ASSP Mag.*, vol. 5, no. 2, pp. 4–24, 1988.

[11] D. Gesbert, M. Kountouris, R. W. Heath, C. B. Chae, and T. Sälzer, “Shifting the MIMO Paradigm,” *IEEE Signal Process. Mag.*, vol. 24, no. 5, pp. 36–46, 2007.

[12] R. Knopp and P. A. Humblet, “Information capacity and power control in single-cell multiuser communications,” *Proc. IEEE Int. Conf. Commun. ICC ’95*, vol. 1, pp. 331–335, 1995.

[13] M. H. M. Costa, “Writing on Dirty Paper,” *IEEE Transactions on Information Theory*, vol. 29, no. 3. pp. 439–441, 1983.

[14] N. Jindal and A. Goldsmith, “Dirty-paper coding versus TDMA for MIMO broadcast channels,” *IEEE Trans. Inf. Theory*, vol. 51, no. 5, pp. 1783–1794, 2005.

[15] F. Kaltenberger, M. Kountouris, L. Cardoso, R. Knopp, and D. Gesbert, “Capacity of linear multi-user MIMO precoding schemes with measured channel data,” in *IEEE Workshop on Signal Processing Advances in Wireless Communications, SPAWC*, 2008, pp. 580–584.

[16] Q. H. Spencer, A. L. Swindlehurst, and M. Haardt, “Zero-forcing methods for downlink spatial multiplexing in multiuser MIMO channels,” *IEEE Trans. Signal Process.*, vol. 52, no. 2, pp. 461–471, 2004.

[17] C. B. Peel, B. M. Hochwald, and a L. Swindlehurst, "A Vector-Perturbation Technique for Communication — Part I : Channel Inversion and Regularization," *Technology*, vol. 53, no. 1, pp. 1–22, 2005.

[18] Z. Shen, R. Chen, J. G. Andrews, R. W. Heath, and B. L. Evans, "Low complexity user selection algorithms for multiuser MIMO systems with block diagonalization," *IEEE Trans. Signal Process.*, vol. 54, no. 9, pp. 3658–3663, Sep. 2006.

[19] J. H. Chang, L. Tassiulas, and F. Rashid-Farrokhi, "Joint transmitter receiver diversity for efficient space division multiaccess," *IEEE Trans. Wirel. Commun.*, vol. 1, no. 1, pp. 16–26, 2002.

[20] C. B. Chae and R. W. Heath, "On the optimality of linear multiuser MIMO beamforming for a two-user two-input multiple-output broadcast system," *IEEE Signal Process. Lett.*, vol. 16, no. 2, pp. 117–120, Feb. 2009.

[21] T. Y. T. Yoo and a. Goldsmith, "Optimality of zero-forcing beamforming with multiuser diversity," in *IEEE International Conference on Communications, 2005. ICC 2005. 2005*, 2005, vol. 1, no. C, pp. 542–546.

[22] T. Yoo and A. Goldsmith, "Sum-rate optimal multi-antenna downlink beamforming strategy based on clique search," in *GLOBECOM - IEEE Global Telecommunications Conference*, 2005, vol. 3, pp. 1510–1514.

[23] Z. Tu and R. S. Blum, "Multiuser diversity for a dirty paper approach," *IEEE Commun. Lett.*, vol. 7, no. 8, pp. 370–372, Aug. 2003.

[24] M. Sharif and B. Hassibi, "On the capacity of MIMO broadcast channels with partial side information," *IEEE Trans. Inf. Theory*, vol. 51, no. 2, pp. 506–522, Feb. 2005.

[25] S. Chen and J. Zhao, "The requirements, challenges, and technologies for 5G of terrestrial mobile telecommunication," *IEEE Commun. Mag.*, vol. 52, no. 5, pp. 36–43, May 2014.

[26] Ericsson, "Ericsson Mobility Report - On the pulse of the networked society," no. June. Stockholm, Sweden, p. 32, 2016.

[27] Fujitsu, "High-Capacity Indoor Wireless Solutions: Picocell or Femtocell," *Fujitsu White Paper*. Tokyo, Japan, p. 10, 2013.

[28] Ericsson White Paper, "5G Energy Performance," no. April. Stockholm, Sweden, pp. 1–14, 2015.

[29] ITU-R, "ITU-R M . 2078: Estimated Spectrum Bandwidth Requirements for the Future Development of IMT-2000 and IMT-Advanced," Geneva, Switzerland, 2006.

[30] Z. Pi and F. Khan, "An introduction to millimeter-wave mobile broadband systems," *IEEE Commun. Mag.*, vol. 49, no. 6, pp. 101–107, Jun. 2011.

[31] F. Boccardi, R. Heath, A. Lozano, T. L. Marzetta, and P. Popovski, "Five disruptive technology directions for 5G," *IEEE Commun. Mag.*, vol. 52, no. 2, pp. 74–80, Feb. 2014.

[32] C. R. Anderson and T. S. Rappaport, "In-building wideband partition loss measurements at 2.5 and 60 GHz," *IEEE Trans. Wirel. Commun.*, vol. 3, no. 3, pp. 922–928, May 2004.

[33] A. V. Alejos, M. G. Sanchez, and I. Cuinas, "Measurement and analysis of propagation mechanisms at 40 GHz: Viability of site shielding forced by obstacles," *IEEE Trans. Veh. Technol.*, vol. 57, no. 6, pp. 3369–3380, Nov. 2008.

[34] M. Marcus and B. Pattan, "Millimeter wave propagation: Spectrum management implications," *IEEE Microw. Mag.*, vol. 6, no. 2, pp. 54–62, Jun. 2005.

[35] U. Johannsen, A. B. Smolders, A. C. F. Reniers, A. R. V Dommele, and M. D. Huang, "Integrated antenna concept for millimeter-wave front-end modules in proven technologies," in *Proceedings of 6th European Conference on Antennas and Propagation, EuCAP 2012*, 2012, pp. 2560–2563.

[36] C. Studer and E. G. Larsson, "PAR-aware large-scale multi-user MIMO-OFDM downlink," *IEEE J. Sel. Areas Commun.*, vol. 31, no. 2, pp. 303–313, Feb. 2013.

[37] S. K. Mohammed and E. G. Larsson, "Per-antenna constant envelope precoding for large multi-user MIMO systems," *IEEE Trans. Commun.*, vol. 61, no. 3, pp. 1059–1071, Mar. 2013.

[38] Hien Quoc Ngo, E. G. Larsson, and T. L. Marzetta, "Energy and Spectral Efficiency of Very Large Multiuser MIMO Systems," *IEEE Trans. Commun.*, vol. 61, no. 4, pp. 1436–1449, Apr. 2013.

[39] E. G. Larsson, O. Edfors, F. Tufvesson, and T. L. Marzetta, "Massive MIMO for next generation wireless systems," *IEEE Commun. Mag.*, vol. 52, no. 2, pp. 186–195, Feb. 2014.

[40] U. U. Johannsen, M. I. Kazim, A. B. Smolders, and M. M. Herben, "Modular antenna array concept for millimeter-wave beam-steering applications," in *Progress in Electromagnetics Research Symposium Proceedings*, 2013, pp. 229–233.

[41] A. Puglielli, N. Narevsky, P. Lu, T. Courtade, G. Wright, B. Nikolic, and E. Alon, "A scalable massive MIMO array architecture based on common modules," in *2015 IEEE International Conference on Communication Workshop (ICCW)*, 2015, pp. 1310–1315.

[42] C. Shepard, H. Yu, and L. Zhong, "ArgosV2: A Flexible Many-Antenna Research Platform," in *Proceedings of the 19th annual international conference on Mobile computing & networking - MobiCom '13*, 2013, p. 163.

[43] J. Vieira, S. Malkowsky, K. Nieman, Z. Miers, N. Kundargi, L. Liu, I. Wong, V. Owall, O. Edfors, and F. Tufvesson, "A flexible 100-antenna testbed for Massive MIMO," in *2014 IEEE Globecom Workshops, GC Wkshps 2014*, 2014, pp. 287–293.

[44] H. Suzuki, R. Kendall, K. Anderson, A. Grancea, D. Humphrey, J. Pathikulangara, K. Bengston, J. Matthews, and C. Russell, "Highly spectrally efficient Ngara Rural Wireless Broadband Access Demonstrator," in *2012 International Symposium on Communications and Information Technologies, ISCIT 2012*, 2012, no. March 2011, pp. 914–919.

[45] H. V. Balan, M. Segura, S. Deora, A. Michaloliakos, R. Rogalin, K. Psounis, and G. Caire, "USC SDR, an easy-to-program, high data rate, real time software radio platform," in *Proceedings of the second workshop on Software radio implementation forum - SRIF '13*, 2013, pp. 25–29.

[46] X. Gao, O. Edfors, F. Rusek, and F. Tufvesson, "Massive MIMO Performance Evaluation Based on Measured Propagation Data," *IEEE Trans. Wirel. Commun.*, vol. 14, no. 7, pp. 3899–3911, Jul. 2015.

[47] F. Kaltenberger, H. Jiang, M. Guillaud, and R. Knopp, "Relative channel reciprocity calibration in MIMO/TDD systems," *2010 Futur. Netw. Mob. Summit*, pp. 1–10, 2010.

[48] H. Huh, A. M. Tulino, and G. Caire, "Network MIMO With Linear Zero-Forcing Beamforming: Large System Analysis, Impact of Channel Estimation, and Reduced-Complexity Scheduling," *IEEE Trans. Inf. Theory*, vol. 58, no. 5, pp. 2911–2934, May 2012.

[49] J. Nam, J.-Y. Ahn, A. Adhikary, and G. Caire, "Joint spatial division and multiplexing: Realizing massive MIMO gains with limited channel state information," in *2012 46th*

Annual Conference on Information Sciences and Systems (CISS), 2012, pp. 1–6.

[50] B. Gopalakrishnan and N. Jindal, "An analysis of pilot contamination on multi-user MIMO cellular systems with many antennas," in *2011 IEEE 12th International Workshop on Signal Processing Advances in Wireless Communications*, 2011, pp. 381–385.

[51] R. R. Muller, L. Cottatellucci, and M. Vehkapera, "Blind Pilot Decontamination," *IEEE J. Sel. Top. Signal Process.*, vol. 8, no. 5, pp. 773–786, Oct. 2014.

[52] A. Ashikhmin and T. Marzetta, "Pilot contamination precoding in multi-cell large scale antenna systems," in *2012 IEEE International Symposium on Information Theory Proceedings*, 2012, pp. 1137–1141.

[53] H. Q. Ngo and E. G. Larsson, "EVD-based channel estimation in multicell multiuser MIMO systems with very large antenna arrays," in *2012 IEEE International Conference on Acoustics, Speech and Signal Processing (ICASSP)*, 2012, no. 1, pp. 3249–3252.

[54] G. Mangqing, X. Gang, G. Jinchun, and L. Yuan'an, "Enhanced EVD based channel estimation and pilot decontamination for Massive MIMO networks," *J. China Univ. Posts Telecommun.*, vol. 22, no. 6, pp. 72–77, Dec. 2015.

[55] F. Fernandes, A. Ashikhmin, and T. L. Marzetta, "Inter-Cell Interference in Noncooperative TDD Large Scale Antenna Systems," *IEEE J. Sel. Areas Commun.*, vol. 31, no. 2, pp. 192–201, Feb. 2013.

[56] H. Yin, D. Gesbert, M. Filippou, and Y. Liu, "A Coordinated Approach to Channel Estimation in Large-Scale Multiple-Antenna Systems," *IEEE J. Sel. Areas Commun.*, vol. 31, no. 2, pp. 264–273, Feb. 2013.

[57] E. Biglieri, J. Proakis, and S. Shamai, "Fading channels: information-theoretic and communications aspects," *IEEE Trans. Inf. Theory*, vol. 44, no. 6, pp. 2619–2692, 1998.

[58] Y. S. Cho, J. Kim, C.-G. Kang, and W. Y. Yang, *MIMO-OFDM Wireless Communications with MATLAB*. Singapore: John Wiley & Sons (Asia), 2010.

[59] S. Coleri, M. Ergen, A. Puri, and A. Bahai, "Channel estimation techniques based on pilot arrangement in OFDM systems," *IEEE Trans. Broadcast.*, vol. 48, no. 3, pp. 223–229, Sep. 2002.

[60] Meng-Han Hsieh and Che-Ho Wei, "Channel estimation for OFDM systems based on comb-type pilot arrangement in frequency selective fading channels," *IEEE Trans. Consum. Electron.*, vol. 44, no. 1, pp. 217–225, 1998.

[61] E. Ientilucci, "Using the singular value decomposition," *Rochester Inst. Technol.*, pp. 1–8, 2003.

[62] M. H. Khan, K. M. Cho, M. Lee, and J.-G. Chung, "A simple block diagonal precoding for multi-user MIMO broadcast channels," *EURASIP J. Wirel. Commun. Netw.*, vol. 2014, no. 1, p. 95, 2014.

[63] J.-J. van de Beek, O. Edfors, M. Sandell, S. K. Wilson, and P. O. Borjesson, "On channel estimation in OFDM systems," in *1995 IEEE 45th Vehicular Technology Conference. Countdown to the Wireless Twenty-First Century*, 1995, vol. 2, no. 1, pp. 815–819.

[64] A. Ancora, C. Bona, and D. T. M. Slock, "Down-Sampled Impulse Response Least-Squares Channel Estimation for LTE OFDMA," in *2007 IEEE International Conference on Acoustics, Speech and Signal Processing - ICASSP '07*, 2007, vol. 3, p. III-293-III-296.

[65] Y. Luan, C. Kan, H. Du, and Q. Zhao, "An improved LS channel estimation algorithm of SC-FDMA," in *2015 IEEE 9th International Conference on Anti-counterfeiting, Security, and Identification (ASID)*, 2015, vol. 7, pp. 128–131.

[66] D. Chu, “Polyphase codes with good periodic correlation properties (Corresp.),” *IEEE Trans. Inf. Theory*, vol. 18, no. 4, pp. 531–532, Jul. 1972.

[67] H. Myung, J. Lim, and D. Goodman, “Single carrier FDMA for uplink wireless transmission,” *IEEE Veh. Technol. Mag.*, vol. 1, no. 3, pp. 30–38, Sep. 2006.

[68] M. Jamal, B. Horia, K. Maria, and I. Alexandru, “Study of multiple access schemes in 3GPP LTE OFDMA vs. SC-FDMA,” *2011 Int. Conf. Appl. Electron.*, pp. 1–4, 2011.

[69] J. G. Proakis and M. Salehi, *Digital Communications*, 5th ed. New York, New York, USA: McGraw-Hill, 2008.

[70] N. Benvenuto and S. Tomasin, “On the comparison between OFDM and single carrier modulation with a DFE using a frequency-domain feedforward filter,” *IEEE Trans. Commun.*, vol. 50, no. 6, pp. 947–955, Jun. 2002.

[71] N. Benvenuto and S. Tomasin, “Iterative Design and Detection of a DFE in the Frequency Domain,” *IEEE Trans. Commun.*, vol. 53, no. 11, pp. 1867–1875, Nov. 2005.

[72] A. Hu, T. Lv, and Y. Lu, “Subspace-Based Semi-Blind Channel Estimation for Large-Scale Multi-Cell Multiuser MIMO Systems,” in *2013 IEEE 77th Vehicular Technology Conference (VTC Spring)*, 2013, pp. 1–5.

[73] D. J. Rabideau, “Fast, rank adaptive subspace tracking and applications,” *IEEE Trans. Signal Process.*, vol. 44, no. 9, pp. 2229–2244, 1996.

[74] R. Badeau, B. David, and G. Richard, “Fast approximated power iteration subspace tracking,” *IEEE Trans. Signal Process.*, vol. 53, no. 8, pp. 2931–2941, Aug. 2005.

[75] F. Xu, Y. Xiao, and D. Wang, “Adaptive semi-blind channel estimation for massive MIMO systems,” in *2014 12th International Conference on Signal Processing (ICSP)*, 2014, vol. 2015–Janua, no. October, pp. 1698–1702.

[76] G. M. A. Sessler and F. K. Jondral, “Low Complexity Polynomial Expansion Multiuser Detector for CDMA Systems,” *IEEE Trans. Veh. Technol.*, vol. 54, no. 4, pp. 1379–1391, Jul. 2005.

[77] J. Hoydis, M. Debbah, and M. Kobayashi, “Asymptotic moments for interference mitigation in correlated fading channels,” in *2011 IEEE International Symposium on Information Theory Proceedings*, 2011, pp. 2796–2800.

[78] M. L. Honig and Weimin Xiao, “Performance of reduced-rank linear interference suppression,” *IEEE Trans. Inf. Theory*, vol. 47, no. 5, pp. 1928–1946, Jul. 2001.

[79] N. Shariati, E. Bjornson, M. Bengtsson, and M. Debbah, “Low-complexity channel estimation in large-scale MIMO using polynomial expansion,” in *2013 IEEE 24th Annual International Symposium on Personal, Indoor, and Mobile Radio Communications (PIMRC)*, 2013, pp. 1157–1162.